25

[redacted]

Coordinated Science Laboratory

UNIVERSITY OF ILLINOIS – URBANA, ILLINOIS

PROGRESS REPORT
FOR
MARCH - AUGUST, 1966

October 31, 1966

The research reported in this document was made possible through support extended the Coordinated Science Laboratory, University of Illinois, by the Joint Services Electronics Program (U. S. Army Electronics Laboratories and U. S. Army Research Office, Office of Naval Research, and the Air Force Office of Scientific Research) under Contract Number DA 28 043 AMC 00073(E).

Portions of this work were also supported by

National Aeronautics and Space Administration

Research Grants NsG-443, NsG-504
NGR 14 005 038, NsG-376

National Science Foundation

Grant NSF GK-36
Grant NSF GK-690

Advanced Research Projects Agency

Through Office of Naval Research
Contract Nonr-3985(08)

Air Force Office of Scientific Research

Grant AFOSR 931.66

Office of Naval Research

Contract
N00014-66-C0010-A01

U. S. Office of Education

Contract OE-6-10-184

Syracuse University Research Corporation

Contract SURC 66124

University of Illinois

as acknowledged in footnotes in the text.

COORDINATED SCIENCE LABORATORY

SUMMARY OF

PROGRESS REPORT FOR MARCH THROUGH AUGUST, 1966

1. Surface Physics

We have demonstrated that the vibrational states of gases adsorbed on metal surfaces can be detected by low-energy electron scattering. The results of the initial measurements of this type are reported and discussed. Additional progress in the design and construction of the apparatus for the measurement of the angular energy distribution of secondary electrons is discussed. Contamination effects have been observed in the study of the adsorption of gases at metal surfaces. These effects have been tentatively related to products from the oil diffusion pump. A high-sensitivity spectrometer for the determination of the energy distribution of ions and electrons leaving a surface under ion or electron bombardment has been designed, and measurements on a prototype model have been made. These measurements show quite promising sensitivity and resolution characteristics. A new experiment involving photon emission from surfaces under ion bombardment is proposed to observe 1) photons originating directly from the ion-neutralization process, and 2) photons resulting from the recombination of electron-hole pairs generated by Auger neutralization. Quantities to be measured are the total yield, the energy distribution of the photons, the dependence on ion species and their energy, and the effect of adsorbed gas on the target.

2. Applied Physics

Further details are given of improvements to the Schuemann suppressor ion gauge which are intended to make it more useful at pressures of 10^{-12} Torr

and lower region. Experiments under way designed to reach pressures low enough to test the limitations of this gauge are also discussed. The status of the cryopumped uhv system to be used for size-effect experiments is discussed. Preliminary results for tunneling experiments intended to show quantum size effects in thin samples are given. Sample-purification techniques for niobium single crystals to be used for tunneling experiments have now produced resistivity ratios as high as 700. The helium-3 refrigerator to be used for this work is now complete. A third design of the cryogenic parametric amplifier is under test. This instrument will, it is hoped, produce a lower noise level than the earlier models.

3. Plasma Physics

Incoherent scattering of microwaves has been used as a diagnostic method to determine the k spectrum of beam-stimulated plasma oscillations. Time-resolved measurements of radiated microwave power are in progress. The Pines-Schrieffer equation has been derived from a hierarchy of equations based on the Bohm-Pines Hamiltonian.

4. Rarefied Gas Dynamics

Professors Hicks, Yen, and Nordsieck presented two papers at the Fifth International Symposium on Rarefied Gas Dynamics at Oxford University July 4 to 8. We have numerical proof of the convergence of our iteration method of solving the Boltzmann equation. In the pseudoshock near the beginning of the relaxation process, we have studied the relaxation of the lateral temperature, the Boltzmann function, and the velocity distribution function.

5. High-Voltage Breakdown

The effect of gas conditioning in suppressing field-emission current by as much as 20 orders of magnitude (at a given voltage) and thereby improving the voltage-holding capabilities of the electrodes in ultrahigh vacuum is explained as due to the blunting of the tips of the cathode protrusions by selective sputtering. Quantitative estimates of the time required to produce noticeable blunting effects agree with experimental observations. At 3×10^{-10} Torr, the measured "half life" of the suppression effect is from one to two weeks for clean tungsten electrodes. Electron-microscope and field-emission-microscope studies of the conditions under which cathode and anode protrusions are formed have been started.

6. Space Science

Maximum-allowable spin rates for gyro-rotor materials are being experimentally determined, beginning with ordinary glasses. The frequency of observation opportunities for the satellite gyro is being calculated via simulation on the CDC-1604 computer. The studies of gas drag are being extended to include the effects of nonuniform heating and orbital regression. New nondegenerate mirror configurations have been devised. The connection between photographic observability and accuracy is being explored by means of optical-analog simulation and computer simulation. Terminal work on the ionosphere program is reported.

7. PLATO

The Control-Data-Corporation gift of a 1604 computer, magnetic-tape system, and line printer was installed in May. The computer is for the sole use of the PLATO group. Improvements in the PLATO hardware for the visual presentation

of material are being implemented. Audio-storage circuitry and equipment for frame-by-frame generation of 16-mm motion-picture sequences are under development. In the spring semester, students completed the PLATO versions of two university credit courses (EE 322 and LIB SCI 195). Comparisons were made in the PLATO portion of the EE 322 course between two types of instructional presentation, inquiry and tutorial. An on-line interpretative compiler for the FORTRAN-programming course has been written. Data from the ARITHDRILL program for low-achieving students gave clear evidence of performance improvement. The SIRA project developed several new PLATO programs in its efforts toward a general fact-retrieval system for the use of authors who are modifying and analyzing lessons. A basic contradiction has been removed in the GIN-1 program developed for the group-interaction studies. Behavioral-science research continues in the learning and retention of verbal materials, propositional control of behavior, satiation of semantic features, animation of abstract visual forms, and pattern-handling capability. Preliminary work necessary for instructional programming in French has been completed. The PLATO system manual has now been distributed on a limited basis to current users for their reactions and suggestions for subsequent revisions.

8. Computer Systems and Applications

The display system is within about a month of initial checkout, and the new 1604 programming system is now in use on an experimental basis. Two special purpose instruments have been completed. One of these, a digital system, processes data from a polarity-coincidence detector used in plasma experiments. The second is a servo system to provide capstan-driving power for the SMP 70-mm-film projection system. Operating statistics for the CSX-1 and the laboratory-owned 1604 are included in this report.

9. Plasma Display

Experiments with a small array have shown that not only can characters be successfully written, retained, and erased, but that the electrical characteristics of the cells are uniform within 5%. The influence of parameter variations on required electrical signals is discussed, spectral measurements of the emitted light are reported, and measurements showing the existence of two stable "on" states are described.

10. Infrared Converter

A new solid-state device utilizing tunneling is proposed for the conversion of infrared to visible light. The results of initial experiments proving the soundness of the device are given. Related to the future fabrication of these devices, procedures for making semiconducting thin films have been tried.

11. Information Science

Significant progress has been made in the algebraic theory of cyclic codes, codes for compound channels, and digital addressing. A new program is initiated in information-retrieval systems. An experimental retrieval system based on citations is being implemented. Results on key-to-address transformations are reported. Also reported are results relating to the connection assignment problem of diagnosable systems.

12. Networks

In the study of linear graphs a new and simpler method has been found for generating all trees of a linear graph by a digital computer. A study of

system reliability has been completed. Also, new results are reported on switching functions and the finding of a minimum feedback cutset with less than four edges. A new proof is given for the existence of a Hamilton circuit in a tree graph. Work on the problems of frequency entrainment and the stability of nonlinear circuits with periodic inputs has been completed. Some results are reported on the occurrence of subharmonic oscillations in parametric circuits. Problems that arise in the stability of distributed systems are also discussed.

13. Control Systems

Several results were obtained in the continuing projects involving parameter-variation effects (sensitivity), stability, and optimal control. Some extensions of sensitivity analysis to nonlinear systems were obtained. Investigation is continuing on connections between optimal and low-sensitivity systems. New insight into the class of perturbations involved in the proof of the Maximum Principle has been achieved. Some related results between controllability and optimality have been explored.

14. Structural System Design

Two studies on the application of system and computer-aided techniques to structural design are described.

15. Switching Systems

Further progress is reported in the generation of test procedures for combinational and sequential networks, the modular decomposition of sequential machines using graph-theoretic methods, and the realization of sequential machines as quasi-linear machines. New investigations which have been started

include a study of the properties of ternary switching circuits, and the design of an error-detecting arithmetic unit. A final report on the algebraic generation and active-network realization of state equations is given.

COORDINATED SCIENCE LABORATORY PERSONNEL

Faculty, Research Associates, and Research Engineers

Compton, W. Dale, Director
Alpert, D.
Anderson, R.
Ash, R.
Barrows, J.
Bitzer, D. L.
Böhmer, H.
Bouknight, W. J.
Brown, R. M.
Chien, R.
Cooper, D. H.
Cruz, J. B., Jr.
Culton, J. W.
Easley, J. A., Jr.
Fenves, S.
Golden, W.
Gooch, J.
Hastings, J. T.
Hicks, B.
Hohn, F.
Huggins, R.
Ichikawa, Y.
Kasami, T.
Killian, T. J.
Kirkwood, B. D.
Knoebel, H. W.
Krone, H. V.
Lee, D. A.
Lyman, E. M.
Lyman, E. R.
Mayeda, W.
Metze, G.
Montague, W. E.
Peacock, R. N.
Perkins, W.
Preparata, F.
Propst, F. M.
Prothe, W. C.
Asst. to Director
Raether, M.
Ray, J.
Resh, J.
Satterthwaite, C. B.
Schuemann, W. C.
Secrest, M.
Skaperdas, D.
Slottow, H. G.
Smith, M.
Sobral, M.
Stake, R.
Steinrisser, F.
Stifle, J.
Trick, T.
Trogdon, R.
Tulumello, A.
Van Valkenburg, M. E.
Voth, B.
Wax, N.
Wu, Y.
Yen, S.

Research Assistants

Anderson, W.
Arndt, G.
Arora, B.
Agashe, S.
Aubuchon, K.
Bahl, L.
Balasaygun, O.
Bleha, W.
Bollinger, L. D.
Bourquin, J.
Carlson, J.
Carr, W.
Chang, J.
Chang, S. C.
Chow, D.
Cooper, T.
Craford, M.
Crockett, E. D.
Cummings, J.
Davies, M.
Depp, S.
duPreez, R. J.
Edwards, D.
Fillman, L.
Gaddess, T.
Gutman, D.
Hartmann, C.
Hosken, R.
Hsu, H. T.
Hsu, J.
Hyatt, W.
Jacobs, J. T.
Jenks, R.
Kamae, T.
Karr, G. R.
Kraatz, J.
Lie, T.
Lum, V.
Marlett, R.
Martens, G.
Marzullo, E.
Mehta, N.
Mendel, C.
Metze, V.
Meyer, J. S.
Minning, L.
Moore, B. K.
Morrison, H.
Murata, T.
Myers, J. L., Jr.
Nishijima, M.
Piper, T.
Reddy, D.
Robinson, J.
Rubovits, J.
Rust, R. D.
Salmon, D.
Schneider, R.
Schoenberger, M.
Schusterman, L.
Tibbetts, G.
Toepke, I.
Toida, S.
Tzeng, K.
Wearing, A.
Willson, R. H.
Wolterbeek, H.

Fellows

Herner, J. P.
Hoyt, R.

Secretaries

Rudicil, J.
Schmidt, R.

Typists and Stenos

Brigham, M.
Butterworth, T.
Curtis, J.
Dewar, V.
Hanoka, N.
Harris, M.
Keel, D.
Lane, R.
Siler, J.
Shaw, C.

Chief Clerk

Drews, C. E.

Accounting Clerk

Potter, R. E.

Draftsmen

Conway, E.
Hollinger, B.
MacFarlane, R. F.

Stumpff, G.
Tracey, R.

Res. Lab. Shop Supr.

Bandy, L. E.

Instrument Makers

Beaulin, W. E.
Bouck, G.
Merritt, K. E.
Zackery, R. L.

Laboratory Mechanics

Bales, R. B.
Burr, J. G.

Storekeepers

Jordan, F.
Lofton, C.
McElwain, W.

Glassblower

Lawrence, W.

Photographer

Fairchild, J.

Werner, R.
Powell, T.

Electronics Engr. Asst.

Carter, E. N.
Gardner, O. E.
Hedges, L.
Neff, E. H.
Vassos, N.

Electronics Technicians

Casale, T. C.
Coad, D. E.
Crawford, G.
Deschene, D. R.
Holy, F. O.
Johnson, M.
Jordan, H.
Knoke, J. H.
Merrifield, F.
Moule, G.
Roberts, G. R.
Schmidt, W.
Streff, L. W.
Susedik, A. J.
Turpin, F. G.

Phys. Sci. Staff Asst.

Thrasher, W.

Student Assistants

Arnold, C.
Babirak, M.
Baltaxe, J.
Balzer, J.
Barkley, N.
Bernhard, W.
Birtcher, R.
Borris, J.
Bullard, C.
Bunting, M.
Butler, S.
Corcoran, J. P.
Daily, J.
Eickert, D.
Everhart, G.
Fancher, D.
Groene, P
Haider, S. G.
Hodges, M.
Holshouser, J.
Hughes, J.
Kulwin, D.
Nanninga, J.
Norton, J.
O'Meara, T.
Panza, K.
Pinsky, H.
Reilly, O.
Ries, R.
Roberts, D.
Rundgren, W.
Samson, C.
Scharf, R.
Smith, S.
Steinberg, L.
Stozek, R.
Sutton, C.
Trombi, P.
Tucker, P.
Walker, M.
Walsh, F.
Williams, R.
Zapatero, G.

PUBLICATIONS AND REPORTS

1. Journal Articles Published or Accepted

D. L. Bitzer, B. L. Hicks, R. L. Johnson, and E. R. Lyman, "The PLATO System: Current Research and Developments," IEEE Transactions HFEG (to appear).

Maryann Bitzer, "Clinical Nursing Instruction Via the PLATO Simulated Laboratory," Nursing Research, 15-2, Spring, 1966.

H. Böhmer and M. Raether, "Incoherent Scattering of Microwaves by Unstable Electron Plasma Oscillations," Phys. Rev. Letters 16, 1145, 1966.

R. T. Chien and V. Lum, "On Golay's Perfect Codes and Step-by-Step Decoding," IEEE Transactions on Information Theory, IT-12, 403.

D. H. Cooper, "Estimation of Fluorescent Decay Times," Rev. Sci. Instr. 37 (in press), Oct. 1966.

D. H. Cooper, "Nonlinear Telegrapher's Equation: Solution and Fourier Analysis," Proc. IEE 113, 1171, 1966.

Y. Ichikawa, "Ion-Oscillations in a Weakly Turbulent Plasma," to be published in Phys. Fluids, August 1966.

E. A. Jackson and M. Raether, "Landau Damping in Inhomogeneous Plasmas," Phys. Fluids 9, 1257, 1966.

R. L. Johnson, "Using the PLATO Teaching System for Computer-Based Instruction in Electrical Engineering," International Journal of Electrical Engineering Education (to appear) Jan. 1967.

T. Kasami, "A Note of Computing Time for Recognition of Languages Generated by Linear Grammars," to appear in Information and Control.

T. J. Lie and Y. Ichikawa, "Thermodynamic Properties of an Electron Plasma," to be published in Rev. Mod. Phys., October 1966.

W. Mayeda, "A Method of Generating Trees and Complete Trees," Denki-Tsushin-Gakuka (Japan), No. 95-7, May 1966 (Japanese).

W. R. Perkins and J. B. Cruz, Jr., "Sensitivity Operators for Linear Time-Varying Systems," Sensitivity Methods in Control Theory, ed. by L. Radanovic, Pergamon Press, pp. 67-77, 1966.

F. P. Preparata, "Convolutional Transformations of Binary Sequences: Boolean Functions and their Resynchronizing Properties," the IEEE Transactions on Electronic Computers (to appear).

J. A. Resh, "A Note Concerning the n-Port Passivity Condition," IEEE Transactions on Circuit Theory, CT-13, 238, June, 1966.

S. Toida, "Some Relationships Among Switching Functions in a Contact Network," IEEE Transactions on Circuit Theory, CT-13, December 1966 (to appear).

T. N. Trick and J. A. Resh, "Transducer Power Gain in Optimally Matched Networks," IEEE Transactions on Circuit Theory, CT-13, December 1966 (to appear).

N. Wax, "On Some Periodic Solutions of the Lienard Equation," IEEE Transactions on Circuit Theory, CT-13, December 1966 (to appear).

2. Meeting Papers

D. L. Bitzer, "Computers in Education" (panel discussion) American Ass'n of Junior Colleges, St. Louis, March 3, 1966.

D. L. Bitzer, "The Use of a Remote Console in Programmed Teaching by Computer," Clinic on Library Applications of Data Processing, Urbana, April 25, 1966.

D. L. Bitzer, "On-Line Computing" (panel discussion) Western Electronic Show and Convention, Los Angeles, August 25, 1966.

D. H. Cooper, "Bessel's Solution for a Two-Tone Finite-Amplitude Source," Meeting of the Acoustical Society of America, Los Angeles, Nov. 3, 1966.

J. A. Easley, Jr. "The Natural Sciences and Educational Research - A Comparison," Annual Spring Conference, State University College, Brockport, N. Y., April 29, 1966.

T. Kasami, S. Lin and W. W. Peterson, "Some Results on Weight Distributions of BCH Codes" presented at the 1966 International Symposium on Information Theory, Los Angeles, California.

E. R. Lyman, "PLATO/CATO," ONR Conference on CAI Languages, Cambridge, Mass., March 2, 1966.

E. R. Lyman, "The PLATO System," USNA Workshop on Computer-Assisted Instruction, Annapolis, August 10, 1966.

G. Metze and S. Seshu, "A Proposal for a Computer Compiler," Spring Joint Computer Conference, Boston, April, 1966.

T. Murata, "Network Topology and Stability of Nonlinear RLC Networks," Fourth Annual Allerton Conference on Circuit and System Theory, October, 1966.

W. W. Peterson and T. Kasami, "Reliability Bounds for Polyphase Codes for the Gaussian Channel" presented at the 1966 International Symposium on Information Theory, Los Angeles, California.

J. A. Resh, "Introduction and Analysis of a Model for Censored Communication," Ninth Midwest Symposium on Circuit Theory, May, 1966.

J. A. Resh, "Signal Processing by Passive Linear Networks," Fourth Annual Allerton Conference on Circuit and System Theory, October, 1966.

T. N. Trick, "Stability of Nonlinear Circuits with Periodic Inputs," Proceeding of the National Electronics Conference, Vol. 22, October, 1966.

T. N. Trick, "Subharmonic Oscillations in Parametric Circuits," Fourth Annual Allerton Conference on Circuit and System Theory, October, 1966.

3. Technical Reports

R-257 An Efficient Recognition and Syntax-Analysis Algorithm for Context-Free Languages, T. Kasami (March, 1966).

R-281 A Theorem on the Minimum Distance of BCH Codes over GF(q), Vincent Lum (March, 1966).

R-282 An Improvement in the State Azioms, James A. Resh (March, 1966).

R-283 Convolutional Transformations of Binary Sequences: Boolean Functions and Their Resynchronizing Properties, Franco P. Preparata (March, 1966).

R-284 Generation of Trees and Complete Trees, Wataru Mayeda (April, 1966).

R-285 Weight Distribution Formula for Some Class of Cyclic Codes, Tadao Kasami (April, 1966).

R-286 FINAL REPORT: Theoretical and Experimental Studies of the Underlying Processes and Techniques of Low Pressure Measurement (April, 1966).

R-287 A Note on Computing Time for Recognition of Languages Generated by Linear Grammars, Tadao Kasami (April, 1966).

R-288 The Absolute Stability of Systems with Multiple Nonlinearities, Michael S. Davies (May, 1966).

R-289 Investigation of Dense Plasma under a Strong Electric Field, Clifford W. Mendel, Jr. (May, 1966).

R-290 Quadratic Differential Systems for Mathematical Models, Richard D. Jenks (May, 1966).

R-291 A Topological Approach to the Stability of Time-Varying and Nonlinear Networks, Tadao Murata (May, 1966).

R-292 On the Generation of Diagnostic Test Procedures, Wendel J. Bouknight (May, 1966).

R-293 On the Design and Testing on Self-Diagnosable Computers, Ralph A. Marlett (July, 1966).

R-294 Algebraic Generation and Active Network Realization of State Equations, G. O. Martens (May, 1966).

R-295 Aerodynamic Torque on a Spinning Spherical Satellite with Application to Measurement of Accommodation Coefficient, Gerald R. Karr (May, 1966).

R-296 A Descriptive List of PLATO Programs, 1960-1966, Elisabeth R. Lyman (June, 1966).

R-297 The Use of Programmed Learning and Computer-Based Instruction Techniques to Teach Electrical-Engineering Network Analysis, Roger L. Johnson (July, 1966).

R-298 Parametric Effects of Radiation on a Plasma, E. A. Jackson (June, 1966).

R-299 An Evaluation of a Bakeout Procedure for Small Glass Ultrahigh Vacuum Systems, F. Steinrisser (June, 1966).

R-300 A Study of System Reliability Using Topological Methods, Glenn H. Stumpff (August, 1966).

R-301 Nonlinear Programming and Multiparameter Sensitivity in Linear Time-Invariant Networks, Gerry L. Kelly (June, 1966).

R-302 Pumping Speed of Getter-Ion Pumps at Low Pressures, Andras Dallos and Fortunat Steinrisser (June, 1966).

R-303 A Capacitively-Coupled Bistable Gas Discharge Cell for Computer-Controlled Displays, Robert H. Willson (June, 1966).

R-304 A Study at High Energy Resolution and at Low Primary Energies of the Secondary-Electron Emission from (100) Tungsten, Thomas C. Piper (July, 1966).

R-305 Covariant Noether Identities in Covariant Field Theories, John R. Ray (July, 1966).

R-306 On Bose-Chaudhuri-Hocquenghem Codes over GF(q), Vincent Lum (July, 1966).

PUBLICATIONS

R-307 Monte-Carlo Evaluation of the Boltzmann Collision Integral, A. Nordsieck and Bruce Hicks (July, 1966).

R-308 On the Accuracy of Approximate Solutions of the Boltzmann Equation, S. M. Yen, Bruce L. Hicks (July, 1966).

R-309 The Effects of the Nodal Regression of the Orbit on the Gravity-Gradient Precession of a Gyroscopic Satellite, James L. Myers, Jr. (July, 1966).

R-310 A Study of Hazards in Ternary Switching Circuits, Louis Abecassis (August, 1966).

R-312 Control-System Synthesis to Minimize Multiparameter Sensitivity, Richard L. Gonzales (August, 1966).

R-317 Weight Distributions of Bose-Chandhuri-Hocquenghem Codes, T. Kasami (August, 1966).

1. SURFACE PHYSICS

F. M. Propst
F. Steinrisser
T. L. Cooper
D. Edwards
M. Nishijima
T. C. Piper
G. C. Tibbetts

1.1 Electron Spectrometry of Solid Surfaces

The electron spectrometer described in previous progress reports has proved to be capable of detecting the vibrational states of specific gas-surface systems.

Figures 1.1-1.5 show the energy distributions of electrons from the (100) surface of tungsten after exposure to various gases. The energy of the incident electrons and the gas species and exposure are indicated on the figures. The exposure indicated for each curve is the product of the uncorrected ion-gauge reading and the exposure time. The ordinate in these curves is the primary energy, E_p, minus the secondary energy, E_s, and is thus equal to the energy an incident electron loses in a scattering event. The very strong elastic peak (100 times as strong as the structure shown in the figure) is centered at $E_p - E_s = 0$.

The tungsten sample is in the form of a ribbon (.003 in. thick), which was cut from an ingot by the spark erosion process.[1] Prior to these measurements, the sample was heated for 100 hours at 1800°K, heated for 10 hours at 2200°K, flashed to 2400°K for a total of 3 hours, and heated to 1300°K in the presence of 5×10^{-7} Torr of oxygen for 30 minutes. Before each measurement, the target was flashed several times to 2400°K for several seconds. It is felt that this treatment produced a clean tungsten surface; however, the vacuum system is

[1] G. G. Tibbetts and F. M. Propst, Rev. Sci. Instr. 34, 1268 (1963).

pumped by an oil diffusion pump (DC-705 pumping fluid), and it is possible that slight carbon or silicon deposits may exist on the surface.

Figure 1.1 shows the distribution obtained after exposing the cleaned target to H_2. There are two peaks in the distribution (135 and 69 meV), which increase with exposure at the same relative rates. The curve for 4×10^{-6} Torr-sec exposure represents approximately saturation; longer exposures producing little change.

The two peaks may be associated with the vibrations of the hydrogen atom, normal and parallel to the surface. To the first approximation, one would expect

$$\omega_p/\omega_n = \sqrt{(E_{diff}/E_{des})},$$

where ω_p and ω_n are the parallel and normal frequencies respectively, and E_{diff} and E_{des}, the energies of diffusion and desorption respectively. Substituting the measured frequencies, we find

$$E_{des} = 3.8\ E_{diff}.$$

This is in reasonable agreement with the value of 4.5 given by Gomer.[2] This approximation neglects the greater anharmonicity present in the parallel potential and assumes equal range for the parallel and normal potentials.

The lack of any frequencies above 135 meV agrees with the observations that hydrogen dissociates upon adsorption. The energy of interaction between the hydrogen atoms after adsorption is probably not appreciably greater than 0.5 eV.

Figure 1.2 shows the spectrum for (100) W exposed to N_2. This spectrum shows a single peak at 67 meV, which is probably the normal vibration of the N-W

---

[2] R. Gomer, R. Wortman, and R. Lundy, J. Chem. Phys. 26, 1147 (1957).

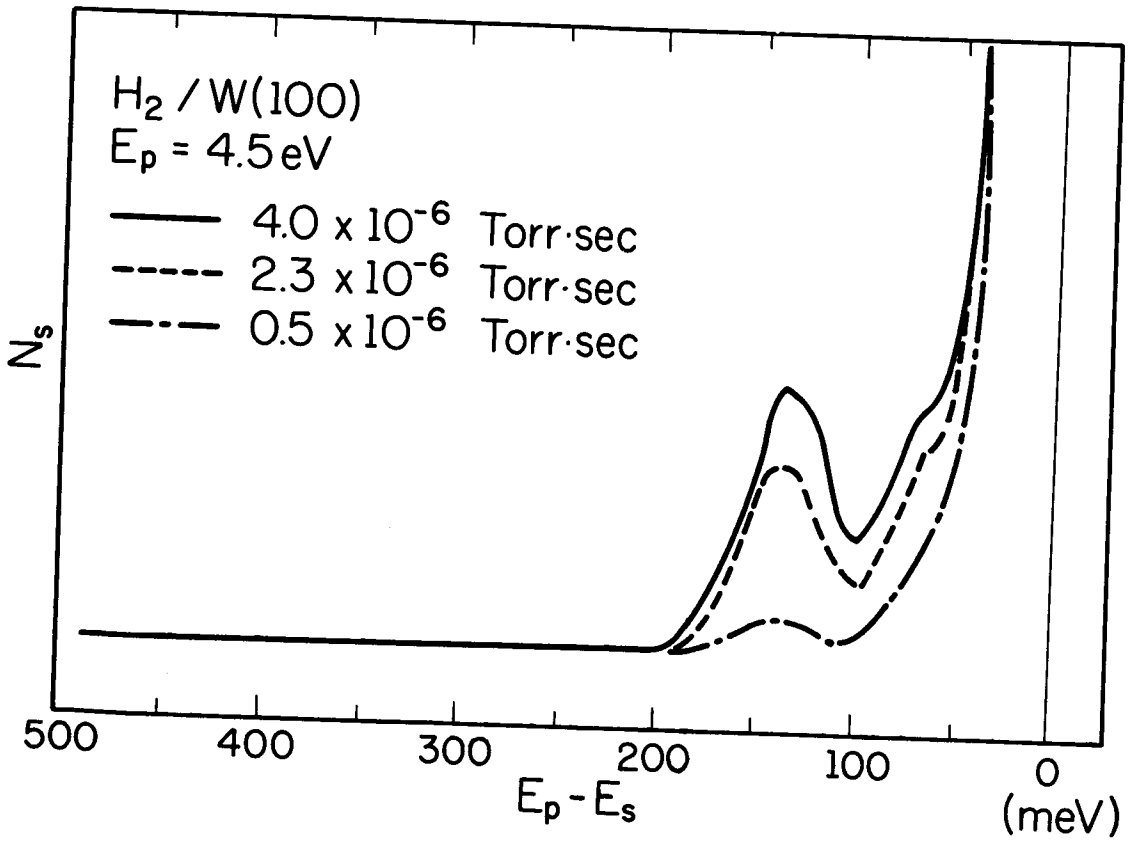

Fig. 1.1. Energy distribution of electrons scattered from 100 W after exposure to H_2.

(OVERLEAF BLANK)

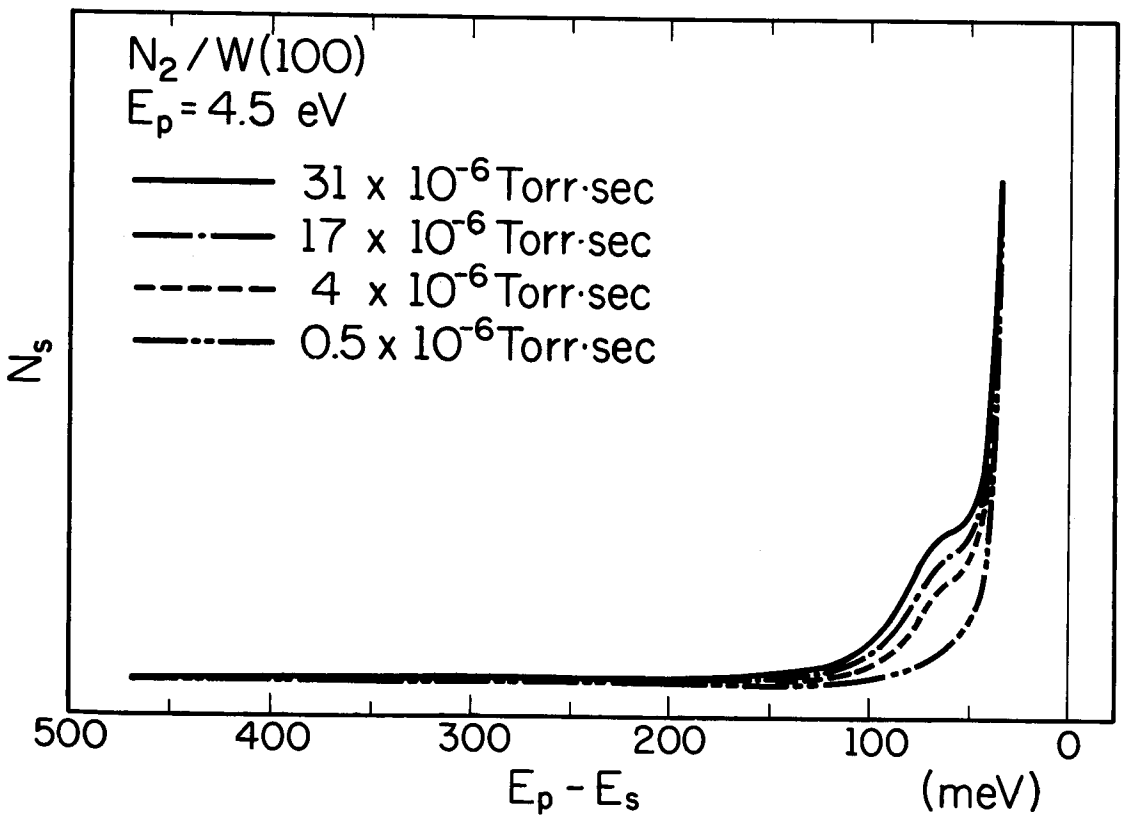

Fig. 1.2. Energy distribution of electrons scattered from 100 W after exposure to N_2.

(OVERLEAF BLANK)

system. As is the case of hydrogen, the lack of higher energy lines implies almost complete dissociation of the nitrogen molecules.

Figure 1.3 shows the spectrum for the surface exposed to H_2O. There are peaks at 77 and 425 meV. The 425 meV-line is a reasonable value for the O-H stretching vibration, and the 77-meV line is probably the normal vibration of the O-W system. The peak at 425 meV does not appear until the 77-meV peak is almost saturated. In Fig. 1.3, the 425-meV peak is not present for an exposure of 5.5 $\times 10^{-6}$ Torr sec, whereas the 77-meV peak is approximately two thirds its saturated height after this exposure. One concludes that in the initial stage of adsorption, the water vapor causes oxidation of the tungsten with dissociation of the hydrogen-oxygen bonds. After approximately a monolayer of oxidation is completed, some overlayer adsorption occurs, preserving at least one of the O-H bonds.

Figure 1.4 shows the distribution for the tungsten exposed to CO. There are two peaks (72 and 258 meV) which are clearly present in these curves. There is also possibly a peak at 135 meV which is not present at low or high coverages, but present only at intermediate coverage. The peak at 258 meV does not appear until the 72-meV peak is saturated. In addition, the intensity of the 258-meV peak is approximately proportional to the CO pressure and disappears when the CO is removed from the system. This 258-meV energy is quite close to the energy of the first vibrational level of free CO (270 meV). This peak is probably due to the weakly-bound α state of adsorbed CO.[3] Due to the heat of the cathode, the sample is somewhat hotter than room temperature (70°C). At these temperatures, the α state completely desorbs; thus, the 258-meV peak is due to the equilibrium coverage in the α state at the ambient pressure. Another interesting conclusion

[3] G. Ehrlich, J. Chem. Phys. 34, 39 (1961).

which can be drawn from these results is that the CO initially adsorbed must be essentially dissociated. The fact that there are no peaks at energies greater than 72 meV for the stably-adsorbed layer implies that the energy of interaction between the carbon and oxygen atoms in the adsorbed phase must be less than about 1 eV. This strongly implies that both the carbon and oxygen atoms are in intimate association with the tungsten surface. This agrees with the conclusions of Madey and Yates,[4] based on the results of isotopic-exchange experiments.

In all of these spectra, the lines which are ascribed to gas-surface bonds are at lower energies than would be expected on the basis of single bonding and the binding energies which have been reported for these gases. Thus, it appears that, in addition to the dissociation of H_2, N_2, H_2O, and CO in the initial stages of adsorption, the H, O, N, and C atoms are held to the surface by multiple bonding.[5]

Finally, Fig. 1.5 shows the distribution obtained after exposing the target to both H_2 and N_2, with the ionization gauge operating during the exposure. This structure does not appear unless the gauge is operating. When the target is exposed to N_2 after exposure to H_2 (gauge off), the hydrogen distribution (Fig. 1.1) disappears and a structure very similar to that of Fig. 1.2 (nitrogen) appears. This indicates replacement of the hydrogen by nitrogen. When the target is exposed to H_2 after exposure to N_2 (again with the gauge off) no changes occur. Thus, the structure of Fig. 1.6 represents an activated reaction. The peak at 404 meV is in good agreement with the energy of singly bonded H-N stretching vibrations and the peak at 174 meV is a typical bending vibration of this bond.

---

[4] T. E. Madey, J. T. Yates, and R. L. Stern, J. Chem. Phys. 42, 1372 (1965).

[5] R. P. Eischens and W. A. Pliskin, Adv. in Catal. X, 1 (1958).

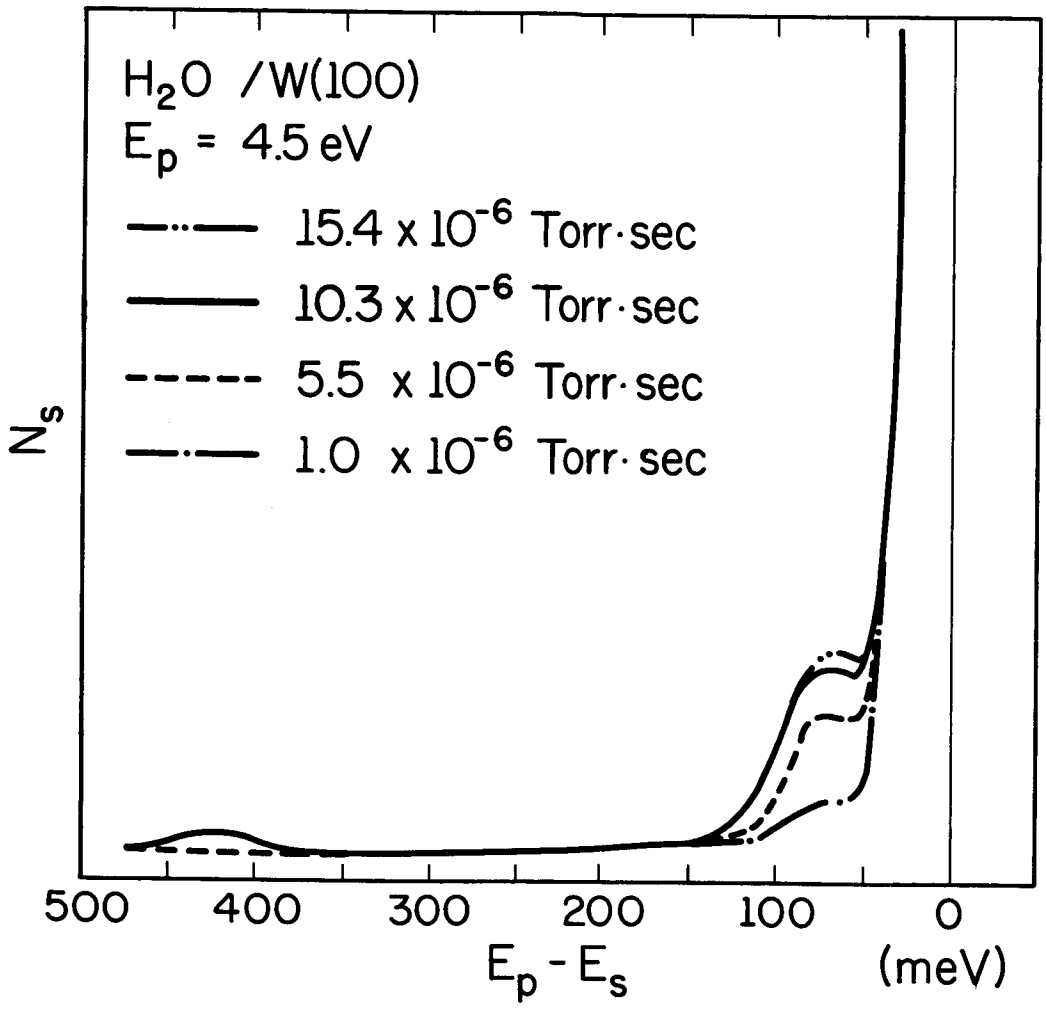

Fig. 1.3. Energy distribution of electrons scattered from 100 W after exposure to H_2O.

(OVERLEAF BLANK)

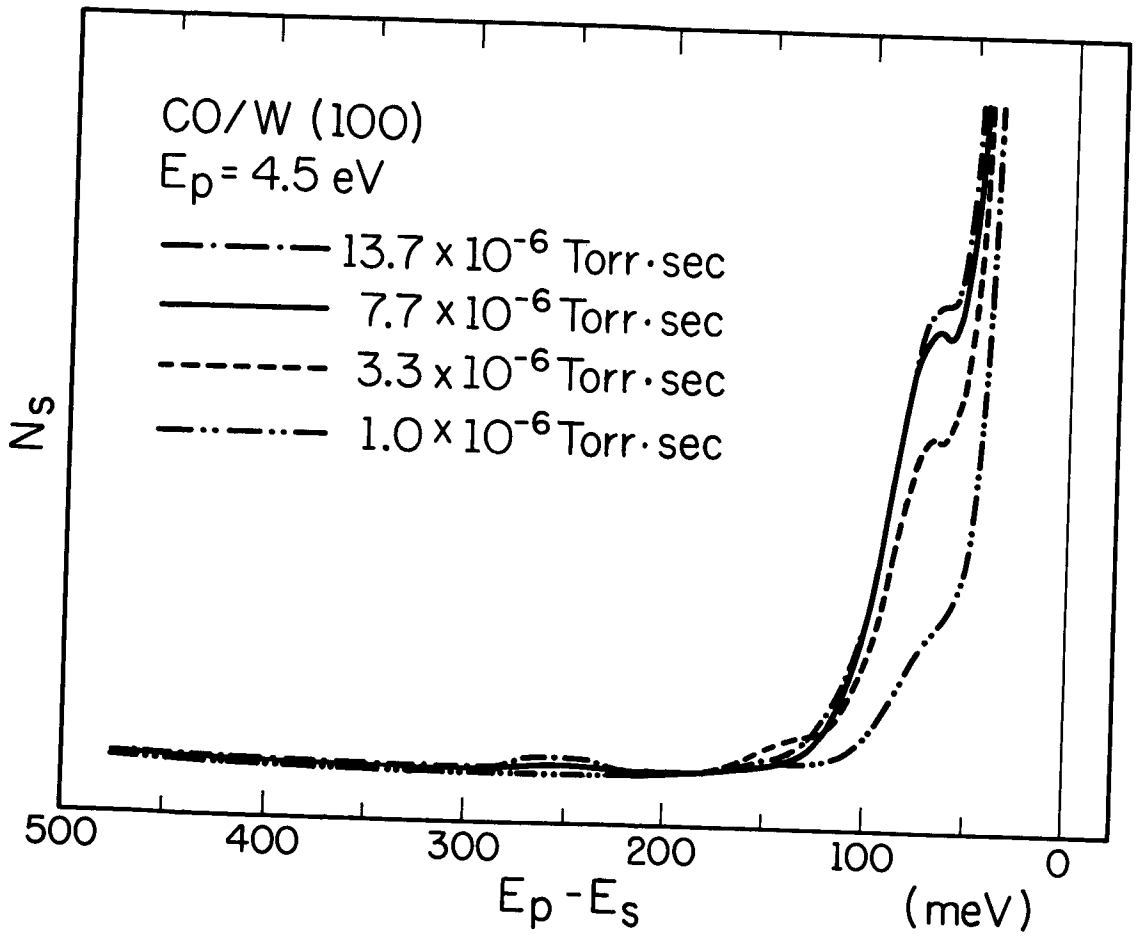

Fig. 1.4. Energy distribution of electrons scattered from 100 W after exposure to CO.

(OVERLEAF BLANK)

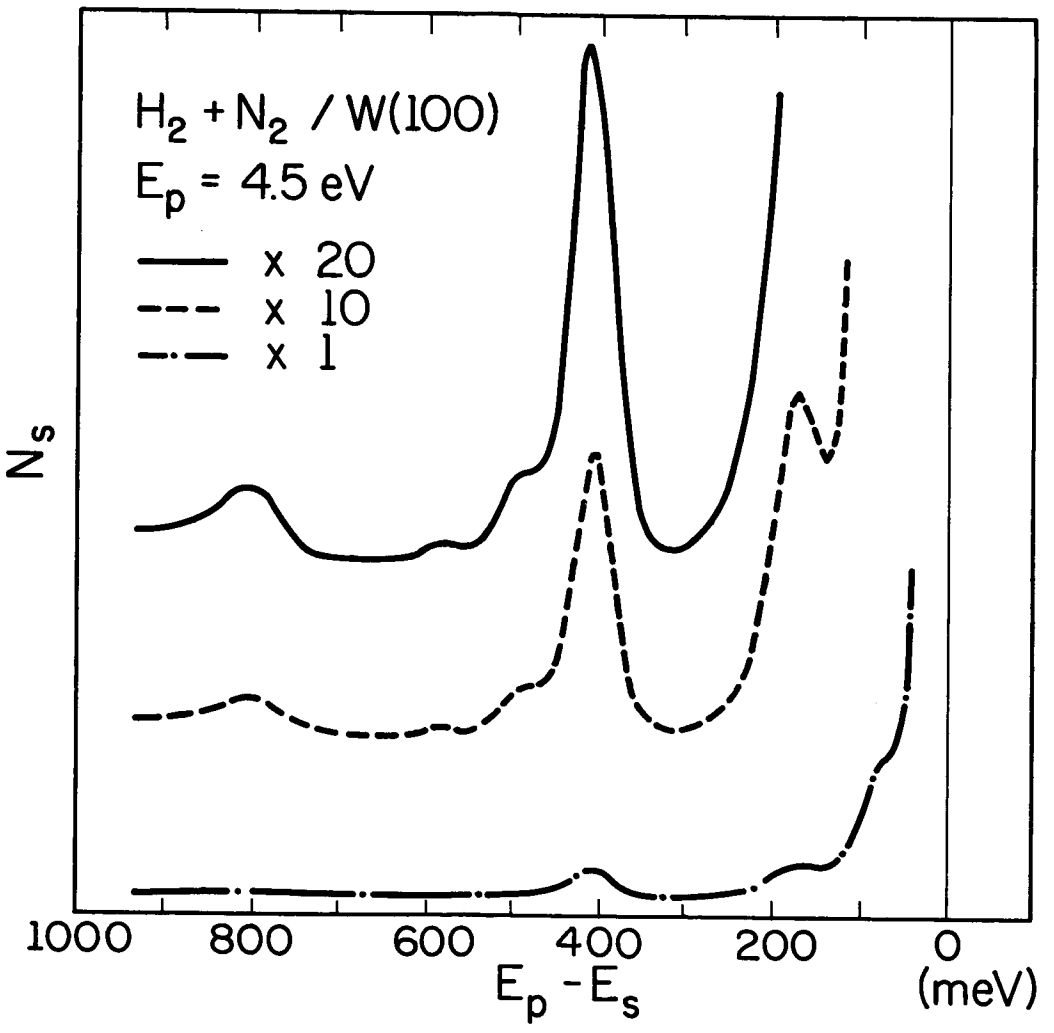

Fig. 1.5. Energy distribution of electrons scattered from 100 W after exposure to H_2 and N_2.

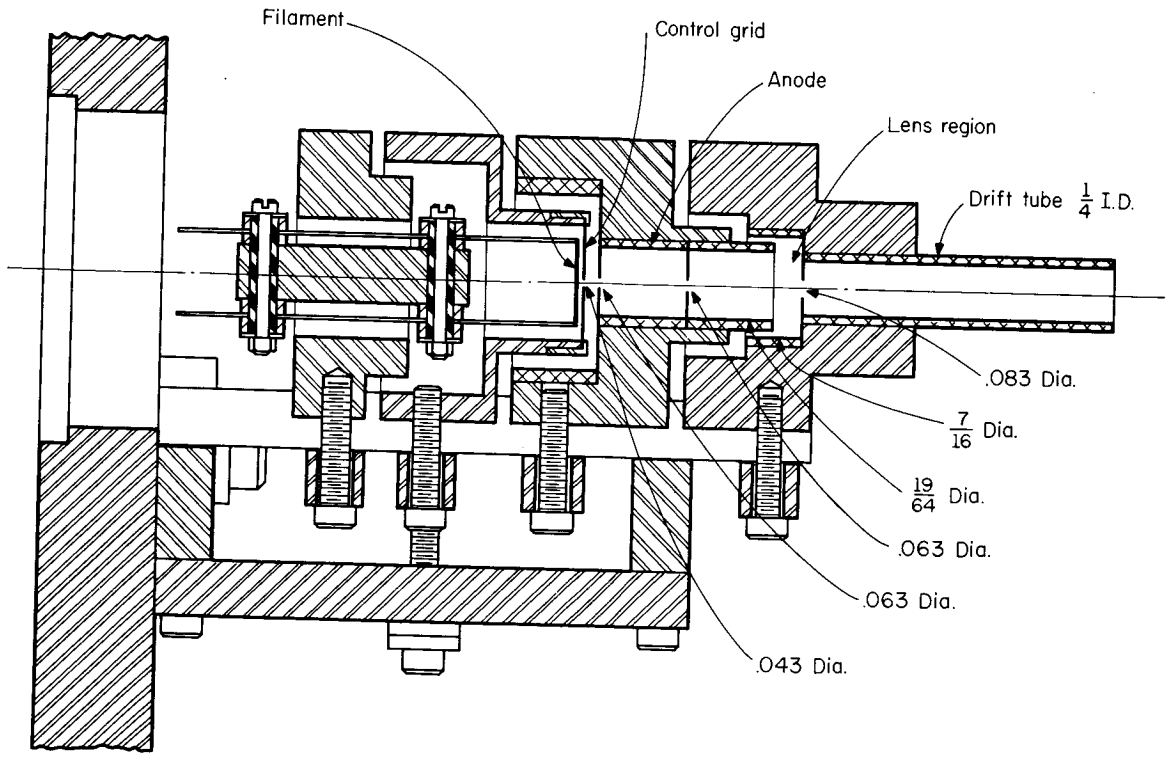

Fig. 1.6 Electron gun.

(OVERLEAF BLANK)

It cannot be definitely stated whether this structure is due to the formation of a hydrogen-nitrogen complex in the gauge which subsequently adsorbs at the sample surface, or is due to production of activated hydrogen in the gauge which then adsorbs on the nitrogen-covered tungsten; however, it is felt that the second process is more likely.

Figure 1.5 also illustrates two other interesting results. First, the excitation of harmonics: The peak at 806 meV is the first harmonic of the 404-meV peak. Other distributions have shown as many as five harmonics at high coverage. Secondly, combination frequencies are excited: There are peaks at 489 and 582 meV. These peaks represent the simultaneous excitation of the 404-meV and the 81- and 174-meV vibrations respectively.

In summary, this work has demonstrated that the vibrational structure of gases adsorbed at solid surfaces can be observed by low-energy electron scattering. We have shown that the spectra of specific gases have been observed, and have discussed some of the interesting but tentative conclusions which can be drawn from these spectra. This technique should find immediate application in the study of catalytic reactions and chemical structures at solid surfaces.

1.2 Angular Distribution of Secondary Electrons

During the past few months, each of four major components of this experiment has been tested and the necessary design modifications made.

1.2.1 Target Assembly. In order to perform a surface experiment, it is necessary to produce a clean surface. For this experiment, cleaning will be accomplished by electron-bombardment heating. A tungsten target was heated with the system to be used for the angular-distribution measurements. The target temperature and temperature gradient were measured with an optical pyrometer,

and it was found that heat losses due to the target clamp were too large. Modifications of the target clamp have been made which will reduce this loss significantly.

1.2.2 Electron Gun. Tests were made with various ion and electron guns. A gun design used by Peria at the University of Minnesota for low-energy electron diffraction proved to be the most successful. (See Fig. 1.6.) Tests made on a prototype of this design demonstrated its capability of producing a spot size of 1/16" diameter, and delivering a current of about 5×10^{-7} amperes up to a few microamperes over an energy range from about 15 eV to 200 eV. This performance was obtained using a voltage ratio (energy of beam in anode region to energy of beam in drift tube) of about 4 and a control-grid voltage a few volts negative with respect to the filament. The filament used for the tests was 20-mil wide and 1-mil thick thoriated-tungsten ribbon.

Inelastic scattering from the walls of the drift tube, although not important for low-energy electron diffraction, must be kept at a minimum when observing inelastic scattering as in the present work. Measurements using a drift tube, the same diameter as that of Peria's guns (1/8 inch), show that a well focused beam is made up of about 25% inelastically-scattered electrons. For this reason, a drift tube of larger diameter, possibly fitted with aperatures (not shown in Fig. 1.6), is being considered for the final design.

1.2.3 Detector Electronics. In order to test the collector and detection system, an electron source was constructed and mounted on the target clamp. The collector, source, and electronics are schematically illustrated in Fig. 1.7. The collector system is essentially a retarding-potential analyzer. Superposing a small ripple voltage ($\Delta V \sin \omega t$) on the retarding potential causes

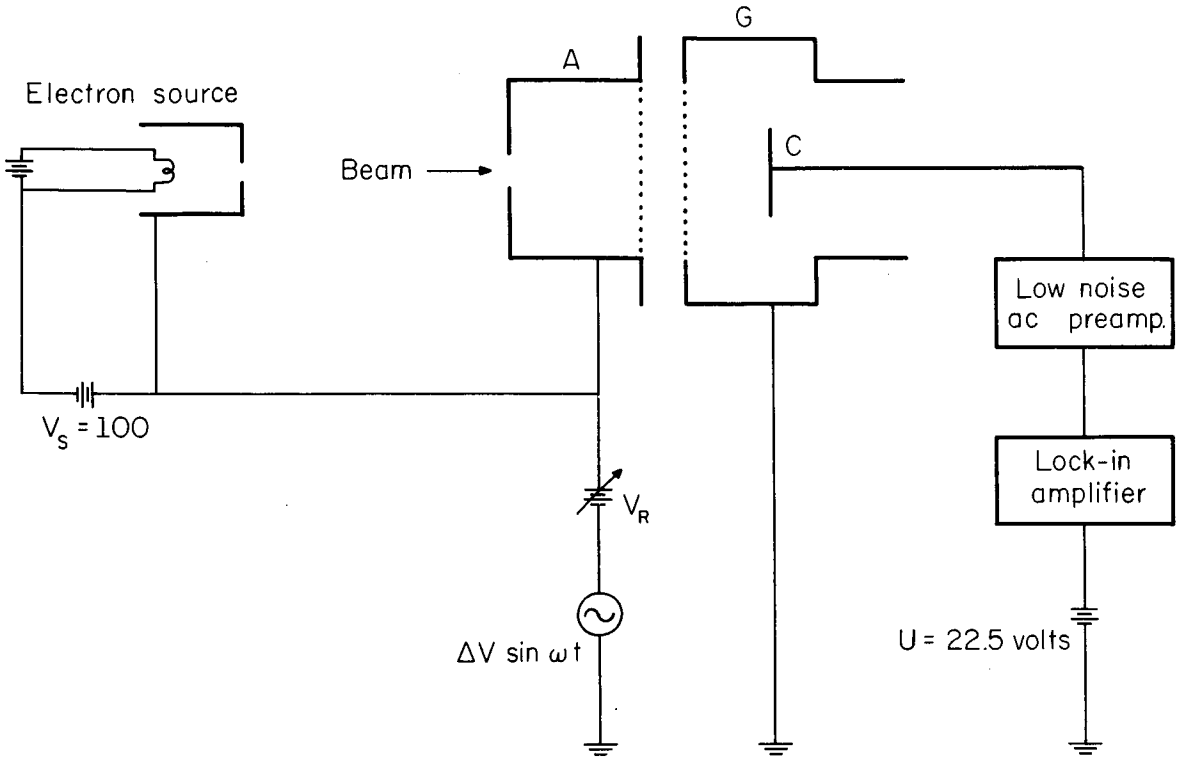

Fig. 1.7. Schematic of collector system and detection electronics.

(OVERLEAF BLANK)

the output of an ac detector (lock-in amplifier) to be proportional to the energy distribution of the incoming beam.

If the beam to be analyzed has an energy distribution dI/dE, electron current per unit energy,[6] the current arriving at the collector[7] C, neglecting the current intercepted by grids, is given by

$$I_c = \int_{eV(t)}^{\infty} (dI/dE)dE = I(\infty)-I(V_R+\Delta V\sin\omega t),$$

where $V(t) = V_R+\Delta V\sin\omega t$, $I(\infty)$ is the total beam current, and $I(V_R+\Delta V\sin\omega t)$ is the current made up of electrons with energy $E \leq (V_R+\Delta V\sin\omega t)e$, where e is the electronic charge.

If we expand in a Taylor series, we have

$$I_c = I(\infty)-I(V_R)-(dI/dE)_{V_R}\Delta V\sin\omega t+\ldots .$$

For small ΔV, we keep only the terms linear in ΔV to obtain

$$I_c \approx I(\infty)-I(V_R)-(dI/dE)_{V_R}\Delta V\sin\omega t.$$

The lock-in amplifier detects only the ac component I_{ac} within a given bandwidth around ω. This is

$$I_{ac} \approx (dI/dE)_{V_R}\Delta V\sin\omega t.$$

Since V_{out}, the lock-in amplifier output, is proportional to the rms ac component,

---

[6] Fig. 1.7 shows a source which will give a large peak around V_S, and a smaller peak at lower energies, due to inelastic scattering from the source aperature. The analysis, however, is for a general distribution.

[7] The beam current arriving at the collector is not necessarily the current collected, due to secondary scattering from the collector. This important effect will be discussed later.

it is,

$$V_{out} \propto (dI/dE)_{V_R}$$

The detection electronics appeared to operate satisfactorily. However, several problems were encountered in the collector system itself: (1) scattering from grid wires; (2) grid-charging effects; (3) changes in effective grid transparency; (4) scattering from the collector plate.

1.2.4 Collector. In order to pursue the above problems in a more straightforward manner, the ac detection electronics were replaced by an electrometer, and dc-retarding-potential measurements were made. The operation of this collector system and another similar collector system has led to the tentative ideas discussed in the following paragraphs concerning the operation of retarding-potential analyzers.

Figure 1.8(a) shows a typical energy distribution to be analyzed. Figure 1.8(b) shows the retarding-potential curve one would expect from an ideal analyzer. Figures 1.9(a) through 1.12(a) show various types of practical retarding-potential analyzers. Figures 1.9(b) through 1.12(b) schematically illustrate the features of the curves obtained when a beam with the energy distribution shown in Figure 1.8(a) is analyzed by these analyzers.

The current to the collector, for the geometry of Fig. 1.9(a) consists of the primary current minus the current due to secondary electrons leaving the collector. The net results are indicated in Fig. 1.9(b). The current decreases as the retarding potential V_R is increased from zero to about 20 volts due to the retardation of the low energy part of the incident beam distribution. The current then remains constant before beginning to increase as the retarding potential is increased. Finally, the current drops to zero as the retarding

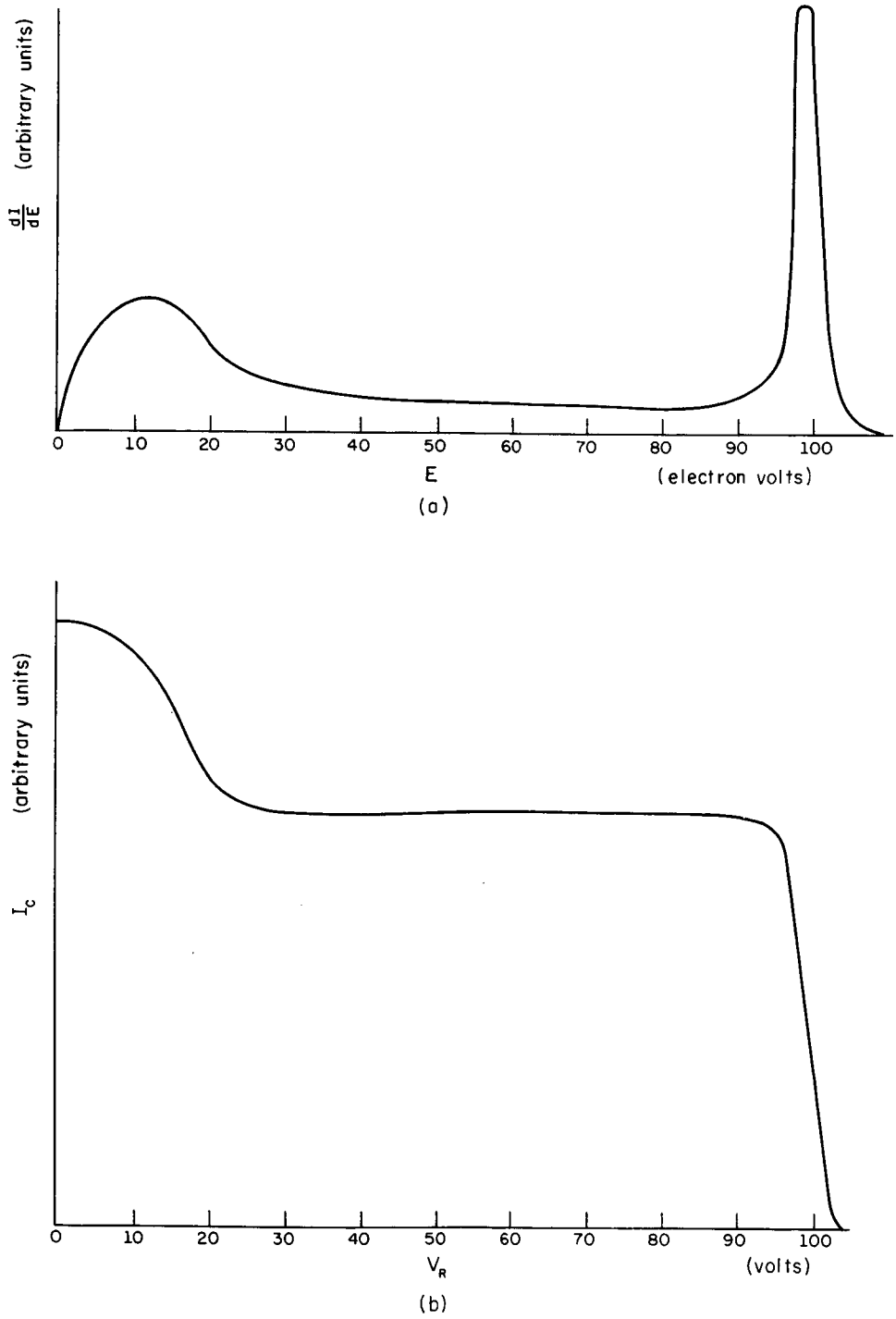

Fig. 1.8. Typical electron energy distribution and idealized retarding-potential curve. The symbols are dI/dE = current per unit energy, E = energy, I_c = collector current, V_R = retarding potential.

(OVERLEAF BLANK)

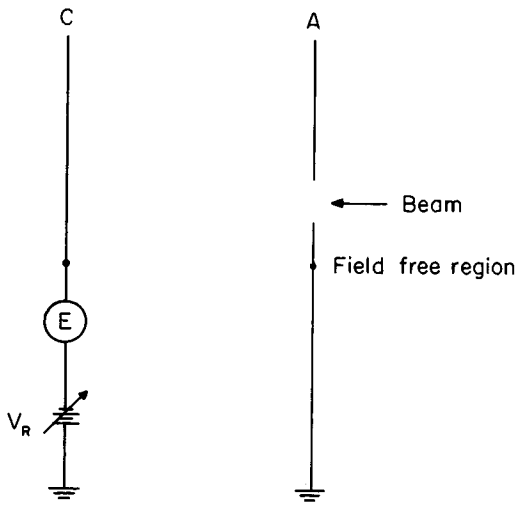

(a)

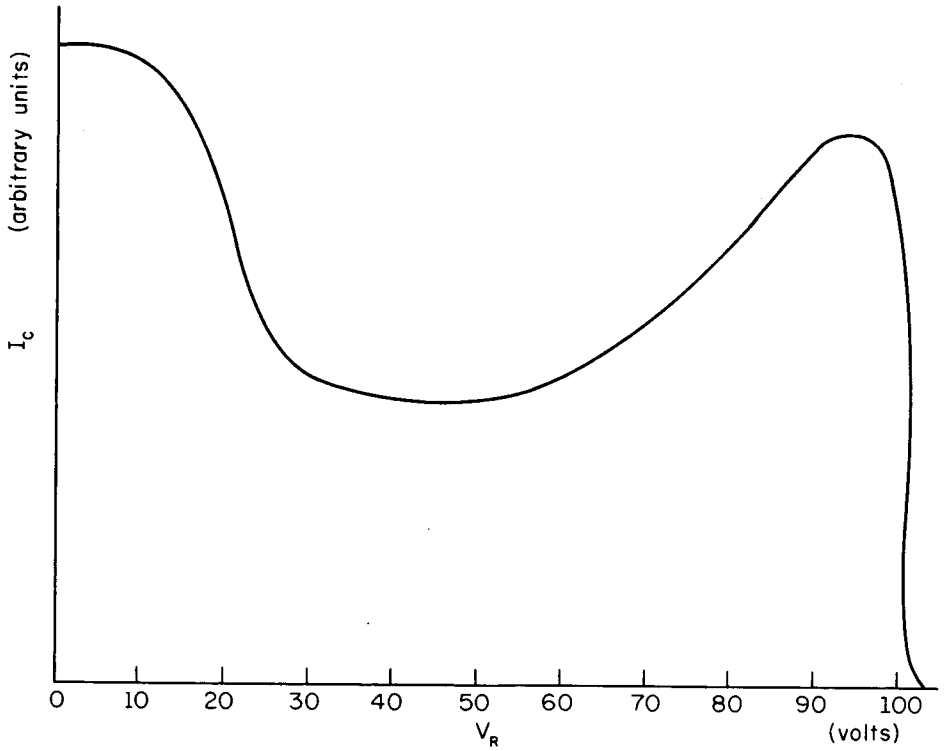

(b)

Fig. 1.9. Retarding-potential system and typical retarding-potential curve from the analysis of the distribution in Fig. 1.8(a). The symbols are C = collector plate, A = aperture, V_R = retarding potential, E = electrometer for measurement of current to collector plate.

voltage reaches the highest energy of the impinging beam (cutoff). The region of constant current is what would be expected, since most of the electrons above 20 eV have sufficient energy to cross the potential barrier until the retarding potential reaches cutoff. The region of increasing current with increasing retarding potential is one of a rather strong decrease in the collector secondary-emission yield as the energy of incidence decreases.[8] As the retarding voltage is increased, the electrons impinge on the collector plate with decreasing energy. This causes the current reflected from the collector to decrease and the net current collected to increase.

Figure 1.10(a) shows the same system as Fig. 1.9(a) except for the addition of a grid (G) at a negative potential U (about 20 V in this case) with respect to the collector (C). This potential forms a barrier to the escape of secondaries of energy not more than eU originating at the collector. Thus, essentially only the elastic secondaries are energetically capable of escaping the collector. (There are few inelastic secondaries formed with energy more than 20 eV.) This leads one to suspect that the rise in current immediately preceding cutoff in Fig. 1.10(b) could be due to a decreasing elastic secondary emission yield with decreasing energy. The systems in Figs. 1.11 and 1.12, however, show that this is not the case.

In the systems shown in Figs. 1.11(a) and 1.12(a), the energy of the electrons striking the collector plate is not a function of the retarding potential V_R. Hence the effect of decreasing electron yield with increasing retarding potential is eliminated. The fact that the retarding curves in Figs. 11(b) and 1.12(b) still exhibit an increase in current in the region just before

---

[8] J. A. Simpson, Rev. Sci. Instr. 32, 1283 (1961).

cutoff indicates that this effect is not due to a change in secondary-emission yield from the collector.

In both systems (Figs. 1.11 and 1.12), the barrier to the escape of low energy secondaries originating at the collector increases as V_R is increased. In Fig. 1.12(a), secondaries formed at the collector escape if their energy is more than eV_R. As V_R is increased, fewer of these secondaries escape, causing a larger fraction of the electrons striking the collector to be collected. This effect, in every measurement performed with our collectors, was sufficiently large to more than offset the decrease in the current striking the collector due to the retardation of the low-energy part of the incident beam distribution. Thus, the current collected, I_c, shown in Fig. 1.12(b), by the system in Fig. 1.12(a) increases as the retarding potential increases from zero until a sufficient barrier to the escape from the collector of inelastic secondaries has been established. In Fig. 1.11, this effect has been eliminated by the addition of a positive potential on the collector, thus establishing a barrier, V_R+U, sufficient to prevent the escape of low-energy secondaries originating from the collector for all values of $V_R>0$.

In an effort to determine the cause of the increase in current before cutoff, the situation shown in Fig. 1.13(a) was simulated on a computer. Making the collector voltage U proportional to the retarding potential was done for computational convenience. All secondary scattering effects were neglected. The incoming beam was made up of 100-eV electrons only. The results are shown in Fig. 1.13(b), where the effective grid transparency (ratio of the collector current to the incident beam current) is plotted as a function of retarding potential V_R. The geometrical transparency (ratio of open area to total area) of the grid used for this calculation was 0.72. The results of this calculation

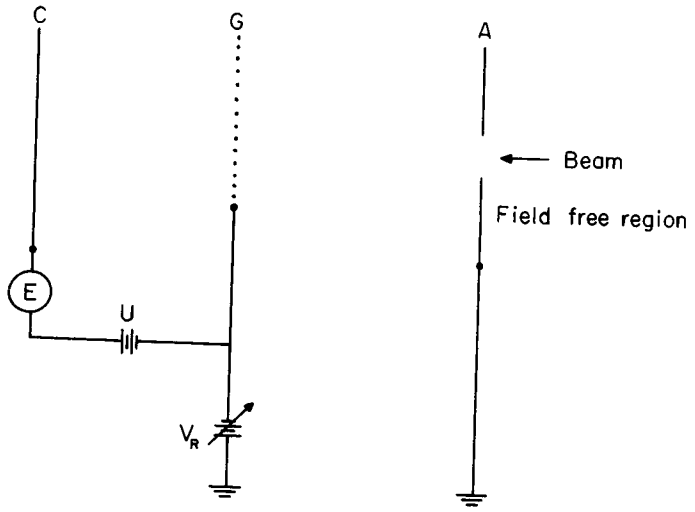

(a)

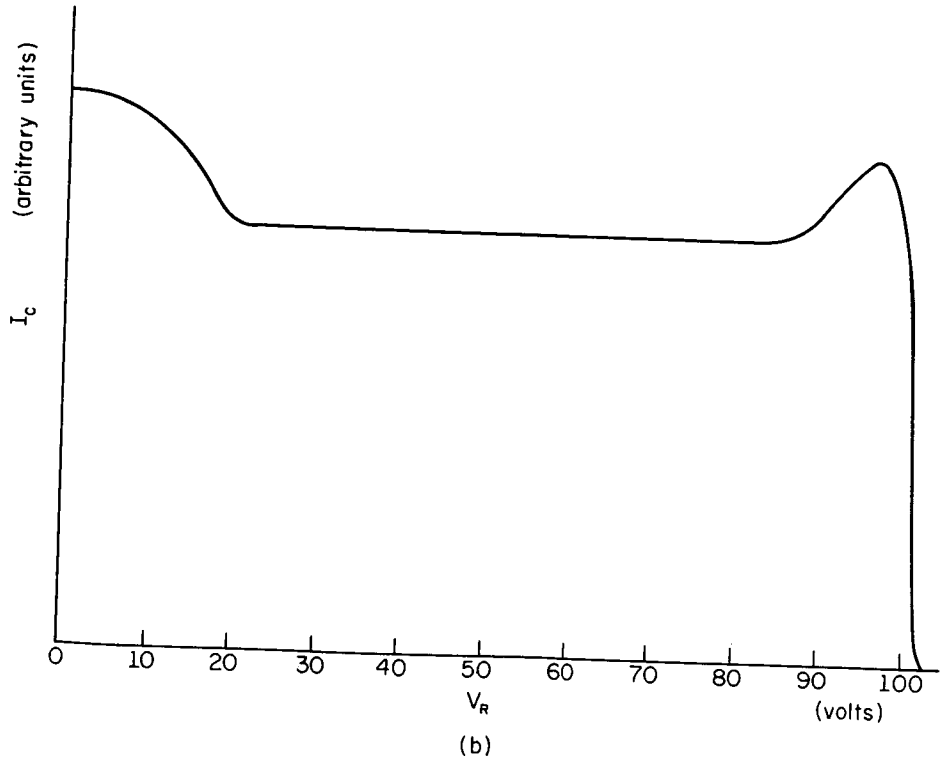

(b)

Fig. 1.10. Retarding-potential system and typical retarding-potential curve from the analysis of the distribution in Fig. 1.8(a). The symbols are G = grid, C = collector plate, A = aperture, V_R = retarding potential, E = electrometer for measurement of current to collector plate, U = accelerating voltage.

(OVERLEAF BLANK)

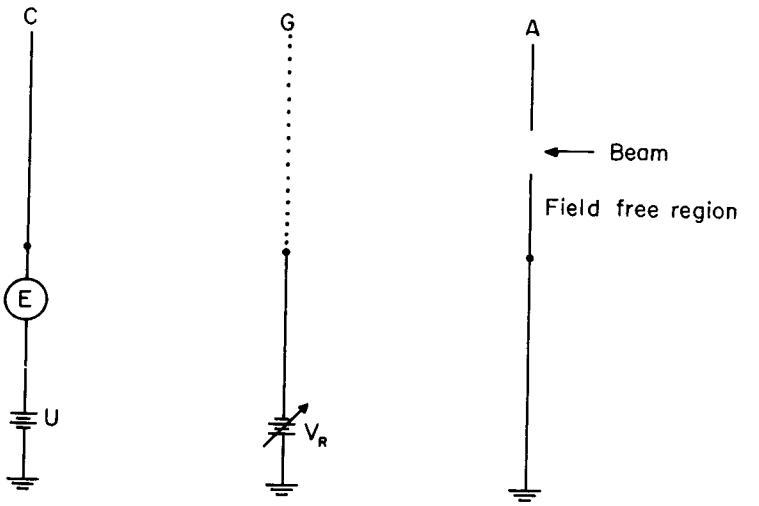

(a)

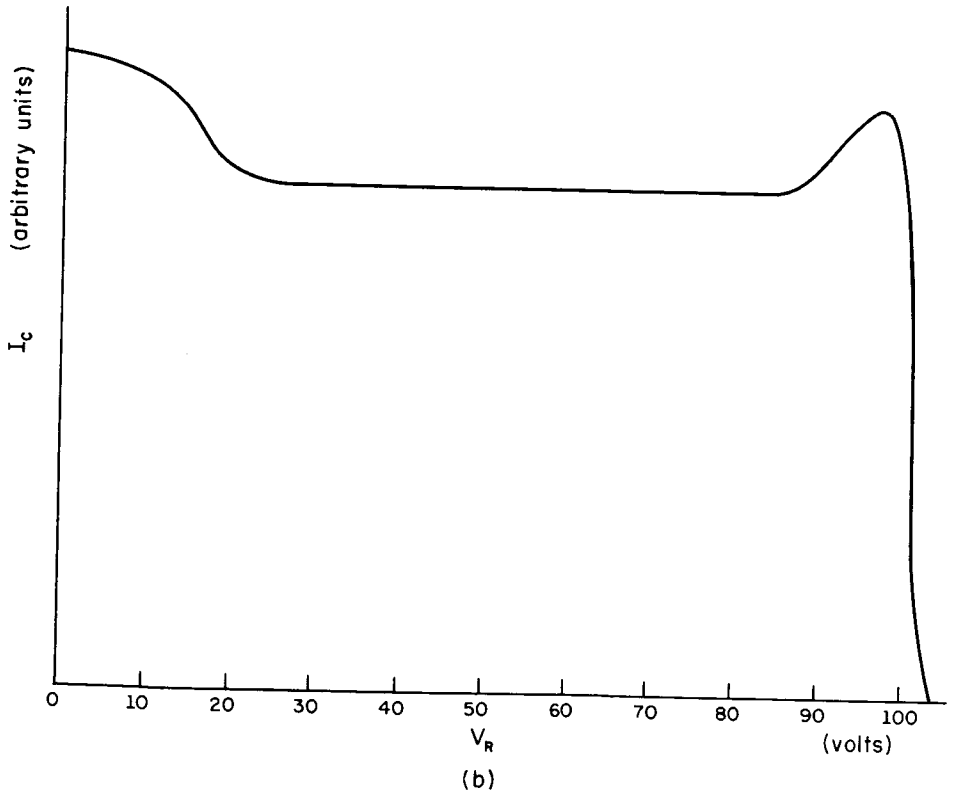

(b)

Fig. 1.11. Retarding-potential system and typical retarding-potential curve from the analysis of the distribution in Fig. 1.8(a). The symbols are G = grid, C = collector plate, A = aperture, V_R = retarding potential, E = electrometer for measurement of current to collector plate, U = accelerating voltage.

(OVERLEAF BLANK)

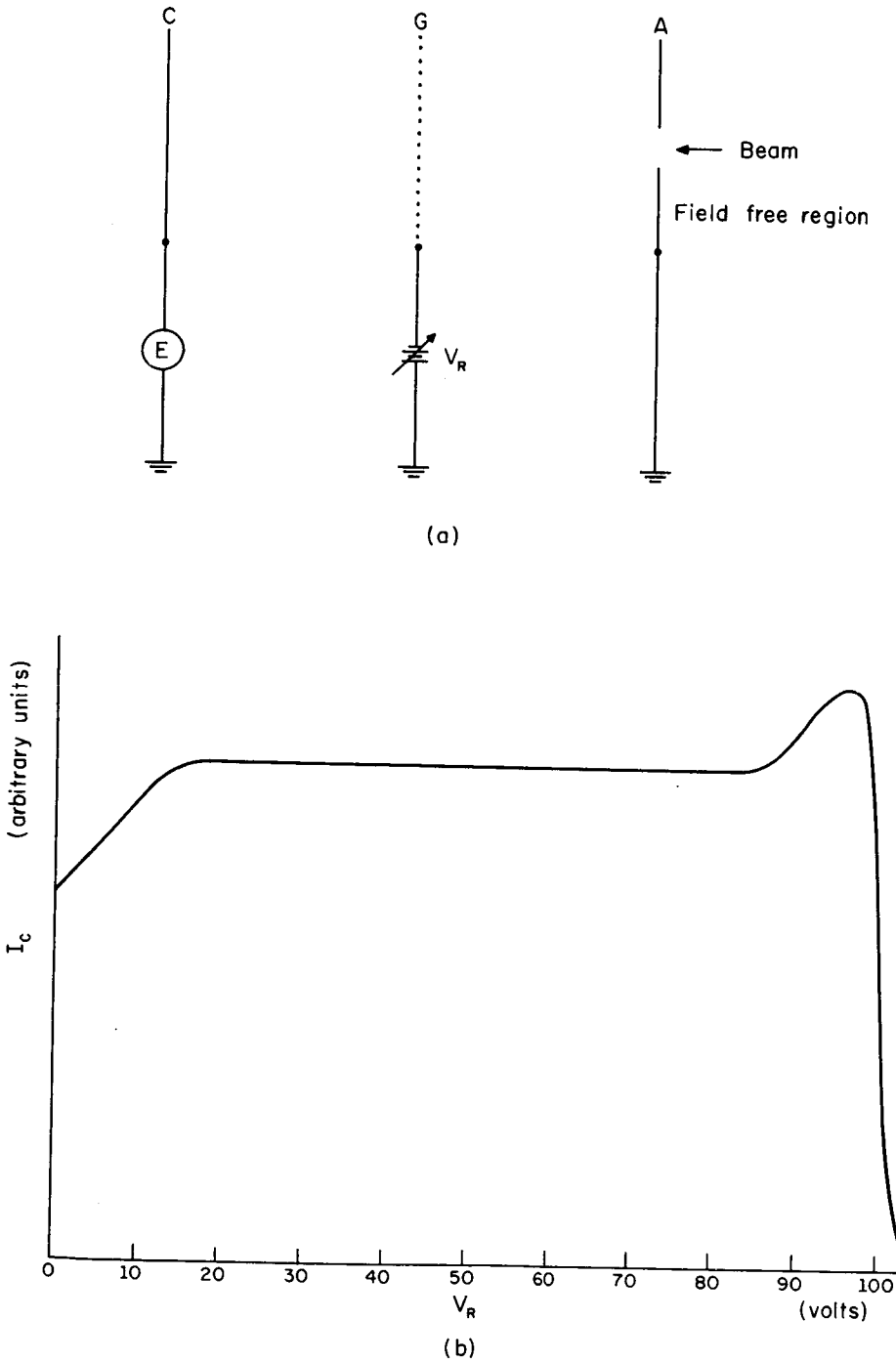

Fig. 1.12. Retarding-potential system and typical retarding-potential curve from the analysis of the distribution in Fig. 1.8(a). The symbols are G = grid, C = collector plate, A = aperture, V_R = retarding potential, E = electrometer for measurement of current to collector plate.

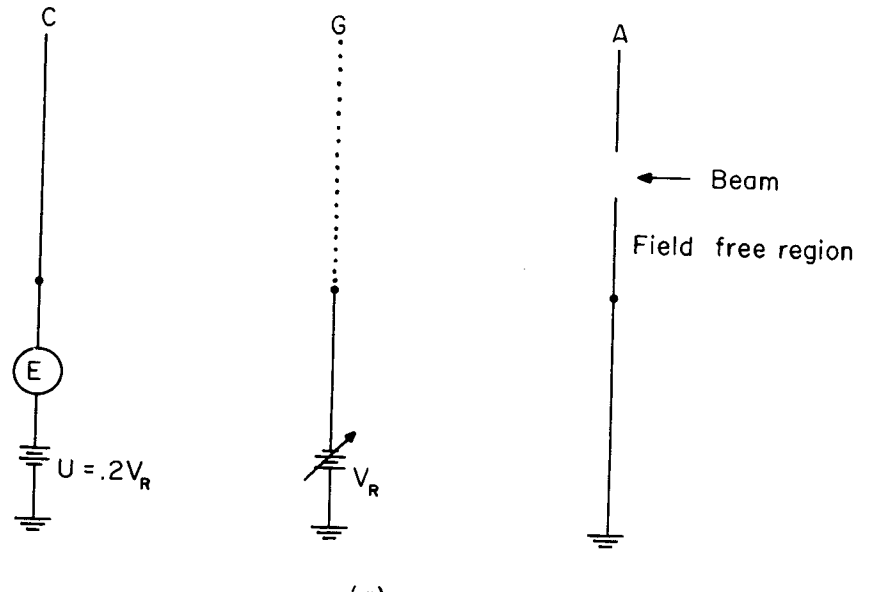

(a)

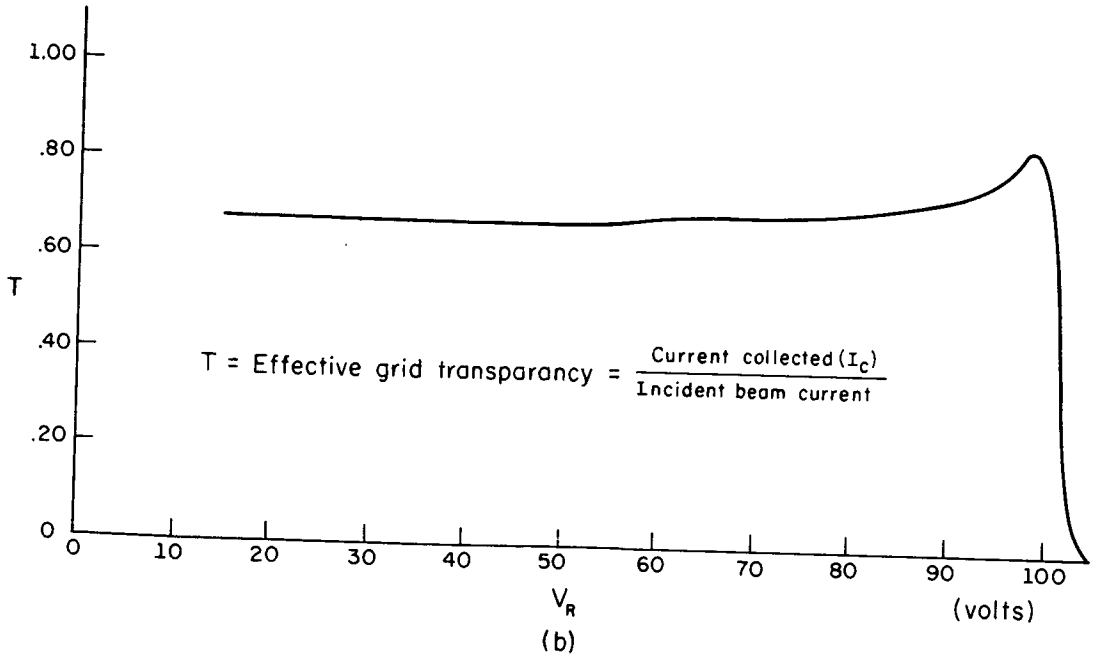

(b)

Fig. 1.13. Retarding-potential system and calculated curve resulting from the analysis of a 100-eV beam. The symbols are C = collector plate, A = aperture, V_R = retarding potential, E = electrometer for measurement of current to collector plate, U = accelerating voltage.

(OVERLEAF BLANK)

demonstrate that the rise in current with increasing retarding potential immediately before cutoff is at least in part due to an increase in effective grid transparency.

The reason for this increase in grid transparency is that the potential on a grid wire is more negative than the potential between wires. Therefore an electric field exists parallel to the plane of the grid which forces electrons away from the grid wires. This field exists only near the grid (about one grid-wire spacing away). In order for the field to alter drastically the path of an electron moving initially on a collision course with a grid wire, the electron must be moving "slowly" through the region where this deflection field exists. Order-of-magnitude calculations show that, for an 100-eV electron to be deflected one grid-wire spacing while within a region of one grid-wire spacing from the grid, the retarding potential V_R must be about 90 volts. (This calculation was done for a grid with geometrical transparency of greater than 90%.) Thus, as the electrons are retarded to near cutoff, they are deflected away from the grid wires, causing the effective transparency of the grid to increase and more current to arrive at the collector plate.

Highly transparent (0.97%) grids made from .001-inch diameter gold-plated moly wires, gold brazed to moly plates have been designed. These grids will

(1) Reduce scattering from the grid wires to less than 3%.

(2) Reduce oxide formation that could result in grid charging.

(3) Reduce the increase in grid transparency to a maximum of 3%.

(4) By comparing curves taken with the retarding systems in 11(a) with those in 10(a), make it possible to estimate the errors in the retarding curves due to elastic reflection from the collector plate.

These measurements were made in an oil-diffusion-pumped bell-jar system, allowing substantial contamination of the electrodes. More quantitative information concerning the operation of retarding analyzers has not been possible because of charging effects due to contaminated electrodes and grids in all our retarding analyzers.

1.3 Adsorption of Gases at Metal Surfaces

Because of the vacuum problems mentioned in the previous progress report, a new target-holding flange has been constructed. The flange has been designed to permit resistance heating of the target through two high-current feedthroughs. Each end of the target is fastened to an interior liquid-nitrogen trap which is heli-arcwelded to the inside lip of the high-current feedthrough. This allows us to cool the target by conduction to the liquid-nitrogen traps.

We have been attempting to clean tungsten targets for a study of nitrogen adsorption. The normal procedure is to heat the target in vacuo for several hours above 2200°K, presumably removing everything but carbon. The carbon is removed by heating in oxygen, which converts it to CO and CO_2.[9]

After heating our targets in vacuo for several hours, we found the room-temperature sticking coefficient to be smaller than 10^{-3}, as compared to the accepted value of 2.[10] Heating the target in oxygen temporarily restored the normal sticking properties of nitrogen, but the target became inert again through two processes:

(1) Continuous flashing in vacuo for about 300 sec.

(2) Adsorption of several monolayers of background gases, followed by a short flash.

---

[9] Becker, Becker, and Brandes, J. Appl. Phys. 32, 411 (1961).

[10] Hill et al., J. Chem. Phys. 44, 2170 (1966).

The second filament in the ion gauge could easily be cleaned by flashing in vacuo so that nitrogen would adsorb with the expected sticking probability.

To analyze these observations, it is important to note that the target is held over the mouth of the liquid-nitrogen trap, which is the only baffle between the oil-diffusion pump and the test chamber, while the ion gauge is much further away from the diffusion pump.

The fact that the ion-gauge filament is not contaminated indicates that the contamination is a specific property of the target, its location, or its supports. All pieces directly in contact with the target are pure tungsten, and no diffusion of other metals over the tungsten was observed when the apparatus was disassembled. Two different tungsten targets were used in this work, one cleaned by electropolishing, and one merely washed with organic solvents. Both of these targets behaved similarly.

Thus, it seems likely that the contamination is the result of the target's location, i.e., in the path of backstreaming diffusion-pump oil. The target could become contaminated either through flashing in the hydrocarbon vapor or through allowing the molecules to accumulate on the target and then flashing to break them down and deposit-out carbon.

The solutions to this problem are obvious: reducing the hydrocarbon concentration by either better trapping of the oil diffusion pump or by changing the method of pumping.

1.4 Photon Emission from Solid Surfaces Under Low Energy Ion Bombardment

1.4.1 Introduction. Of the many processes which can occur when an ion hits a solid surface, the emission of a photon has been investigated very

little. Sternberg[11] calculated that the yield for He^+-ions on tungsten should be about 10^{-4} photons/ion. Böhmer and Lüscher[12] obtained experimental results which differed strongly from the theoretical predictions. It cannot be excluded, however, that they observed metastable atoms instead of photons.[13] Photon emission from copper under He^+-ion bombardment was also observed by Tolk.[14]

1.4.2 Brief Description of the Photon Emission Process. The process responsible for photon emission and the energy-level diagram for the ion-metal system is drawn in Fig. 1.14. An ion approaching the surface is neutralized at a distance d by an electron from the conduction band of the metal. The energy gained by the electron is radiated in the form of a photon with energy $h\nu$. (The by-far dominant process occurring after ion neutralization is a radiationless Auger process where a second electron from the conduction band takes up the energy.) The maximum photon energy is $h\nu_{max} = E_i - \phi$, where E_i is the ionization potential of the ion and ϕ is the work function of the metal. For He^+-ions on tungsten, $h\nu_{max} = 20$ eV.

Another source of photons can be recombination radiation of an electron-hole pair which is generated when an electron is excited in an Auger neutralization process, but does not leave the solid. To our knowledge, nobody has studied this process in metals.

It is the goal of this experiment to study (a) photons originating directly from the ion-neutralization process, and (b) photons due to recombination

---

[11] D. Sternberg, Ph.D. thesis, Columbia University, 1960 (unpublished).

[12] H. Böhmer and E. Lüscher, Phys. Letters 5, 240 (1963).

[13] H. D. Hagstrum, Phys. Rev. 123, 758 (1961).

[14] N. Tolk, Ph.D. thesis, Columbia University, 1966 (unpublished).

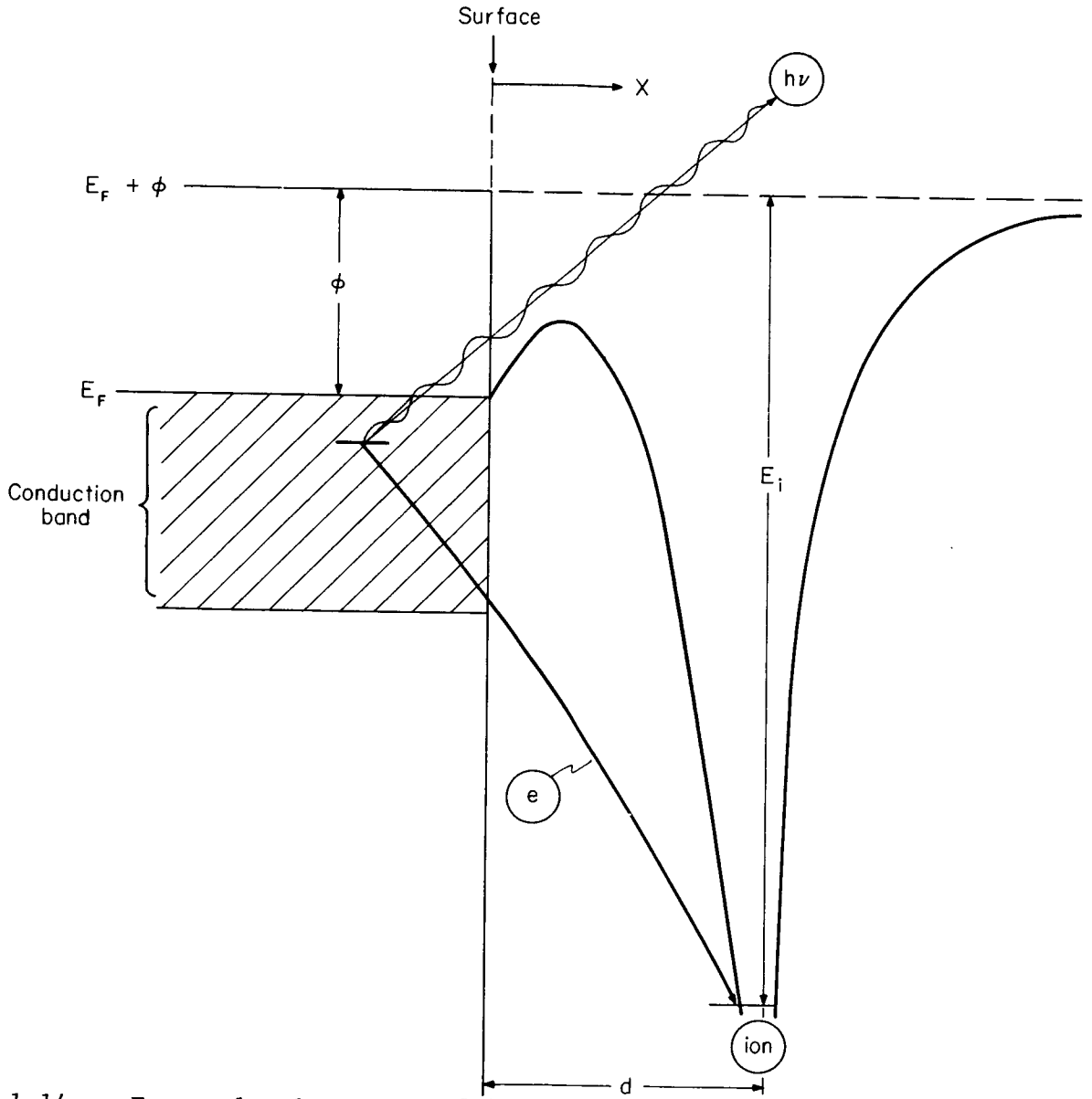

Fig. 1.14. Energy-level diagram of ion-metal system, showing emission of a photon after ion neutralization.

(OVERLEAF BLANK)

of electron-hole pairs which are generated by Auger neutralization. The important numbers are the total yield, the energy-distribution of the photons, the dependence on ion species and energy, and the dependence on gas coverage of the target material.

1.4.3 Experimental Setup. Figure 1.15 shows the setup. A bakeable stainless steel vacuum chamber capable of reaching a pressure of less than 10^{-10} Torr contains the following parts:

a) An ion source which gives 10^{-7}A ion current at the target at 100-eV ion energy,

b) A target (tungsten of other material) which can be lifted and outgassed by electron bombardment far away from the detection region to avoid contamination,

c) A platinum-coated reflector which receives photons from half the solid angle (platinum has a reflection coefficient of not less than 15% for photons of an energy from 2 to 25 eV, and it does not change its reflectivity upon frequent exposure to atmosphere),

d) A particle multiplier which receives not less than 90% of the photons reflected from the platinum reflectors, and

e) A set of different high-frequency cut-off filters which can be put in front of the particle multiplier.

The particle multiplier counts individual photons with an energy not less than 4 eV. One has to take care that no particles which can produce a count, other than photons, can enter it. This problem is not completely solved.

The apparatus for this experiment is under construction. The most difficult part is the ion source which still needs a few improvements. Another problem will be the alignment of all the parts inside the vacuum system.

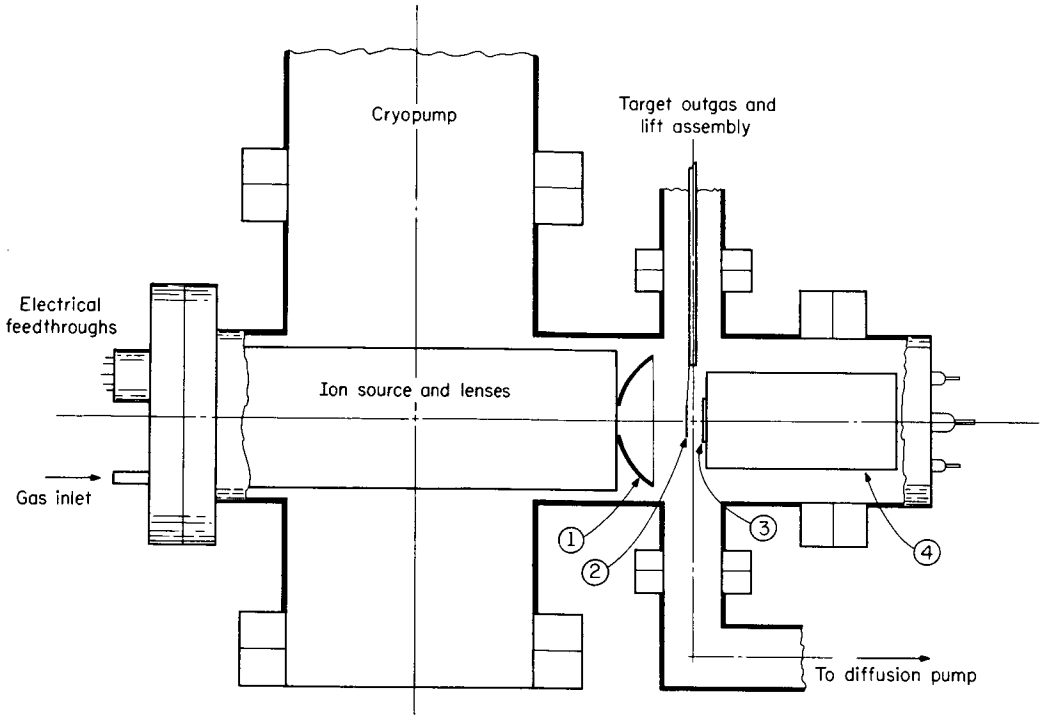

① Mirror
② Target
③ Optical filter
④ Photo multiplier

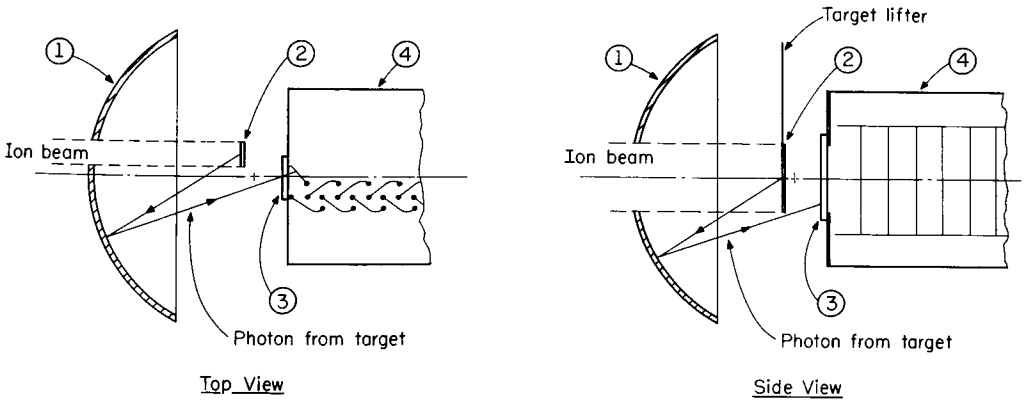

Details of Target Area

Fig. 1.15. Schematic illustration of vacuum system and components used for photon experiment.

(OVERLEAF BLANK)

R. N. Peacock
D. Alpert
W. P. Bleha
M. G. Craford
J. W. Culton
J. T. Jacobs
R. P. Ries
J. Robinson
W. C. Schuemann
F. Steinrisser

2.1 Vacuum Instrumentation[†]

2.1.1 Introduction. The principal activity of the vacuum group during the period covered by this report has been related to improving the low-pressure characteristics of the Schuemann suppressor gauge, and such vacuum work as was necessary to the continuation of this aim.

2.1.2 Further Development of the Schuemann Suppressor Gauge. The Schuemann suppressor gauge, in the forms made following the original invention, or in the commercial version as now manufactured by RCA, is not capable of utilizing the full potential of the suppressor concept. The problem of accurate total-pressure calibration at pressures below 10^{-10} Torr has not been solved by any generally available gauge. Thus, further development of the suppressor gauge has been undertaken to overcome problems associated with the early models.

Specifically, the problems with the gauge have been those of outgassing the electrode structure to make possible operation at pressures as low as 10^{-12} Torr, Barkhausen oscillations, and problems associated with the mechanical structure of the electrodes.

In the past few months, several new forms of the gauge have been built and tested. Special effort has been given to choosing a design and electrode materials such that the metal components could be outgassed. To improve the outgassing properties further, all of the recent gauges have utilized a spherical bulb, which aids in keeping the envelope cool during outgassing. The geometry now used, with attention to grid-filament spacing has apparently eliminated

[†]Supported in part by the National Aeronautics and Space Administration under Grant NsG-376.

space-charge oscillations. The construction has been simplified by supporting all electrodes other than the ion collector from a single header. This gauge, of which a photograph is shown in Fig. 2.1, has operated effectively at pressures in the mid 10^{-12}-Torr range. Lower pressures have not been available to continue tests further. Figure 2.2 shows that the operation of the gauge has an insignificant effect on the partial pressures of the residual gases as measured with a GE 90° spectrometer. The very small CO peak which appears with the gauge "on" is barely above spectrometer dark current.

2.1.3 Efforts to Reach Lower Pressures--Glass Systems. The metal valves used to isolate the trap from the working portion of the system during baking are the major source of gas (H_2) in our present glass systems. In the hope of removing this limitation, we have made a glass valve similar to those reported in the literature.[1,2] The second model is presently being tested for leakage conductance, and all indications are that such a valve will be useful. If the hydrogen from the metal valve is eliminated, the dominant residual gas in the systems will be helium.

Thought has been given to two possible ways of reducing the helium limit. One would be to use a glass with a small permeability for helium, such as an alumino-silicate glass. Another would be to use a large cell ion pump with a significant pumping speed for helium at very low pressures.

2.1.4 Lower Pressures--Metal Systems. Although the outgassing rates per unit area are usually much higher for stainless steel than for glass after equal baking, it should be possible to make metal-gasketed stainless-steel systems

---

[1] R. Decker, J. Appl. Phys. 25, 441 (1954).

[2] A. H. Turnbull, R. S. Barton, and J. C. Riviere, An Introduction to Vacuum Technique (Wiley, N.Y., 1962), pp. 126-127.

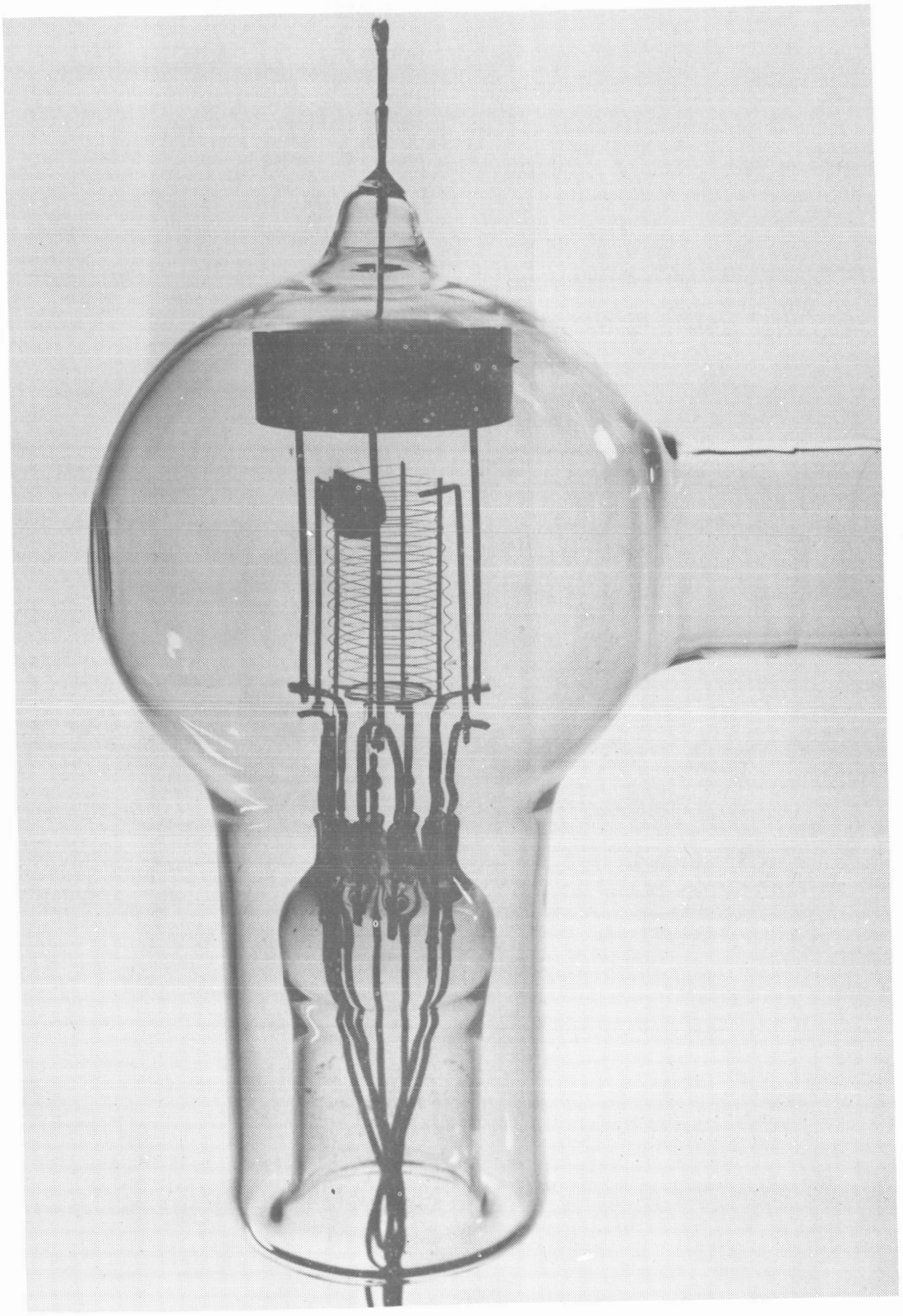

Fig. 2.1. Photograph of the type of suppressor ionization gauge now under test.

(OVERLEAF BLANK)

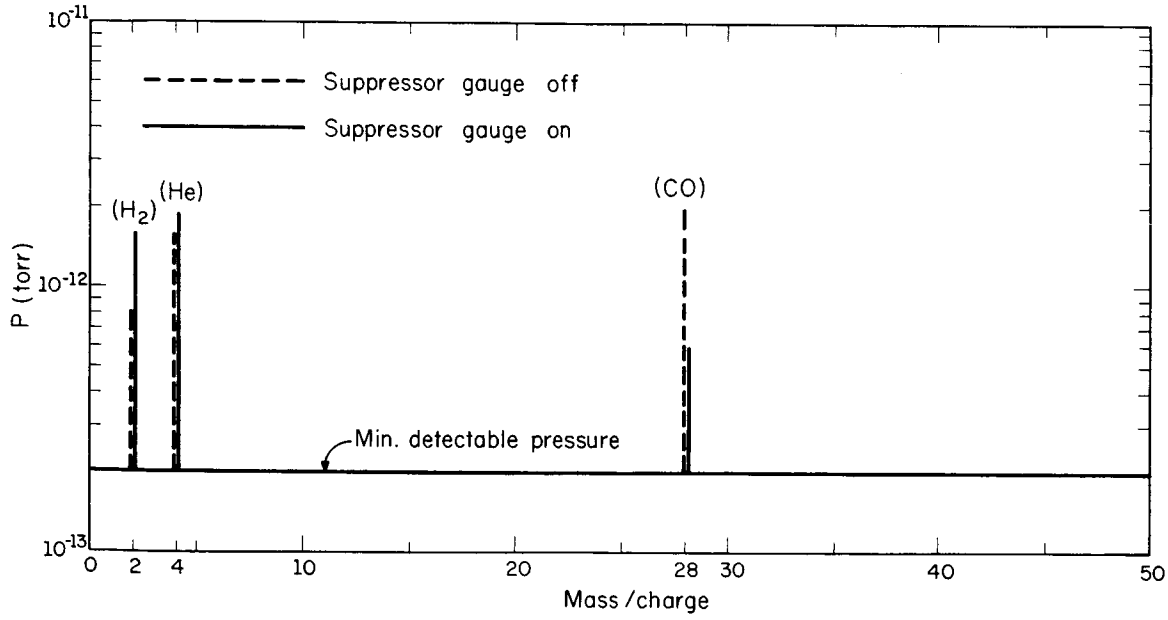

Fig. 2.2. Mass spectra showing the effect of operating the suppressor ionization gauge.

(OVERLEAF BLANK)

reach pressures as low as 10^{-12} Torr. Larger pumping speeds are possible in steel systems because of greater conductances, and it is more convenient to use large getter areas with large pumping speeds for active gases. Further, special techniques have been developed by Petermann at the Battelle Institute, Geneva (private conversation) which reduce the hydrogen evolution by forming an oxide barrier on the stainless-steel surface.

A steel system designed for comparing ionization gauges is in preparation. It is presently evacuated with an ion pump built in the laboratory, and made for high speed at low pressure. Titanium sublimation is also included. The initial results have been encouraging with pressures reaching as low as 8×10^{-11} Torr. The only significant residual gas is hydrogen. The system is now being outfitted with a well-trapped diffusion pump to maintain low pressures during bakeout, and to thus reduce the saturation of the metal by the gases present during bakeout. The diffusion pump will be valved-off from the stainless system during normal operation.

2.2 Size Effects in Thin Films

2.2.1 Introduction. The vacuum system necessary to perform the size-effect experiments mentioned in previous reports is under test and construction. The main progress has been to develop and test a cryopump. The experiments on this system are reported below.

2.2.2 Cryopump Tests. The persistent failure of the gold o-ring seals used with the Swagelocs on the cryopump liquid feedthrough has caused them to be discarded. The faulty joints were replaced by welds. The modified cryopump was installed on the ultrahigh vacuum system. The unit was leak tested using the Varian-Assoc. partial-pressure gauge (PPG). A mass spectrum of the entire

system before bakeout indicated that hydrogen had the largest partial pressure (1.3×10^{-8} Torr).

The system was baked for 11 hours at 300°C. The system was still leak tight. However, the partial pressure of hydrogen was the same. This indicated that the use of a titanium sublimation pump (TSP) during bakeout might help remove the excessive amount of hydrogen.

The system was isolated from the unbaked region and the baked ion pump started. After pumping all night, the hydrogen pressure reached 1.9×10^{-9} Torr. Liquid nitrogen was put in the cryopump shroud. After it had cooled to liquid-nitrogen temperature, the helium dewar was filled with liquid helium. By pumping on the helium with a roughing pump, a total pressure of 5×10^{-11} Torr was obtained.

The total holding time for the helium was about 30 minutes. The total holding time for liquid nitrogen was 40 hours. These times are compatible with the proposed size-effect experiments.

A Varian-Assoc. TSP was installed in the unbaked region of the system. A current control for the TSP was built in our laboratory.

An attempt was made to bakeout the system with the aid of the TSP. However, a sizeable leak was now found to have developed in the cryopump. The cryopump was dismantled and the helium dewar disconnected. Using a helium leak detector, the leak was found to be in a weld in the stainless steel. The cryopump has been delivered to the machine shop for repairs.

Meanwhile a feedthrough collar which was built in our shop was installed and leak tested. A superconducting level detector to be used in the cryopump was also built.

2.2.3 Size-Effects Experiments. Investigation of quantum size effects was initiated. In order to use recent developments in superconductive-tunneling

procedures, we began a cooperative effort with Dr. E. L. Wolf of the Materials Research Laboratory. Considerable effort resulted in a simple technique for cleaving mica in a vacuum. A thin gold film was deposited on the cleaved mica. Tunneling measurements on this first sample were inconclusive. More samples will be prepared and measured in the future.

J. T. Jacobs.

2.3 Superconductive Tunneling in High-Purity Single-Crystal Niobium

Work is continuing in the attempt to obtain a niobium crystal of sufficient purity to study the anisotropy of the superconducting energy gap. As mentioned previously, the best commercial crystals available are not adequate.

Recently we have used radio-frequency induction heating to outgas a commercial crystal in high vacuum. The crystal, a 2-in×½-in rod, is suspended in a water-cooled quartz tube. We are able to maintain a pressure of 3×10^{-9} Torr, while heating the crystal at 2000°C. In a first attempt, we have succeeded in increasing the resistivity radio ($R_{300^\circ K}/R_{4.2^\circ K}$) of a high-purity commercial crystal from 100 to 400. A second, more thorough, processing of another crystal gave a ratio of 700. We wish to obtain a resistivity ratio of about 1500. A partial-pressure analysis of the residual gases during heating showed nitrogen to be the most common gas resulting from the sample processing.

A helium-3 refrigerator has been completed, allowing us to make measurements at 0.3°K, instead of the 1.2°K we are able to attain using helium 4. It is necessary to operate at this temperature in order to determine whether or not niobium has a second energy gap.[3]

M. G. Craford

---

[3] Lawrence Yun Lung Shen, N. M. Senozan, and N. E. Phillips Phys. Rev. Letters 14, 1025 (1965).

2.4 Picovoltmeter

A third version of the picovoltmeter (superconducting parametric amplifier) is being tested at the present time. The new version is more rugged and considerably smaller than previous models. This version is the first to use multiple input and output coils. The use of multiple-coil systems permits a higher gain-bandwidth product for the system. The gain-bandwidth product is also enhanced in this version by an extremely high-Q (10^4) vibrating system, achieved by a tuning fork which carries the vibrating portion of the amplifier. The tuning fork is used as the frequency-determining element of the pump-frequency oscillator, thus eliminating stability problems created by the extremely high Q. The tuning fork allows a balanced vibrating system, and should permit a reduction of the type of noise which limited the sensitivity of the previous model, i.e., noise created by the vibration of the output coils in the residual magnetic fields remaining after shielding.

A more detailed report on the cryogenic picovoltmeter will be made at the conclusion of tests now in progress.

3. PLASMA PHYSICS[†]

M. Raether
W. Bernhard
H. Böhmer
L. D. Bollinger
W. E. Carr
J. Chang
R. W. Hosken
R. W. Huggins
Y. Ichikawa
E. A. Jackson
T. Lie
C. A. Manning
C. W. Mendel
H. J. Pinsky

3.1 Beam-Plasma Interaction

3.1.1 Incoherent Scattering of Microwaves by Unstable Plasma.

An effort was made to detect the incoherent scattering of microwaves by the beam stimulated plasma oscillations.

The possibility of using incoherent scattering of electromagnetic waves by plasma oscillations as a diagnostic tool has received considerable attention recently.[1] The importance of this method for the investigation of unstable plasmas has been emphasized by Ichimaru, Pines and Rostoker[2] and by W. E. Drummond.[3] Arunasalam and Brown[4] have observed incoherent scattering from the unstable ion-acoustic mode in a dc discharge, and scattering by driven

---

[†]Supported in part by the University of Illinois.

[1]K. L. Bowles, Phys. Rev. Letters, 1, 454 (1958); J. Res. Nat. Bur. Sta., 66D, 395 (1962). T. P. Dougherty and D. T. Farley, Proc. Roy. Soc. (London), A259, 79 (1960). E. E. Salpeter, Phys. Rev., 120, 1528 (1960). J. A. Fejer, Can. J. Phys., 38, 1114 (1960). M. N. Rosenbluth and N. Rostocker, Phys. Fluids, 5, 776 (1962). H. L. Berk, Phys. Fluids, 7, 917 (1964). F. W. Perkin, E. E. Salpeter, and K. O. Yngvesson, Phys. Rev. Letters, 14, 579 (1965). F. D. DuBois and V. Gillinski, Phys. Rev., 133, A1308, A1317 (1964). The observation of collective effects in the scattering of laser light by plasmas has been reported in a number of papers, cf. W. E. R. Davis and S. A. Ramsden, Phys. Letters 8, 179 (1964). H. J. Kunze, E. Fünfer, B. Kronast, and W. H. Kegel, Phys. Letters, 11, 42 (1964). See also P. W. Chan and R. A. Nodwell, Phys. Rev. Letters 16, 122 (1966).

[2]S. Ichimaru, D. Pines, and N. Rostocker, Phys. Rev. Letters, 8, 231 (1962).

[3]W. E. Drummond, Phys. Fluids, 5, 1133 (1962).

[4]V. Arunasalam and S. C. Brown, Phys. Rev., 140, A471 (1965).

plasma oscillations has been demonstrated in two recent publications.[5]

The experimental arrangement is sketched in Fig. 3.1. An electron beam of 0.5 A, 15-21 keV, and 2 μsec duration is injected into the afterglow of a pulsed discharge in neon at a pressure of 3×10^{-2} Torr. Discharge and electron beam are triggered at a repetition frequency of 15 Hz. By varying the delay between the initiation of the discharge and the injection of the beam, the beam can be exposed to plasma densities in the range between 10^{13} and 10^{11} electrons/cm^3. The decay time for the plasma is 300 μsec so the plasma density can be taken as constant during the time the beam is on. In the region of interest the plasma is at room temperature as inferred from the ambipolar diffusion coefficient. The beam instability, however, increases the electron temperature by a factor of 6 for beam currents in excess of 300 mA. The plasma is illuminated under a variable angle by a 300-mW, 27-GHz CW signal from a klystron. A receiving horn, mounted at an angle with respect to the axis of the discharge, is coupled to a receiver via a high-pass filter of 29-GHz cut-off frequency. The received signal is mixed in a balanced mixer with local oscillator, variable between 38 and 34 GHz. The difference frequency of 70 MHz is amplified by an if amplifier of 8-MHz bandwidth. The if amplifier is gated on during the beam pulse and the rectified output is detected in a synchronous fashion by a lock-in amplifier.

The planes of polarization of the transmitting and receiving horns are such that the E vector is perpendicular to the axis of the electron beam. Under these conditions the scattered intensity per solid angle is given by

$$dP_s/d\Omega = 2Nr_o^2(P_o/F)S(k,\omega)\ \Delta\omega$$

---

[5] R. A. Stern and N. Tzoar, Phys. Rev. Letters 15, 485 (1965). Y. G. Chen, R. F. Leheny, and T. C. Marshall, Phys. Rev. Letters 14, 184 (1965), Phys. Rev., 140, A471 (1965).

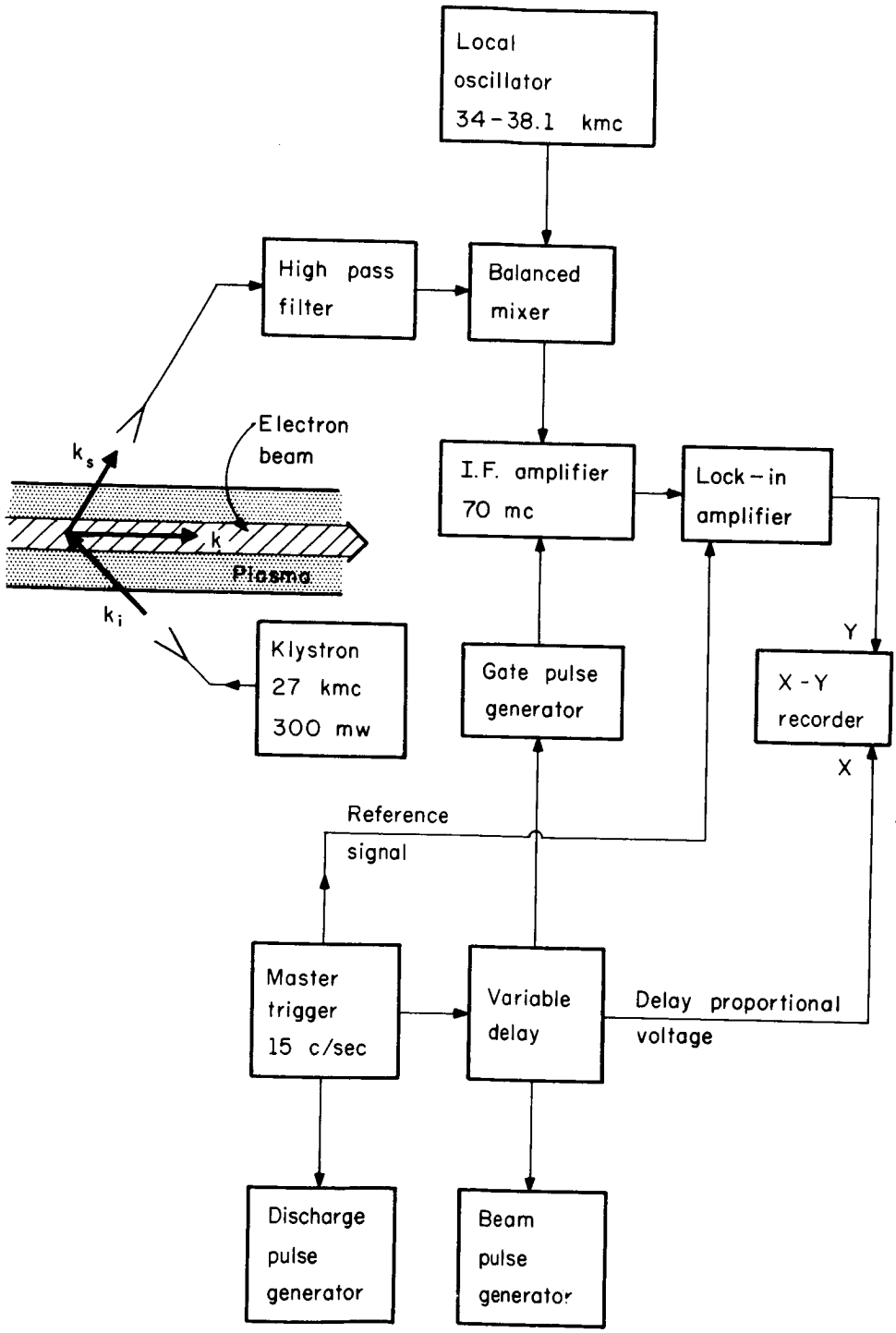

Fig. 3.1. Schematic of the experiment.

(OVERLEAF BLANK)

where N is the total number of electrons in the scattering volume, r_o the classical electron radius, P_o/F the incident power density, $\Delta\omega$ the receiver bandwidth and $S(k,\omega)$ the dynamical form factor of the density fluctuations. $\underset{\sim}{k}$ and ω are determined by $\underset{\sim}{k} = \underset{\sim}{k}_s - \underset{\sim}{k}_i$, $\omega = \omega_s - \omega_i$ where $\underset{\sim}{k}_i$ and ω_i are wave vector and frequency of the incident radiation, while $\underset{\sim}{k}_s$ and ω_s represent the scattered radiation. In the present experiment the most unstable $\underset{\sim}{k}$ is expected to be parallel to the direction of the electron beam. By varying the angles between $\underset{\sim}{k}_i$ and $\underset{\sim}{k}$ as well as between $\underset{\sim}{k}_s$ and $\underset{\sim}{k}$, one could select $\underset{\sim}{k}$ values from 4 to 10 cm^{-1}.

Figure 3.2 shows a recorder trace of the received power as a function of electron density in the vicinity of the scattered signal. The two neighboring peaks are due to radiation at higher harmonics of the plasma frequency.

Figure 3.3 shows a plot of scattered power versus k as inferred from the angular distribution. The maximum of the scattering is expected to occur for the most unstable k, which is given to a good approximation by $k_{opt} = \omega/u_o$, where u_o is the beam velocity and ω the frequency of the most unstable mode. This is true for a cold as well as a warm beam, the corrections due to finite beam density and thermal velocity spread being within the accuracy of the measurement. The value of k_{opt} can be changed by varying either u_o or ω. Both parameters were varied, and the result is shown in Fig. 3.3b where the experimental values of k_{opt} are plotted versus ω/u_o together with the theoretical curve. The width of the k spectrum is determined primarily by the angular resolution of the microwave horns, so that a comparison with theoretical predictions based on the quasilinear theory[6] is not possible at the moment. The appearance of strong radiation at harmonics of the plasma frequency would indicate, however, that mode-mode coupling

---

[6] V. D. Shapiro. Soviet Physics JETP, 17, 416 (1963). Ya. B. Fainberg and B. D. Shapiro, Soviet Physics JETP, 20, 937 (1965).

terms give rise to strong density fluctuation at these frequencies and that these terms may no longer be considered to be small. We seem to be faced, therefore, with a case of "strong turbulence," for which no satisfactory theories seem to exist at the present time. The magnitude of the scattered power indicates that the beam-plasma interaction has enhanced the fluctuation spectrum by a factor 10^9-10^{10} over the thermal equilibrium value.

H. Böhmer
M. Raether

3.1.2 Time-Resolved Measurements. In order to time-resolve the build-up of plasma oscillations, the beam plasma experiment was modified so that the beam and the gate pulse operate at 30 Hz while the plasma is pulsed and detection is done at 15 Hz. This eliminates any gating and beam-pulse feedthrough. Any plasma-pulse feedthrough is detected, but is negligible because the gate is off when the plasma is pulsed.

A new 70-MHz amplifier with 15-MHz width was installed. It can be gated on and off in 0.3 μsec. This amplifier is used with X-band and K-band detectors to examine the growth of the plasma oscillations. To do this, the gate pulse is kept at a constant delay after the start of the beam pulse, and their delay time in the afterglow is varied. The detector output plotted versus delay is therefore equivalent to the plot of the oscillation spectrum at a particular time after the beam initiation.

Surprisingly, two discrete lines are found separated by about 0.5 GHz for a plasma frequency of 32 GHz (Fig. 3.4). The higher frequency line appears shortly after beam onset and then becomes smaller while the lower frequency line increases. As the beam is turned off the lower frequency line disappears and the higher line reappears temporarily (Fig. 3.5). This behavior was found

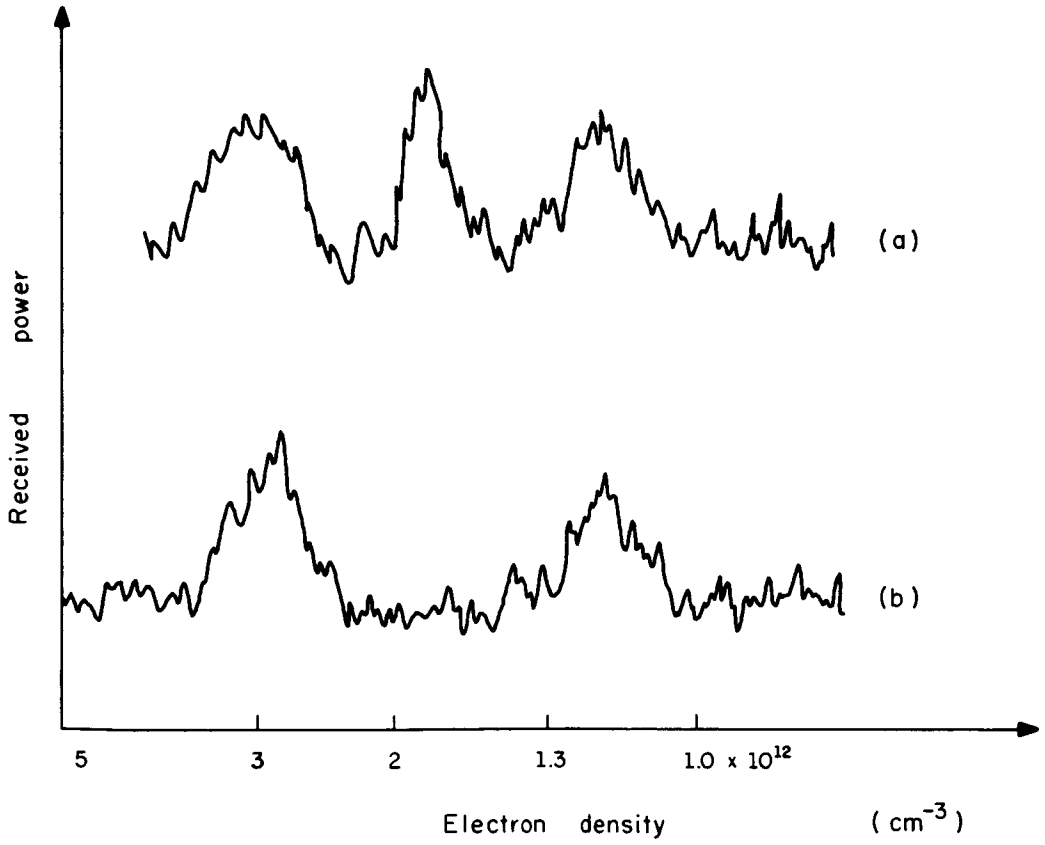

Fig. 3.2. Received power versus electron density. Upper trace: Microwave power on; Lower trace: Microwave power off.

(OVERLEAF BLANK)

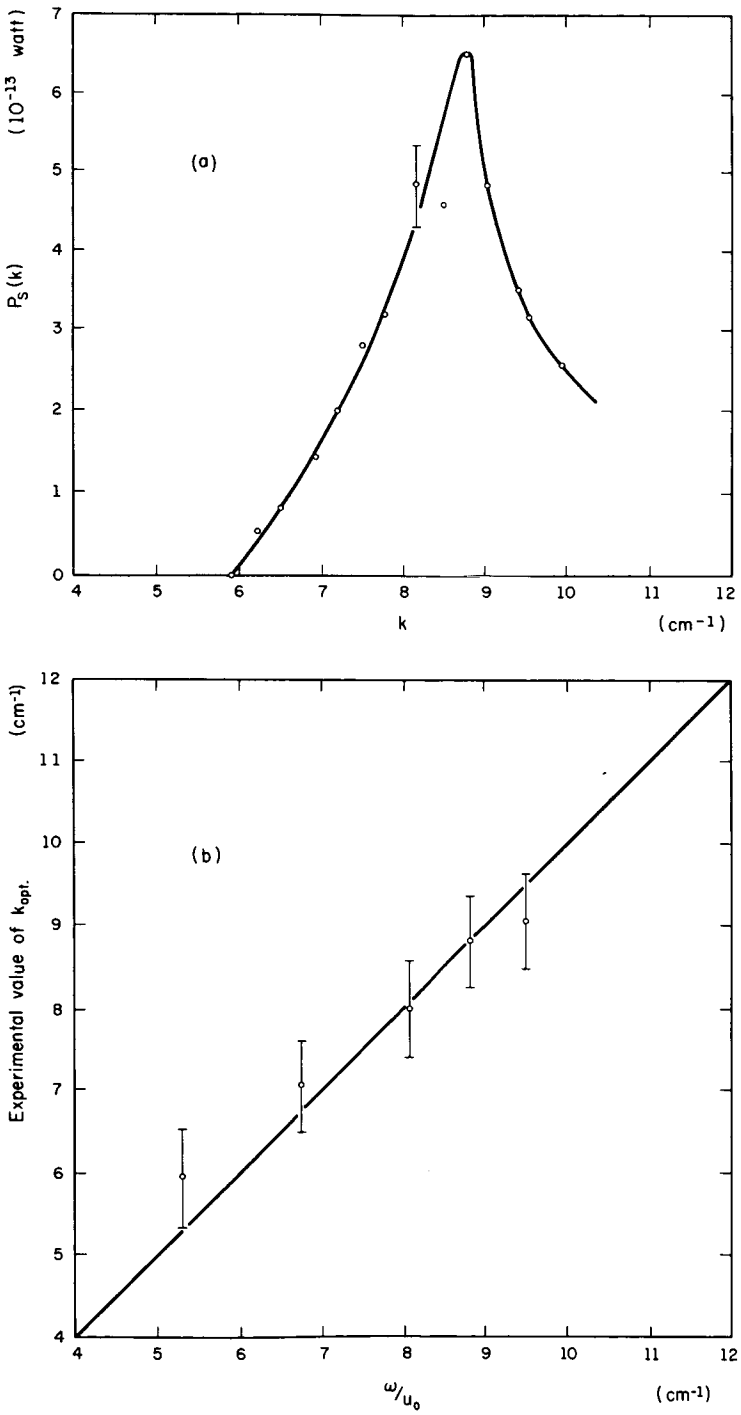

Fig. 3.3. a) Scattered power as a function of wavenumber of the unstable waves.
b) Experimental Values of k_{opt} as a function of ω/u_o.

(OVERLEAF BLANK)

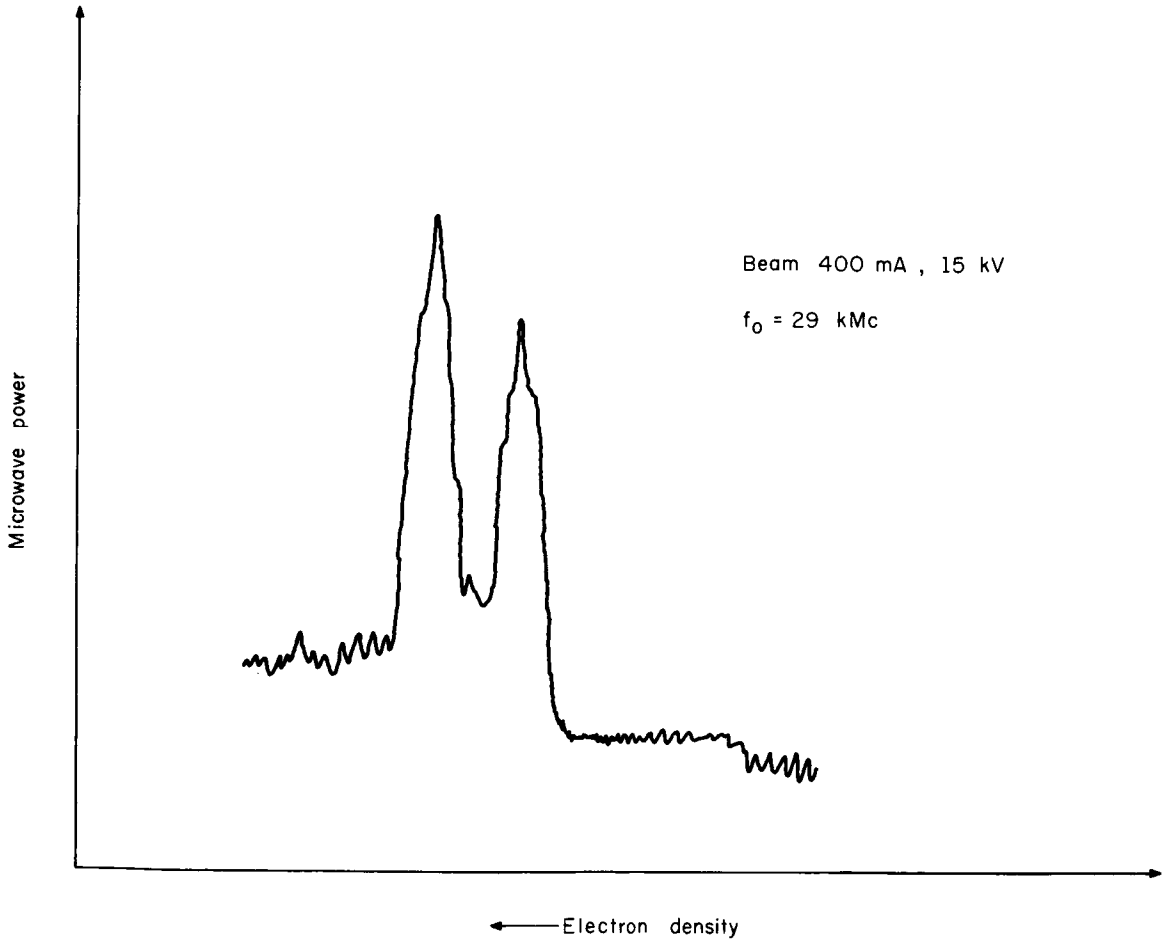

Fig. 3.4. Spectrum as a function of electron density for a short sampling interval.

(OVERLEAF BLANK)

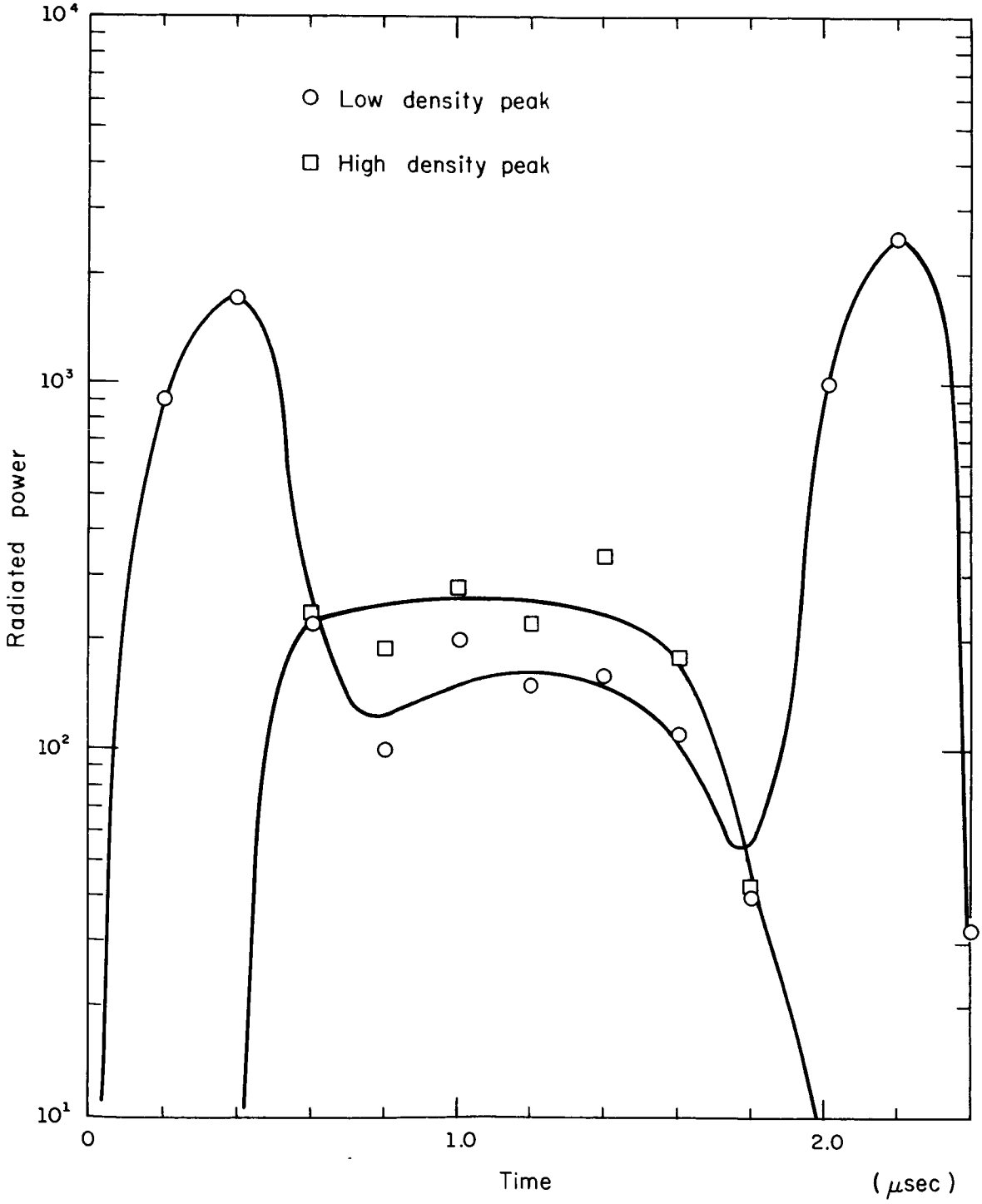

Fig. 3.5. Time-resolved spectrum.

(OVERLEAF BLANK)

for both 32 and 8 GHz. The splitting was smaller at 8 GHz and the lines were not distinct. The origin of this effect is not understood at the moment; it will be the subject of future investigations.

H. Böhmer
C. Mendel

3.2 Equilibrium Electron Gas

In continuation of work on the equilibrium properties of a classical electron gas,[7] we attempt to formulate kinetic equations based on the picture of field-particle scattering. We start with the Hamiltonian,

$$H = \sum_{i=1}^{n} (1/2m)[p_i+(e/c)\underset{\sim}{A}(x_i)]^2 + (1/8\pi)\int |\underset{\sim}{E}(x)|^2 d^3x, \tag{1}$$

where $\underset{\sim}{E}(x)$ is electric field strength and $\underset{\sim}{A}(x)$ its vector potential, so that

$$\underset{\sim}{E}(x) = -\frac{e}{c}\frac{\partial}{\partial t}\underset{\sim}{A}(x).$$

$\underset{\sim}{E}(x)$ and $\underset{\sim}{A}(x)$ are expanded in Fourier series:

$$\underset{\sim}{E}(x) = \sum_{\underset{\sim}{k}} \underset{\sim}{E}_k e^{i\underset{\sim}{k}\cdot\underset{\sim}{x}},$$

$$\underset{\sim}{A}(x) = \sum_{\underset{\sim}{k}} \underset{\sim}{A}_k e^{i\underset{\sim}{k}\cdot\underset{\sim}{x}}.$$

If we put

$$\underset{\sim}{A}_k = \hat{a}_k Q_k \sqrt{(4\pi c^2)}, \tag{2a}$$

$$\underset{\sim}{E}_k = \hat{a}_k P_{-k} \sqrt{(4\pi)}, \tag{2b}$$

then Q_k and P_k are canonical variables of the field, for electrons we use

---

[7] To be published in 1966 October issue of Rev. Mod. Phys.; CSL Report R-276, Univ. of Ill. (1966).

second-quantized operators c_p and c_p^+. In these variables the Hamiltonian H is written

$$H = \sum_{\underset{\sim}{p}} \epsilon_p c_p^+ c_p - \frac{1}{2}\sum_{\underset{\sim}{k}}(P_k P_{-k} + \omega_p^2 Q_k Q_{-k}) + \sum\sum_{\underset{\sim}{k}\underset{\sim}{p}} m(\underset{\sim}{p},\underset{\sim}{k}) Q_k c_p^+ c_{p-k}$$

$$- \sum_{\underset{\sim}{k}\neq\underset{\sim}{k}'} \sum_{\underset{\sim}{p}} \sum \ell(\underset{\sim}{k},\underset{\sim}{k}') Q_k Q_{-k'} c_p^+ c_{p-k+k'}, \tag{3}$$

in which $\epsilon_p = \hbar^2 p^2/2m$, $m(\underset{\sim}{p},\underset{\sim}{k}) = v_{p-k}^p \sqrt{(4\pi e^2/k^2)}$ with $\hbar v_{p-k}^p = \epsilon_p - \epsilon_{p-k}$, $\ell(\underset{\sim}{k},\underset{\sim}{k}')$ $= (2\pi e^2/m)(\hat{a}_k \cdot \hat{a}_{k'})$, and $\omega_p^2 = 4\pi n e^2/m$. The commutation relations are

$$[Q_k, P_{k'}] = i\hbar\delta_{kk'} \qquad \text{etc.},$$

$$\{c_{\underset{\sim}{p}}, c_{\underset{\sim}{p}'}^+\} = \delta_{\underset{\sim}{p},\underset{\sim}{p}'} \qquad \text{etc.}$$

and field operators commute with particle operators. The Hamiltonian H is supplemented by the divergence theorem,

$$S_k |\Psi_n\rangle = 0 \tag{4a}$$

with

$$S_k = P_{-k} - i\sqrt{(4\pi e^2/k^2)} \sum_{\underset{\sim}{p}} c_{\underset{\sim}{p}}^+ c_{\underset{\sim}{p}+\underset{\sim}{k}} \tag{4b}$$

where $|\Psi_n\rangle$ is an eigenfunction,

$$H|\Psi_n\rangle = E_n|\Psi_n\rangle.$$

One can show that the operator S_k commutes with H, hence is constant in time:

$$i\hbar \frac{\partial S_k}{\partial t} = [S_k, H] = 0.$$

Based on the Hamiltonian (3) we set up operator equations. Taking their ensemble average we get a hierarchy of equations. Neglecting higher order

correlations, which is equivalent to self-consistent field approximation or random phase approximation, we have

$$i\hbar \frac{\partial}{\partial t}\langle c_p^+ c_p \rangle = -i\Sigma_{\underset{\sim}{k}} (\underset{\sim}{k}\cdot\frac{\partial}{\partial \underset{\sim}{p}}) m(\underset{\sim}{p},\underset{\sim}{k}) \mathrm{Im}\langle Q_k c_p^+ c_{p-k}\rangle \tag{5}$$

and

$$i\hbar \frac{\partial}{\partial t}\langle Q_k c_p^+ c_{p-k}\rangle = -i\hbar\langle P_{-k} c_p^+ c_{p-k}\rangle - \hbar v^p_{p-k}\langle Q_k c_p^+ c_{p-k}\rangle$$

$$-m(\underset{\sim}{p},k)\langle Q_k Q_{-k}\rangle (\underset{\sim}{k}\cdot\frac{\partial}{\partial \underset{\sim}{p}})\langle c_p^+ c_p\rangle . \tag{6}$$

Through the subsidiary condition (4) we have

$$\langle P_{-k} c_p^+ c_{p-k}\rangle = i\sqrt{(4\pi e^2/k^2)}\langle c_{p-k} c_{p-k}\rangle [1-\langle c_p^+ c_p\rangle]$$

$$+i\sqrt{(4\pi e^2/k^2)} \sum'_{p'\neq p-k} \langle c_{p'}^+ c_{p'+k} c_p^+ c_{p-k}\rangle , \tag{7}$$

while the equation for $\langle c_{p'}^+ c_{p'+k} c_p^+ c_{p-k}\rangle$ is

$$i\hbar \frac{\partial}{\partial t}\langle c_{p'}^+ c_{p'+k} c_p^+ c_{p-k}\rangle = \hbar(v^{p'+k}_{p'} - v^p_{p-k})\langle c_{p'}^+ c_{p'+k} c_p^+ c_{p-k}\rangle$$

$$-m(p'+k,k)(\underset{\sim}{k}\cdot\frac{\partial}{\partial \underset{\sim}{p}'})\langle c_{p'}^+ c_{p'}\rangle\langle Q_k c_p^+ c_{p-k}\rangle$$

$$-m(p,k)(\underset{\sim}{k}\cdot\frac{\partial}{\partial \underset{\sim}{p}})\langle c_p^+ c_p\rangle\langle Q_{-k} c_{p'}^+ c_{p'+k}\rangle . \tag{8}$$

From the equations (6), (7), and (8) we solve for $\langle Q_k c_p^+ c_{p-k}\rangle$.

We take the classical limits: $\hbar \to 0$.

$$v^p_{p-k} \to \underset{\sim}{k}\cdot\underset{\sim}{v} \tag{9a}$$

$$\frac{1}{\hbar}\underset{\sim}{k}\cdot\frac{\partial}{\partial \underset{\sim}{p}} \to \frac{1}{m}\underset{\sim}{k}\cdot\frac{\partial}{\partial \underset{\sim}{v}} \tag{9b}$$

$$\langle c_p^+ c_p\rangle \to n f_o(v) \tag{9c}$$

and denote

$$-\langle Q_k Q_{-k}\rangle = V_k(t) \tag{10a}$$

$$\sqrt{(4\pi e^2/k^2)}\langle Q_k c_p^+ c_{p-k}\rangle = ng(\underset{\sim}{k},\underset{\sim}{v},\underset{\sim}{t}). \tag{10b}$$

After taking Laplace transform of the equations (6), (7), and (8), the problem is reduced to solving singular integral equation:

$$k(u+\omega)\epsilon^+(k,u+\omega)\bar{g}(k,u,\omega) = i\bar{a}_o(k,u,\omega)+i(4\pi e^2/k^3\omega)\bar{f}_o(u)$$

$$+(4\pi e^2/m)u\bar{f}_o'(u)V_k(\omega)-(\omega_p^2/k)u\bar{f}_o'(u)\int_{-\infty}^{+\infty} du'\,\bar{g}^{(*)}(k,u',\omega)/(u'-u-\omega), \tag{11}$$

where

$$g(\underset{\sim}{k},\underset{\sim}{v},\underset{\sim}{\omega}) = \int_0^\infty dt\, g(\underset{\sim}{k},\underset{\sim}{v},\underset{\sim}{t})e^{ik\omega t},$$

$$\bar{g}(k,u,\omega) = \int_{-\infty}^{+\infty} dv_2 \int_{-\infty}^{+\infty} dv_3 g(\underset{\sim}{k},\underset{\sim}{v},\underset{\sim}{\omega})$$

with $\underset{\sim}{k} = (k,0,0)$, and $\underset{\sim}{v} = (u,v_2,v_3)$, $\epsilon^+(k,u+\omega)$ = dielectric constant, and $a_o(\underset{\sim}{k},\underset{\sim}{v},\underset{\sim}{\omega})$ = a function involving initial conditions. One can solve equation (11) exactly through techniques as outlined in the books by, e.g. Muskhelishvili,[8] Balescu,[9] and Montgomery-Tidman.[10]

Depending on how one groups terms, one can express the final results in two ways. One is

---

[8] N. I. Muskhelishvli, "Singular Integral Equations," Noordhoff N.V., Groningen, Holland, 1953.

[9] R. Balescu, "Statistical Mechanics of Charged Particles," Interscience Publishers, New York, 1963.

[10] D. C. Montgomery and D. A. Tidman, "Plasma Kinetic Theory," McGraw-Hill, New York, 1964.

$$\frac{\partial}{\partial t} f_o(\underset{\sim}{v}) = \sum_k (\pi\omega_p^2/mnk^2) W_k(t) (\underset{\sim}{k}\cdot\frac{\partial}{\partial \underset{\sim}{v}}) \delta(\underset{\sim}{k}\cdot\underset{\sim}{v}-\omega_k) (\underset{\sim}{k}\cdot\frac{\partial}{\partial \underset{\sim}{v}}) f_o(\underset{\sim}{v})$$

$$+\sum_k (2\pi^3 e^2 \omega_p^4/mk^4\gamma_k) (\underset{\sim}{k}\cdot\frac{\partial}{\partial \underset{\sim}{v}}) \delta(\underset{\sim}{k}\cdot\underset{\sim}{v}-\omega_k)$$

$$\times\int d^3v' \left[f_o(\underset{\sim}{v}') (\underset{\sim}{k}\cdot\frac{\partial}{\partial \underset{\sim}{v}}) f_o(\underset{\sim}{v}) - f_o(\underset{\sim}{v}) (\underset{\sim}{k}\cdot\frac{\partial}{\partial \underset{\sim}{v}'}) f_o(\underset{\sim}{v}')\right] \delta(\underset{\sim}{k}\cdot\underset{\sim}{v}-\underset{\sim}{k}\cdot\underset{\sim}{v}') \tag{12}$$

$$\frac{\partial}{\partial t} W_k(t) = -2\gamma_k W_k(t) \tag{13}$$

and the other way is

$$\frac{\partial}{\partial t} f_o(\underset{\sim}{v}) = \sum_k (4\pi^2 e^2/mk^2) \left[\frac{1}{m}\mathcal{E}_k(t) (\underset{\sim}{k}\cdot\frac{\partial}{\partial \underset{\sim}{v}}) \delta(\underset{\sim}{k}\cdot\underset{\sim}{v}-\omega_k) (\underset{\sim}{k}\cdot\frac{\partial}{\partial \underset{\sim}{v}}) f_o(\underset{\sim}{v})\right.$$

$$\left.+\omega_k (\underset{\sim}{k}\cdot\frac{\partial}{\partial \underset{\sim}{v}}) f_o(\underset{\sim}{v}) \delta(\underset{\sim}{k}\cdot\underset{\sim}{v}-\omega_k)\right] \tag{14}$$

$$\frac{\partial}{\partial t} \mathcal{E}_k(t) = -2\gamma_k \mathcal{E}_k(t) + (4\pi^2 ne^2/k^2)\omega_k^2 \int d^3v\ f_o(\underset{\sim}{v}) \delta(\underset{\sim}{k}\cdot\underset{\sim}{v}-\omega_k), \tag{15}$$

where

$$\mathcal{E}_k(t) = W_k(t) + (4\pi^2 ne^2/k^2)(\omega_k^2/2\gamma_k) \int d^3v\ f_o(\underset{\sim}{v}) \delta(\underset{\sim}{k}\cdot\underset{\sim}{v}-\omega_k) \tag{16}$$

and it can be shown that

$$(1/4\pi) |\underset{\sim}{E}_k|^2 = \tfrac{1}{2}[\mathcal{E}_k(t) + \mathcal{E}_{-k}(t)]. \tag{17}$$

We note that the first term of the right-hand side of equation (12) is what one obtains in the quasi-linear theory starting from Vlasov's equation[11] and the second is the well-known Balescu-Leonard collision integral term. The coupled equations

[11] W. E. Drummond and D. Pines, Ann. Phys. 28, 478 (1964).

(14) and (15) are essentially identical with those of Klimontovich[12] and Pines and Schrieffer.[13] These equations are valid either for stable or unstable system. For the latter case one has to consider mode-mode coupling, i.e., to go beyond random phase approximation to be able to explain the stabilization process. One should note that in the present theory no assumption is made about the homogeneity of the system.

It is straightforward to extend our theory to consider motions of ions. The final results are identical again with those of Pines and Schrieffer.[13]

Taejourn Lie
Yoshi H. Ichikawa

---

[12] Yu. L. Klimontovich, JETP 36, 999 (1959) (translation).

[13] D. Pines and J. R. Schrieffer, Phys. Rev. 125, 804 (1962).

4. RAREFIED GAS DYNAMICS

B. L. Hicks
M. Jordan
H. J. Schmidt
M. A. Smith
Y. Wu
S. M. Yen

Boltzmann Equation[†]

Professors Hicks and Yen attended the Fifth International Symposium on Rarefied Gas Dynamics at Oxford University July 4 to 8, 1966, and presented two papers, one by Nordsieck and Hicks and the other by Yen and Hicks. The papers provoked much interest because we described the first and only method of evaluating the Boltzmann collision integral for conditions far from equilibrium. These papers, therefore, marked the beginning of a new era in applications of the Boltzmann equation to problems in kinetic theory.

The usefulness of all of the papers presented at the symposium was reduced because at the most only 12 minutes was allowed for a presentation. The calibre of the papers was quite variable, but the contacts established with scientists from many European countries was most worthwhile.

In the Progress Report for February, 1966, we reported a least-squares correction of the collision integral which insures that the conservation laws are satisfied for shock waves. We discovered that it was best to weight the corrections in proportion to the square of the value of the collision integral as we had done earlier with the pseudo-shock.

With the new weighting of the correction we made a series of tests of the convergence of the iteration method of solving the Boltzmann equation for a shock wave. We made calculations for a Mach number of 2.5 with 3 to 17 positions within a shock. Tests indicated that convergence could be clearly

[†]This work was supported in part by the Office of Naval Research under Contract No. ONR N00014-66-C0010-A01.

demonstrated if we used the same set of collisions for each iteration. With the same set of samples for each iteration, our current results show rapid convergence even for small samples of collisions. We are also testing the uniqueness of the solutions and appear to be getting favorable results. Both types of tests are continuing and will be expanded to include other Mach numbers.

We have been studying the relaxation of the lateral temperature, the Boltzmann function, and the velocity distribution function for the pseudo-shock near the beginning of the relaxation process (collision number η less than 0.2). Mach numbers considered are 1, 2, and 4. The lateral temperature appears to relax exponentially, and the relaxation curves (plotted against η) for different Mach numbers appear to be similar. (These findings are in agreement with the results of the previous study as given in CSL Report R-236.) However, the Boltzmann function deviates slightly from exponential behavior for M = 2 and 4. We have obtained the relaxation curves of the velocity distribution function for ten to fifteen selected velocity bins. We may divide these curves into two groups:

(1) those with exponential relaxation similar to the lateral temperature (the rate of relaxation varies with the location of the velocity bin); (2) those with non-exponential relaxation.

5. HIGH-VOLTAGE BREAKDOWN[†]

E. M. Lyman
D. Alpert
W. R. Anderson
G. Arndt
T. C. Casale
D. A. Lee
J. S. Meyer
W. Schuemann
H. E. Tomaschke

5.1 The Effect of Gas Pressure on Electrical Breakdown and Field Emission

One of the significant consequences of the physical picture for the initiation of electrical breakdown between metallic electrodes in ultrahigh vacuum, as previously reported,[1] has been the development of a physical explanation for the so-called "gas effect" which has often been noted but heretofore not understood. Several authors[2,3,4] have noted that when a gas was introduced into the vacuum system to a pressure of about 10^{-4} Torr, the predischarge currents were typically reduced and the breakdown properties improved. The observed effects were not strongly dependent upon the nature of the gas; in particular, no significant differences were noted as between noble and molecular gases of comparable mass. We have observed similar effects when gas is admitted to systems containing clean tungsten electrodes.

Since the gap spacings in most of the above experiments were smaller than the mean free path for atomic collisions, the "gas effect" could not readily be attributed to interactions in the volume; yet an effect sensitive to the

---

[†]Supported in part by the National Aeronautics and Space Administration under Grant NGR 14 005 038 and by the University of Illinois.

[1]D. Alpert, D. A. Lee, E. M. Lyman, and H. E. Tomaschke, J. Vac. Sci. Technology 1, 35 (1964).

[2]C. M. Turner, Phys. Rev. 81, (1951).

[3]J. L. McKibben and K. Boyer, Phys. Rev. 82A, 315 (1951).

[4]E. G. Linder and S. M. Christian, J. Appl. Phys. 23, 1213 (1952).

pressure, but not to the chemical nature of the gas, seemed to be equally difficult to ascribe to atomic interactions at the electrode surfaces.

To explain this so-called "gas effect," we assume as a starting point the breakdown model[1] based on field emission from submicroscopic projections. When gas is introduced, the significant decrease in field emission is here attributed to the selective sputtering of the emitting whiskers by ions formed in the volume by electron bombardment of the gas molecules. If the ions were created uniformly in the gap volume, the probability of striking a given projection would be very small indeed, since the cross-sectional area of an individual emitter lies in the range of 10^{-12} to 10^{-10} cm^2. However, as is suggested by the schematic representation in Fig. 5.1, the formation of ions by impinging electrons is not uniformly distributed; on the contrary, it is restricted to localized regions adjacent to the emission sites. Hence, these ions have a much higher probability of striking the corresponding emitting projection, and they do so with sufficient energy to cause sputtering and thus a change in geometrical shape.

In view of the complex dependence of the probability of ionization on the energy of colliding electrons, it is not easy to make an accurate calculation of the number and distribution of the ions formed in the volume. However, it is possible to make certain order-of-magnitude estimates which provide quantitative support and added plausibility for the above picture. Consider the following hypothetical situation, which is derived from a rather typical experimental observation (with tungsten electrodes). For a broad area configuration with electrodes of about 3 cm diameter and 1 mm gap spacing, the breakdown voltage is approximately 60 kV, while the total current just prior to breakdown is of the order of 200 μA. Let us consider the ion production at some value below breakdown, say at an applied voltage, V_A, of 48 kV where the emission current is about 10 μA.

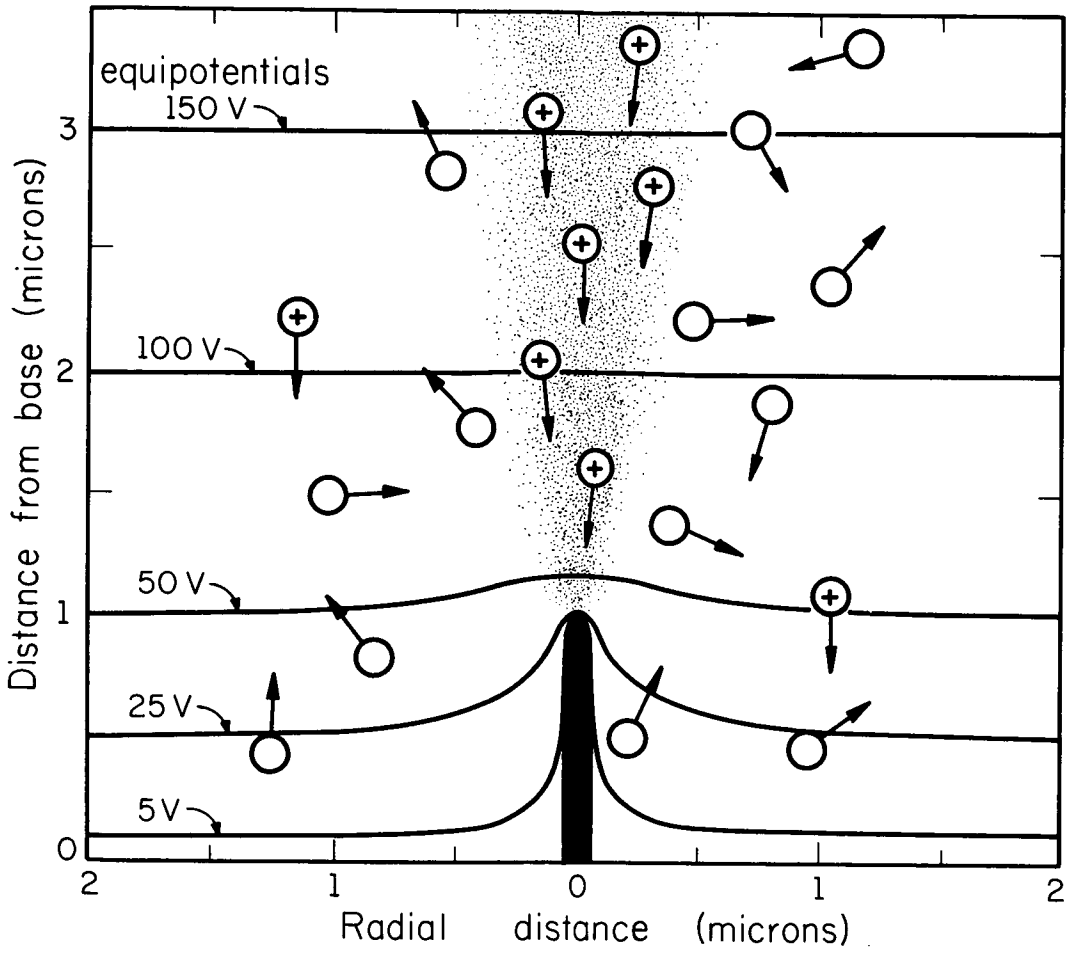

Fig. 5.1 Schematic representation of selective ion bombardment of a one-micron (10^{-4}-cm) projection. Calculated equipotentials are shown for an average electric field of 5×10^5 V/cm.

(OVERLEAF BLANK)

At a pressure (for nitrogen) of 10^{-4} Torr, the overall probability of forming ions in the volume by electron collision is estimated to be approximately 10^{-5} ions per electron for the above gap spacing. This assumes an average ionization efficiency of about 10% of the maximum value, which is approximately 10 ions/electron/cm path length/Torr, for an electron energy of 100-200 eV. (The efficiency drops off considerably for higher energies.) If the resulting ion current, 10^{-10} A were uniformly distributed over the entire cathode area, the number of ions striking unit area per second under these conditions would be about 10^{8} ions/cm^2/sec. This corresponds to the deposition of a monolayer of ionized gas in 10^{7} seconds, i.e., in the order of months, and would not result in rapid sputtering of the emitter tips.

The shape of a typical emitting whisker can be approximated by a prolate spheroid, as shown in the figure, roughly 10^{-4} cm in height and 10^{-5} cm in base diameter. Typically, the emitting area is some small fraction (a few percent) of the base area, and, for the dimensions shown, the localized enhancement of the electric field at the tip is approximately 100. Hence, even allowing for the spreading due to space charge,[5] the electrons traverse the gap in narrow pencil-like beams, originating only at the sharpest projections. Furthermore, the highest probability for ion production lies in the portion of the electron trajectory in which its energy is of the order of 100 eV, i.e., in the cylindrical microvolume immediately above the whisker and roughly of the same dimensions, as shown schematically in the figure.

When the applied voltage is 80% of the breakdown value, the local field at the emitter tip is approximately 5×10^{7} V/cm, while the average electric

---

[5] G. E. Vibrans, MIT Lincoln Laboratory Tech. Report 308 (1963). "Computation of the Spreading of an Electron Beam Under Acceleration and Space-Charge Repulsion."

field within the gap (for an enhancement factor of 100) is about 5×10^5 V/cm. As indicated by the calculated equipotentials superimposed in the figure, the energy of the electrons impinging on the neutral gas molecules ranges from 50 eV at a distance of 1.8×10^{-5} cm to 100 eV at 10^{-4} cm above the emitter tip. Corresponding energies are transferred to the ions when they impinge on the emitter surface. A crude calculation indicates that under these conditions of field and gas pressure, the current density is sufficient ($8 \times 10^5 A/cms^2$) that a sizeable fraction (several percent) of the neutral gas molecules entering the microvolume are ionized. In view of their proximity, a large fraction of these will strike the projection; the resulting rate of arrival of energetic ions at the emitting tip corresponds to tens of monolayers of gaseous ions per second at a pressure of 10^{-4} Torr.

Since energies of 50 to 100 eV are quite sufficient to cause sputtering or similar dislocation damage to the emitting whisker, this effect can readily explain a significant change in its shape. Assuming a typical sputtering efficiency of a few percent, a measurable change might be expected within minutes. It is estimated that the most rapid change in enhancement factor, β, under the above conditions occurs for projections about one-micron high. For smaller projections, the sputtering ions are not so strongly focused on the tip since they are created far from it; hence, β changes more slowly because the sputtering rate is low. For larger projections, since the fractional rate of removal of material is roughly inversely proportional to the linear dimensions, the rate of change of β is also less than for the one-micron whiskers. The exact rate of change of the enhancement factor would therefore depend on the size and shape of the projection, the gas and its pressure, the ionization probability, and the sputtering rates for the ions and electrode material in question.

Two experiments of a preliminary nature have been carried out to test the qualitative conclusions presented above. In the first, a small tungsten electrode was inserted into a modified field-emission microscope,[6] and the applied voltage adjusted to give a field-emission current of 10^{-6}A. With the voltage off, argon gas was admitted to a pressure of about 3×10^{-5} Torr. The voltage was then raised to the value at which the current reached its former value of 10^{-6}A. With the voltage off, argon gas was admitted to a pressure of about 3×10^{-5} Torr. The voltage was then raised to the value at which the current reached its former value of 10^{-6}A. With the voltage held constant at this value, the current was observed to rise rapidly to a maximum value of about 10^{-5}A (in a matter of a minute or less) and then to decrease more gradually to a new equilibrium value of 2 or 3×10^{-7}A. The time elapsed for the entire process was of the order of a few minutes. If the voltage was thereupon increased, the process would repeat, although the magnitudes of the current and time interval might vary, depending on the previous treatment of the cathode.

It seems reasonable to postulate that the initial increase in current is due to a sharpening of the whisker by the initial sputtering at glancing angles; the subsequent decrease in current is attributed to a more gradual dulling process as the tip of the projection is eroded away. Although changes in the work function of the emitting projection might also account for the changes in the emission current, the lack of sensitivity of the effect to the chemical nature of the gas suggests that this is not the dominant process.

In the second set of experiments the apparatus included the 3.5-cm diameter flat electrodes cut from a single-crystal tungsten boule and mechanically

---

[6] H. E. Tomaschke, University of Illinois Coordinated Science Laboratory Thesis, Report 192 (1964). "A Study of the Projections on Electrodes and Their Effects on Electrical Breakdown in Vacuum."

and electrically polished, as described[1]. After bakeout at 450°C and repeated breakdown runs in ultrahigh vacuum, the breakdown voltage approached a reproducible value of 36 kV ± 10% at a gap spacing of 0.71 mm. Thus, at breakdown, the average field, F_o, in the gap was 5.1×10^5 V/cm ± 10%. The emission current just below the breakdown point was 100 μA. The enhancement factor, β, as deduced from the Fowler-Nordheim plots was also fairly reproducible at β = 126 ± 10% and the critical field $F_{crit} = \beta F_o$ at the emitter tips at breakdown was 6.4×10^7 V/cm, in substantial agreement with earlier results.

Argon gas was then introduced into the system to a pressure of 10^{-4} Torr while the voltage was held at 28 kV. The initial current of 5 μA increased immediately to 10 μA, then fell slowly over a period of several hours to 0.5 μA. The x-ray yield was at all times proportional to the current, showing that the current was mainly due to electrons having the full gap energy. Additional gas treatments, totaling about 15 hours, further suppressed the current to about ½% of its original value, where it remained, or decreased slightly when the system was evacuated. The enhancement factor of the conditioned surface was measured to be 90, with a corresponding increase in breakdown voltage to 41 kV.

In a second type of experiment with the broad-area electrodes, after admitting gas at 10^{-4} Torr, the current was held constant at 100 to 300 μA by continuously adjusting the voltage upward as surface conditioning proceeded. In one run, the enhancement factor was lowered to 26 with an accompanying increase in the breakdown voltage to 116 kV, corresponding to an average field in the gap of $F_o = 1.6 \times 10^6$ V/cm at breakdown. It should be remarked that the volt-ampere characteristic from which β is deduced cannot be measured with gas present because the surface changes occurring during the measurement render the data unreproducible.

Table I. Vacuum Insulation Properties of Flat Tungsten Electrodes 3.5 cm in Diameter

	V_{BD}(kV)	β	F_{crit}($\frac{MV}{cm}$)	F_o($\frac{MV}{cm}$)	area(cm^2)
A. Gap = 0.71 mm					
1. New, baked out	36	126	64	0.51	7.6×10^{-11}
2. After low-current gas conditioning	41	90	52	0.58	
3. After outgassing anode	59	71	59	0.83	8.1×10^{-12}
4. After anode outgas and gas conditioning	116	26	43	1.63	1.6×10^{-9}
5. Ratio: $\frac{\text{Row 4}}{\text{Row 1}}$	3.2	1/4.8	1/1.5	3.2	21.
B. Gap = 0.25 mm					
6. New, baked out	13	94	49	0.52	5.2×10^{-12}
7. After gas conditioning	22	60	53	0.88	2.9×10^{-10}
8. After gas conditioning, anode at LN temp.	33	36	47	1.32	7.2×10^{-10}
9. After anode outgas and gas conditioning	52	19	40	2.08	3.5×10^{-9}
10. Ratio: $\frac{\text{Row 9}}{\text{Row 6}}$	4.0	1/4.9	1/1.2	4.0	67.

The observed vacuum-insulation properties of the electrodes at gap spacings of 0.71 mm and 0.25 mm at various stages of the gas conditioning are illustrated in Table I.

From the table it can be seen that the combination of selective sputtering and anode outgassing may decrease the enhancement, β, by a factor of about 4 with a corresponding increase of the voltage-holding capabilities by a factor of 3 to 4. In one run at 0.25-mm gap, a value of $\beta = 14.5$ was achieved with a breakdown voltage of 81 kV corresponding to an average field in the gap of over 3×10^6 V/cm.

The emitting area increases greatly as the sharp tips are blunted during selective sputtering. Consequently, the predischarge emission current near breakdown for the conditioned electrodes may be from one to two orders or magnitude higher than for the fresh electrodes. As a practical matter in vacuum insulation, anode heating and x-radiation may become a more serious problem because of the combination of high voltage and high current. On the other hand, even taking into account the increase in area, a reduction in enhancement factor from 100 to 20 should, on theoretical grounds, be accompanied by a reduction in field-emission current by almost 20 orders of magnitude. Experimentally, for the 0.25-in gap with 81-kV breakdown voltage, the current dropped to our lowest measurable value (10^{-10} A) at an applied voltage of 42 kV corresponding to an average field in the gap of 1.7×10^6 V/cm.

Estimates of the time constants for blunting of the new sharp whiskers formed during a spark were made by observing the fading of the transition radiation that appears on the anode opposite a new emitter point. At 10^{-4} Torr and 1 mA emission current, the fading of a sharp blue spot into the general blue background (due to many weaker emitters) occurred in a few seconds. At 10^{-5} Torr, the time

constant was of the order of tens of seconds except for giant emitters which heated the anode spot white hot. As predicted above, these large protrusions were not noticeably affected by the sputtering and could only be burned off with great difficulty at high currents (5 mA). After blunting of the sharpest whiskers, the rate of decrease of enhancement factor is small. Conditioning to the point indicated in Row 9 of the table required about 20 hours.

These results differ in one important way from those of earlier workers who reported that the voltage holding properties returned to their original characteristics (breakdown voltage) almost immediately after the gas was removed and the system evacuated. Preliminary observations on this system (at 3×10^{-10} Torr) indicate a time of the order of a week or two for the increase of β by a factor of two. It can only be conjectured here that the surface contamination in these earlier experiments may have contributed to the redevelopment of sizeable protuberances as soon as the selective sputtering process was terminated or that the conduction and its suppression were associated with inherently different physical mechanisms. It may also be conjectured that the final values of breakdown parameters reached in our experiments represent an equilibrium between blunting and regeneration of protrusions on the cathode.

Our detailed experiments have thus far been carried out only with tungsten electrodes. It will be of considerable interest to continue these studies with other materials as well, to determine the effects of selective ion bombardment and the rate of formation of new whiskers after the gas is removed.

E. M. Lyman
D. Alpert
D. Lee

5.2 Flicker Effect

The object of this work is to study the so-called flicker effect in field emission which may be postulated to be due to the adsorption and desorption of gas molecules at emission sites. The interesting characteristic of the effect is the rigorously bistable nature of the current from the flickering spot on the field-emission pattern of an emitting tip. By obtaining Fowler-Nordheim plots of the current-voltage characteristics of the spots in the "on" and "off" modes, one might hope to provide some quantitative clues as to the physical phenomenon involved.

A simplified version of the Young-Müller[7] apparatus was constructed in which a small portion of the emission pattern from the cathode tip was passed through a small hole in the anode and the current was collected in a Faraday cup. Two versions of the apparatus were constructed. In the first, the portion of the emission pattern striking the anode hole was selected by magnetic deflection, which, due to the nature of the design, interacted with the accelerating voltage and gave non-linear Fowler-Nordheim plots. In the second, the tip and an anode ring were mechanically rotated to admit the desired portion to the cup.

The operation of the second version appears to be satisfactory, but no data have been obtained with it. The experiment will be resumed at a later date.

5.3 Whisker Production

5.3.1 Field-Emission Study. In previous work[8] with closely-spaced, small electrodes it was found that under certain conditions, namely with a

---

[7] R. D. Young and E. W. Müller, J. Appl. Phys. 33, 91 (1962).

[8] H. E. Tomaschke, University of Illinois, Coordinated Science Laboratory, Thesis, Report R-192 (1964).

gas-covered anode, numerous, fine, whisker-like projections could be produced on the emitter. (These whiskers were observed with an electron microscope.) The production of these whiskers was associated with an "unstable" behavior of the emission characteristics in which large current fluctuations were observed. It was decided to continue this study using field-emission techniques. The procedure used was as follows: First the emission pattern from an emitter was viewed on a screen. Next, an anode was interposed between the emitter and screen and was positioned at a small distance from the emitter. This anode was purposely not outgassed so that ions produced at its surface could bombard the emitter surface and, in theory, produce sites for whisker growth. The third step was to swing the anode out of the way and again view the emission pattern on the screen. The presence of whiskers would be expected to produce a number of new spots of illumination on the screen.

The experimental apparatus included a phosphor-coated disk mounted on a press at one end of the cylindrical bell jar. From the same press, support wires projected out past the disk into the bell jar. An emitter which faced the disk was mounted on these support wires. The emitter consisted of the blunt end of a 3-mil tungsten wire spotwelded to a 10-mil tungsten filament. A press mounted on a metal bellows was attached to the other end of the bell jar. A loop of 10-mil tungsten wire serving as the anode was spotwelded to the support wires from this second press. This loop could be interposed between the emitter and the disk.

Although the data obtained from this apparatus are relatively meager, the results have all been negative. That is, after placing the anode next to the emitter and operating in the "unstable" mode, i.e., with large current

fluctuations, for periods as long as one hour, there were no indications in the emission pattern that whiskers had been produced on the emitter.

In continuing this study, it now seems necessary to look carefully for differences in the present procedure as compared with that used previously (in the electron-microscope case) in which fine whiskers were observed. One obvious difference is that in the previous case the cathode was alternately subjected to ion bombardment in an ultrahigh vacuum and then subjected to electron bombardment in an oil-contaminated system.

5.3.2 Electron-Microscope Study. In addition to the search for whisker production using the field-emission microscope as the detector, a search using an RCA Electron Diffraction Unit (a prototype of the Type EMD) in the shadow electron-microscope mode of operation has been started. Electrodes have been mounted in the specimen chamber. The blunt end of a 3-mil tungsten wire has been used as the cathode electrode. This electrode is mounted on a 10-mil tungsten loop for heating purposes. The electropolished end of a 100-mil tungsten rod has served as the anode. The gap spacing has been about 5 mils.

Changes in the cathode profile due to electrical breakdown have been observed. Both the destruction and the formation of projections have been noted.

Attempts to measure field-emission currents in order to plot F-N curves have been unsuccessful due to the large current fluctuations. Some reduction in fluctuation has been obtained by operating the cathode at elevated temperatures. Presumably this reduces the amount of contamination on the cathode.

Preliminary attempts to produce whiskers by operating in the "unstable" mode have given negative results. However, because of the poor vacuum conditions

it is questionable whether or not the observed current fluctuations are due to the same conditions as those which were present in the ultrahigh vacuum system in which the "unstable" mode was originally observed.

H. E. Tomaschke

(OVERLEAF BLANK)

6. SPACE SCIENCES

H. W. Knoebel
D. O. Skaperdas
D. H. Cooper
W. J. Bouknight
T. Chen
J. D. Gooch
G. R. Karr
B. D. Kirkwood
H. V. Krone
E. Marzullo
N. Mehta
H. C. Morrison
J. L. Myers, Jr.
R. Palamara
J. R. Ray
L. Schusterman
J. Shu

6.1 Gyro Materials[†]

In order to discover any problems associated with the use of glass under severe centrifugal stress, glass disks were spun to the bursting point in a motor-driven test fixture. According to elasticity theory, the maximum stress for a solid, spinning sphere is at the center and is approximately given by[1]

$$\sigma_{max} = \rho\omega^2 r^2 (3+2\mu)/(7+5\mu)$$

where ρ is the density, ω is the angular spin, r is the radius and μ is Poisson's ratio. For a thin, solid disk, the maximum stress is also at the center and is, to good approximation,

$$\sigma_{max} = \rho\omega^2 r^2 (3+\mu)/8$$

For glass, $\mu \approx 0.16$ so that the numerical factors become 0.425 and 0.395 for the sphere and disk, respectively. Hence, the maximum stresses are nearly the same for identical materials, diameters, and spin speed, which justifies the use of disks for this test.

[†]This work was supported in part by the National Aeronautics and Space Administration under Grant NsG 443.

[1]C. Chree, Cambridge Phil. Soc. Trans., Vol. 14, Part 3, (1889), p. 292.

Adequate protection was provided to absorb the energy when the glass structure failed. The glass disks were made of ordinary plate-glass window, 12 inches in diameter and 1/8 inch thick. An aluminum spindle was bonded at the center of the glass disk and the resulting structure was checked for balance about the spindle. The first glass disk sample was spun about its attached spindle and the speed slowly increased to 166 Hz, at which point the glass disk shattered into small particles. The second sample, which was not balanced as well as the first, failed at 145 Hz. The maximum stresses for the disk and sphere spinning at 150 Hz are about 3200 psi and 3400 psi, respectively. If the spin speed is reduced to 100 Hz, the maximum stress for the sphere becomes 1530 psi since the stress is proportional to the square of the spin rate. These tests tentatively indicate an upper spin-speed limit of about 100 Hz for the spherical glass satellite, with an adequate safety factor. Further spin tests will be conducted with better balanced disks and with the actual material when it has finally been selected for its proper volume resistivity at the satellite operating temperature.

D. Skaperdas

6.2 Satellite Observation Times and Mirror Normal Angles[†]

A digital computer program has been written to determine typical times of observation of a sunlight-illuminated satellite. At each instant of time for which the satellite is observable, the following quantities are computed: the slant range and elevation of the satellite, the unit-vector normal to a hypothetical mirror on the satellite which would reflect sunlight to the observing

[†]This work was supported in part by the National Aeronautics and Space Administration under Grant NsG 443.

station, and the angle of incidence of sunlight on the mirror. On a given pass, an actual observation is predicted if one or more of the satellite's mirror normals lie in the range of the hypothetical values calculated.

The program is initially being used to determine which mirror normals would produce the highest number of reflections to a given ground station. For a gyroscope-satellite in a circular equatorial orbit at 1000 km altitude, computer results show that ground stations within 17° of latitude from the equator would be able to track the satellite for about 1000 passes in one year (neglecting clouds). With the spin axis aligned along the Vernal Equinox, the maximum number of reflections from a single mirror is about 400 per year. These results are indicated in Fig. 6.1 for stations at 0° and 16.5° latitude, where the number of reflections in one year has been plotted vs. the mirror-normal angle measured from the spin axis. It is evident that mirror-normal angles between 40° and 140° would give the best results for the conditions given.

J. L. Myers, Jr.

6.3 Gas Drag[†]

The work on gas drag reported in earlier Progress Reports has been extended to include the effects of non-uniform heating and orbital regression. This work has been completed and is available from the Coordinated Science Laboratory.[2] When applied to the aerodynamic analysis, the orbital-regression

---

[†]This work was supported in part by the National Aeronautics and Space Administration under Grant NsG 443.

[2]Karr, G. R., "Aerodynamic Torque on a Spinning Spherical Satellite with Application to Measurement of Accommodation Coefficients," Report R-295, Coord. Science Lab, University of Illinois, Urbana, Ill., May, 1966.

analysis reveals the necessary orbital parameters needed to minimize the aerodynamic torque. The non-uniform heating effect is of the same class as surface roughening by dust particles, radiation damage, and other effects which cause localized changes in the surface accommodation coefficient, possibly giving rise to a torque. The non-uniform heating analysis, therefore, provides an example of the precession to be expected from this class of external effects.

The satellite spin axis parallel to the sun line in the orbital plane, as shown in Fig. 6.2, was taken as the worst case in calculating the non-uniform heating effect. The half surface always in the sunlight was assumed to have a uniform temperature and accommodation coefficient higher than the other half surface not illuminated by the sun's rays. The aerodynamic torque equations in a nonregressing orbit were then employed to find the maximum total angular precession occurring in one year. The precession rate is periodic and the angular deviation of the spin axis varies from zero to a maximum in a period of half a year. The maximum value, shown in Fig. 6.3, is seen to depend upon the accommodation-coefficient difference and the orbital altitude. At 600 miles, however, the precession can be kept to less than one-tenth the Schiff effect if the accommodation-coefficient difference is less than .01, a value which is reasonable in view of the experimental data available on this effect.

The orbital-regression analysis applied to the aerodynamic-torque problem results in solutions which are similar to the gravity-gradient analysis. The solutions are separable into two parts. One term will be of the same type as for the nonregressing orbit. The other part of the solution will contain terms of the orbital-regression frequency. These last terms have magnitudes dependent upon the orbital parameters and cannot, in general, be neglected. In order to keep these magnitudes low, certain tolerances are imposed on the orbital parameters.

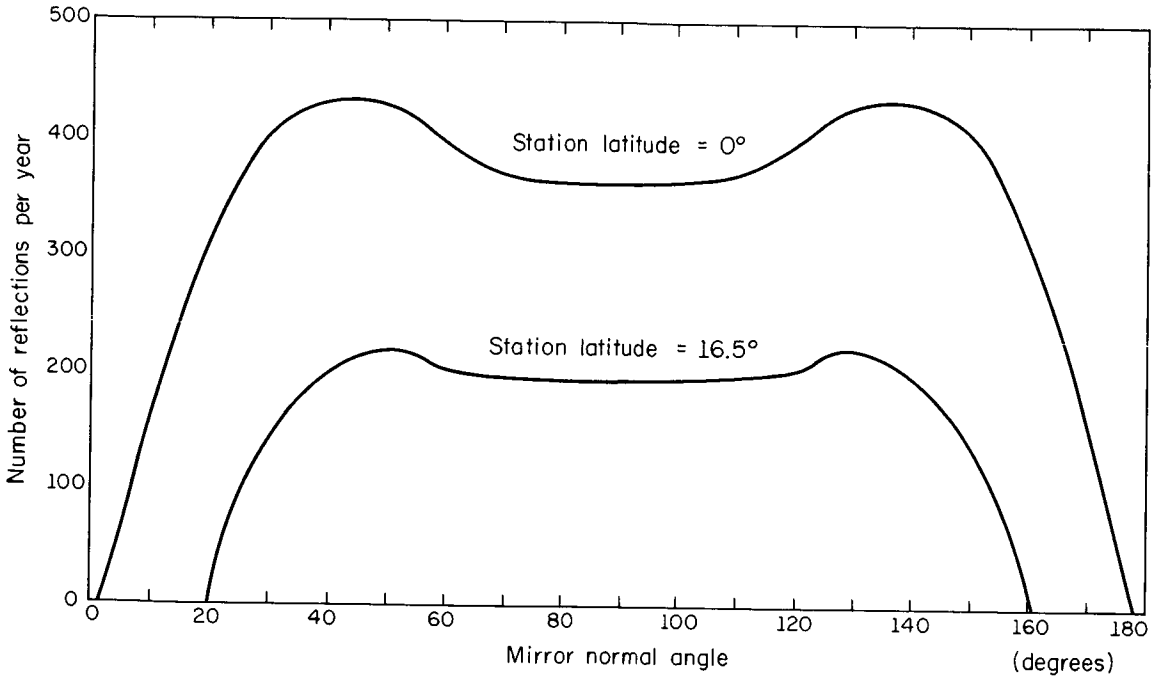

Fig. 6.1. Possible number of observations from two different stations plotted as a function of the angle of the mirror normal relative to the spin axis.

(OVERLEAF BLANK)

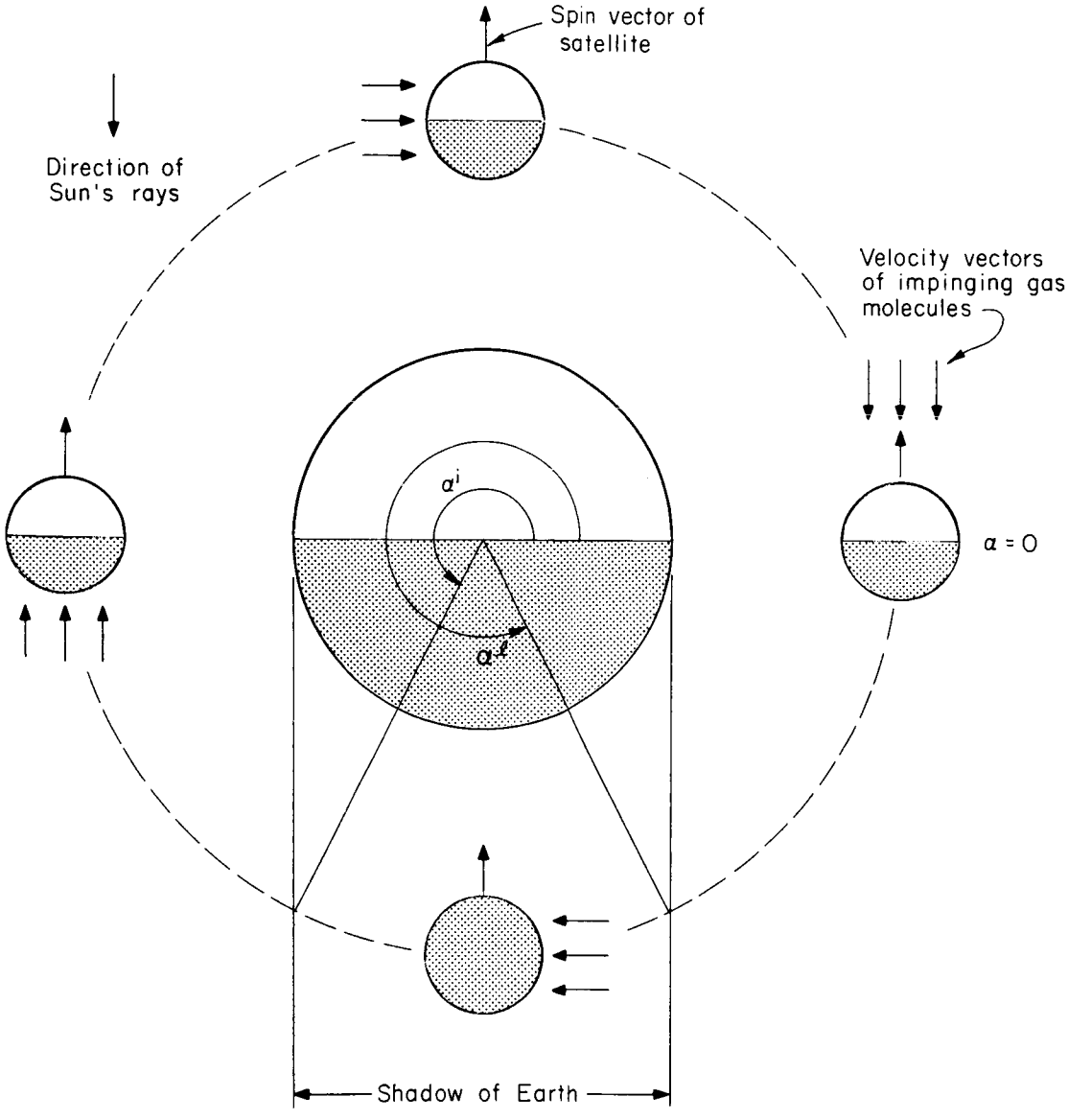

Fig. 6.2. Diagram showing opportunities for an interaction between gas drag and a nonuniform heating for an equatorial orbit.

(OVERLEAF BLANK)

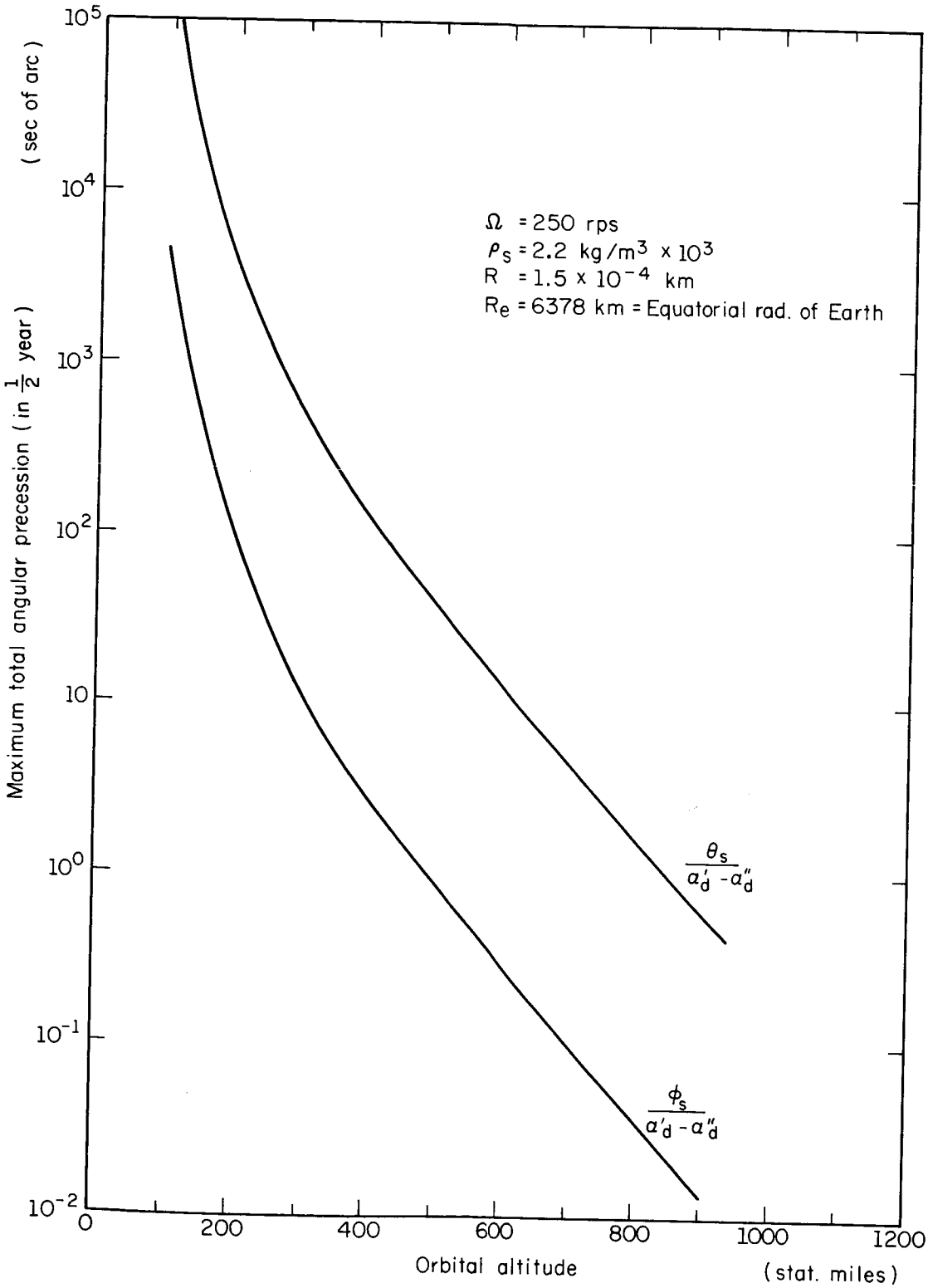

Fig. 6.3. Aerodynamic precession resulting from nonuniform heating plotted as a function of altitude.

(OVERLEAF BLANK)

For example, for the polar orbit, the following condition is obtained:

$$\Delta\epsilon/\alpha_d = 2(-2\delta \pm .056i) \text{ arc sec}$$

where $\Delta\epsilon$ is the satellite spin axis deviation from its original orientation, α_d is the accommodation coefficient, δ is the spin axis deviation in radians from the orbital plane, and i is the inclination in radians of the orbital plane normal to the equatorial plane. For a given $\Delta\epsilon/\alpha_d$ this equation establishes the tolerances for the orbital parameters δ and i.

G. R. Karr

6.4 Nondegenerate Mirror Configuration[†]

The previously-proposed mirror configuration, using mirrors identified as the facets of a truncated icosahedron, has involved a degeneracy of mirror-normal-to-spin-axis angles. For example, the choice of the normal to one of the pentagonal facets as the spin axis has involved a five-fold degeneracy, there being five facets at each angle for six angles, not counting the spin facets. Any error in fixing the spin axis, ranging from several seconds of arc to as much as 900 seconds, would provide a partial splitting of the degeneracy, partial in the sense that the glitter flash pattern would be broadened into a complicated difficult-to-analyze pattern, as described previously.[3]

The difficulty in analysis of such patterns is not one of principle, but may require the analysis of photoelectric data in addition to the photographic

[†]This work was supported in part by the National Aeronautics and Space Administration under Grant NsG 443.

[3]Prog. Report for March, April, May, 1965, p 16, Coord. Science Lab., Univ. of Illinois Urbana, Ill.

data, because of the limited resolution in the latter. Such analysis could prove very costly. Removal of the degeneracy could be achieved by placing the spin axis away from any facet normal by more than 0.25^{o} (900 seconds) figure. The result could, for the same mirror configuration, be 32 different mirror angles with a five-fold reduction in the number of flashes in each pattern. While there would be a slightly more than five-fold increase in the number of opportunities (angle diversity) to make flash-pattern observations, there is some doubt as to whether the observing net could exploit this increase effectively. Also, since the individual flashes would not be resolved, this degeneracy removal would cost a five-fold reduction in photographic exposure. Such a large cost is felt to be decisive against this means of degeneracy removal.

The choice of a fewer number of facets reduces the cost, in terms of a sacrifice in photographic brightness, for removing redundancy. The five-fold loss in number of facets is almost exactly made up by a slightly more than five-fold gain in individual facet area through choosing a cube of the same weight as the truncated icosahedron. There still remains the six-fold diversity of facet angles. An alternate choice would be the tetrahedron of the same weight, but with four facets each offering an 80% increase in area over the individual cubic facets, but also offering only a four-fold diversity in angles. These two also have spherical figures of inertia.

A comparison in merit for these two is not altogether straightforward, however. The loss in angle diversity for the tetrahedron could be important for the proposed observation net. Also, it will undoubtedly be the case that one would want to "round-off the corners" of these figures to make the stress pattern, under high-speed rotation, conform more nearly to that for spherical objects. Such a decision will seriously damage the apparent area advantage

of the tetrahedron. The choice appears to lie with the cube.

A decision to "round-off the corners" of the cube offers the opportunity to make part of the surface into a specularly-reflecting sphere. This part of the surface could then be used to photograph the object at such times that the glitter flashes would not be observed, using a tracking camera, and obtaining supplementary orbit data. Such data could be especially helpful during the early days of the experiment.

For a camera tracking with an angular speed error of ϵ percent, the effective exposure time is $(100/\epsilon)\theta r/v$, in which θ is the resolution of the camera, about 25×10^{6}m/0.5m = 5×10^{-5} radian, r is the slant range, taken to be 2500km, and v is the orbital speed taken to be 7.5km/sec. If the luminous flux is F at the satellite, taken to be 1.25×10^{5}lumens/m^2, then the flux at the camera is $Fd^2/16r^2$, in which d is the diameter of the sphere, taken to be 0.3m. The exposure E at the camera must be 8×10^{-11}lumen-sec/m^2 to achieve the reliable density of 0.3 to 0.4 logarithmic units above background. The required tracking accuracy is $\epsilon = (100/E)(\theta/v)(Fd^2/16r)$, which is 2.34%, using the above numbers. If only half the area of the body be devoted to such a spherical surface the tracking accuracy would have to be about 1.2%. One would expect this to be achievable with the help of telemetered data obtained during the launch phase.

The cost of providing such a continuous-tracking facility is such as to reduce the facet area to about half what it would have been for the cube. However, it is unfair to levy all this cost against continuous tracking, since the corners of the cube would be rounded-off anyway. In addition to providing the spherical surface, it would be necessary to remove some material to provide a salient moment of inertia. The desired adjustment would involve two flats on a sphere, each having a diameter about 10% of the spherical diameter.

These flats would locate the spin axis, be located on the spherical part of the surface, and serve as spin facets, since little area is required for that function. A complete model has been worked out based on a 3-inch diameter, shown in Fig. 6.4.

The specifications of this model scaled to a 0.3-m diameter offer the following parameters: the spherical diameter is 30cm; the total area of the six facets is one half the area of the 30-cm sphere, each facet being 17.32cm in diameter, with an area of $236cm^2$; the flat-to-flat diameter is 24.5cm; and the angles of the mirror normals relative to the spin axis are 42, 54, and 72 degrees, with provision for two 3-cm spin facets.

To begin the calculation of photographic observability, it is interesting to calculate first the slant range at which the individual flashes begin to be resolved. For greater ranges, the photographic exposure varies inversely with the slant range. For the shorter ranges, it varies inversely with the square of the range. For a speed of 7.5km/sec and a flash rate of 100Hz, the flash spacing along the orbit is 75m. This subtends an angle of 5×10^{-5} radian for a slant range of 2.5×10^6m or 2500km.

At a spin rate of 100Hz, the maximum flash duration is 7 microseconds. Using a mirror area of $236cm^2 = 2.36 \times 10^{-2} m^2$, one "sees," at a slant range of 2500km a portion of the sun's disc through $2.36 \times 10^{-2} / (2.5 \times 10^6)^2 = 0.38 \times 10^{-14}$ sterradian. However, the sun's disc subtends 0.68×10^{-4} sterradian, a reduction in luminous flux by the factor 0.56×10^{-10}. Thus the incident flux of 1.25×10^5 lumens/m^2 becomes, at the camera, 0.7×10^{-5} lumen/m^2. At 7 microseconds, the exposure is 4.9×10^{-11} lumen-sec/m^2. This is a little more than half the nominal value of 8×10^{-11} cited above.

Doubling the spin rate would reduce the resolving range by half, quadruple the light intensity, and halve the exposure time, so that the exposure

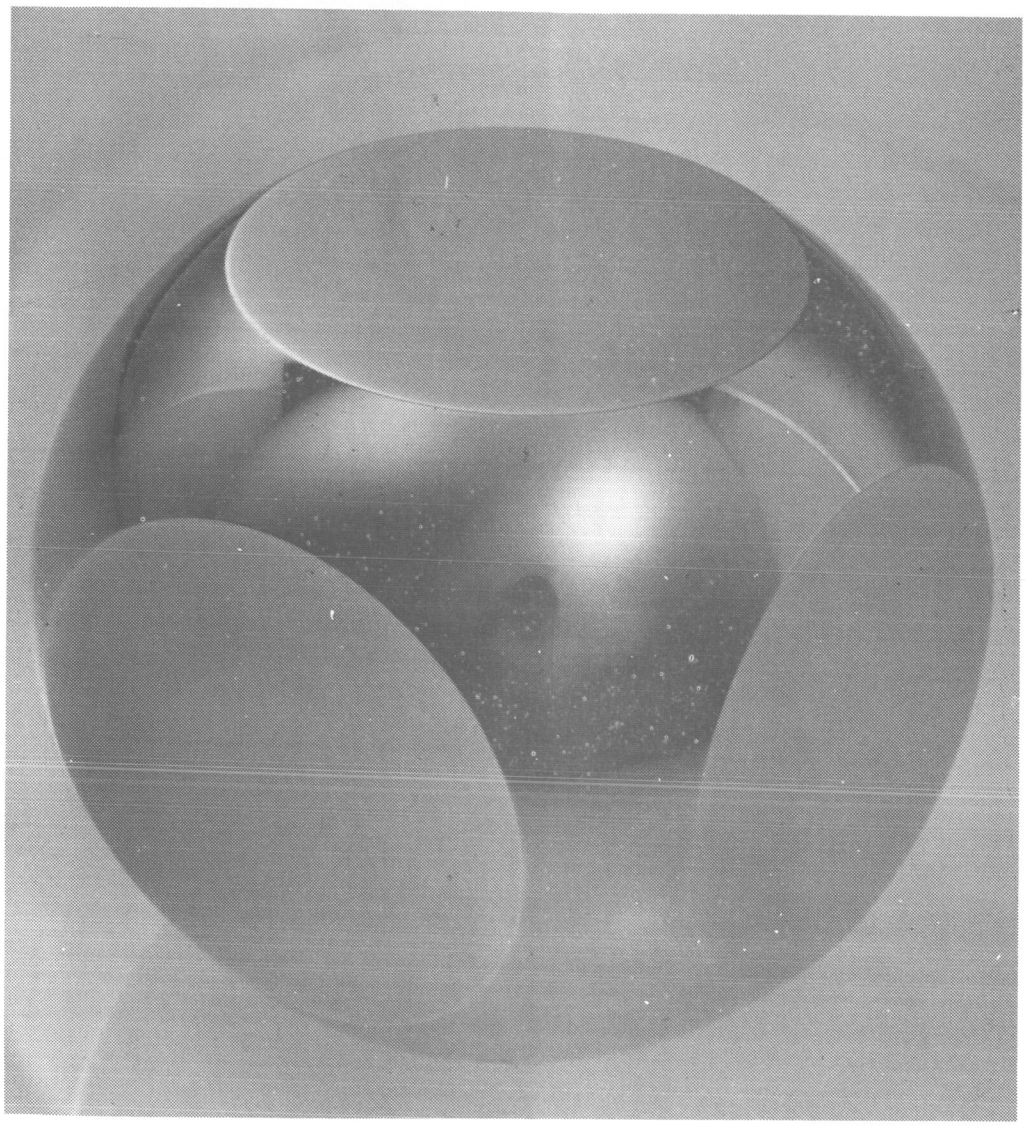

Fig. 6.4. Model of sphere modified by cubic-oriented flats consuming half the area of the sphere. In addition two small flats would be provided to establish a salient moment of inertia and to serve as spin facets. The spherical surface provides a facility for continuous orbit tracking to supplement the spin-axis tracking facility provided by the reflecting flats.

(OVERLEAF BLANK)

would be 9.8×10^{-11} at that range, but, obeying the inverse-first-power law, fall to 4.9×10^{-11} at 2500km. Halving the spin rate, on the other hand, would move the resolving range to 5000km, one of no interest, but would double the exposure at 2500km. At the same time, it would halve the number of flashes in the pattern and reduce the accuracy in estimating the center of the pattern in a way to compensate to a degree for the increased exposure for individual flashes. In this way, it is seen that the photographic effect is not very sensitive to spin rate.

The present numbers tend to suggest a possible need for a four-fold increase in facet area such as would obtain for a diameter of 0.6m. A definitive resolution of such a question must, however, await a determination of the relation between the accuracy of measurement and the photographic exposure produced by the flash pattern.

Before turning to that discussion, it may be noted that studies involving the use of more sensitive cameras than the Baker-Nunn, or the use of a combination of photographic and photoelectric data analysis, have not yet been undertaken.

6.5 Photographic Observability and Accuracy[†]

The basic photographic sensitivity of the Smithsonian Astrophysical Observatory's Baker-Nunn cameras, used in the above analysis and reported previously,[4] is an important factor in the optical design of the satellite spin-axis-orientation readout system. This sensitivity needs to be interpreted,

---

[†]This work was supported in part by the National Aeronautics and Space Administration under Grant NsG 443.

[4]Prog. Report for Sept., Oct., Nov., 1965 p 1, Coord. Science Lab., Univ. of Illinois, Urbana, Ill.

however, in terms of the accuracy with which the angular position of a flash pattern may be estimated from the Baker-Nunn photographs. Apart from errors in the measuring apparatus itself, errors in knowledge of the position of cataloged stars, and errors involving the mechanical stability of the photographic film, observation errors arise from a signal-to-noise competition involving film noise and a signal represented as the tapered, symmetrical density pattern of the photographed flash pattern. The latter errors may be expected to be signal-strength dependent, so that it would be important to be assured of sufficient signal strength (photographic exposure) such that the signal-dependent errors would not be appreciably larger than the instrumental errors.

The present experience is that "hard-edge" Baker-Nunn images, in which a usable density (0.3 logarithmic units or more) is developed, allow a determination in position to within about ± 1.1 seconds of arc. This number correlates well with the nominal 10 seconds-of-arc resolution for the camera, is compatible with the requirements of the relativity experiment, assuming some redundancy in observations during an undisturbed data-taking period, and it should be regarded as a goal in fixing the minimum-acceptable photographic exposure for the individual flash pattern. That minimum-acceptable exposure fixes the satellite mirror aperture but places no bounds on the spin rate so long as more than one flash may be assured to fall within the interval of resolution of the camera.

The minimum acceptable exposure is being determined by two approaches, direct photographic simulation and computer-based simulation. In each case it is assumed that the estimation of the image center is obtained by a weighted-average technique resembling a center-of-gravity estimation. This is illustrated schematically in Fig. 6.5. The upper part of the figure shows what a densitometer

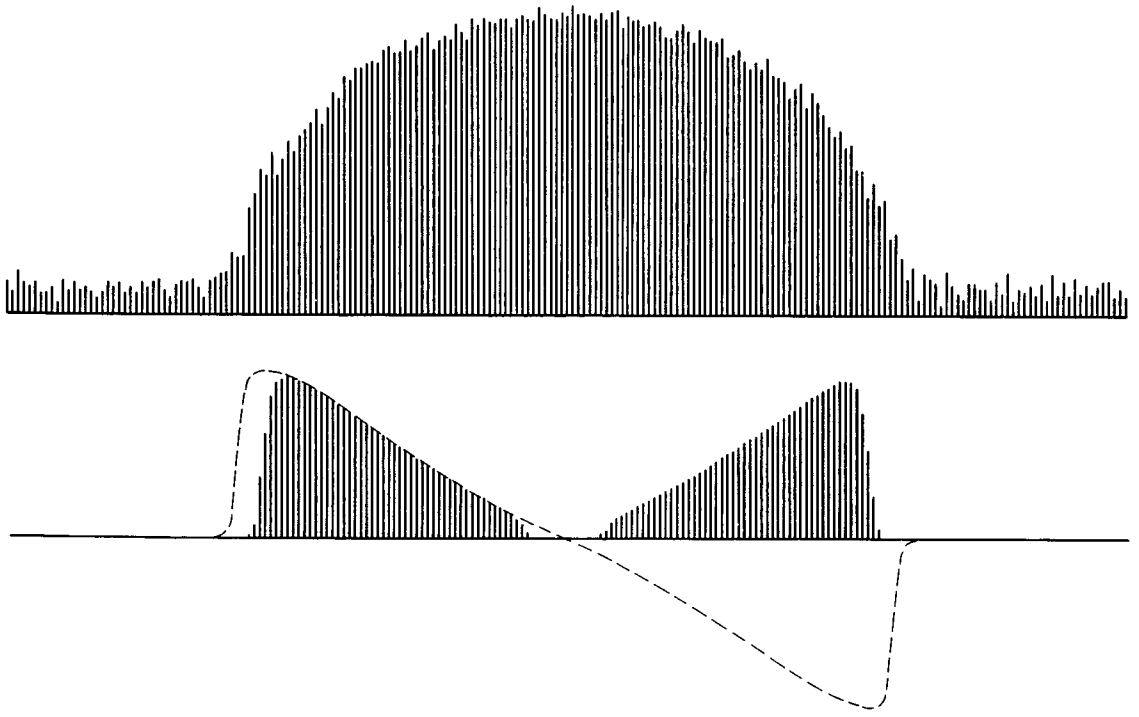

Fig. 6.5. Illustration of center-estimation procedure. The upper half shows, schematically, a densitometer tracing through a photograph of the expected flash pattern. A roughly semicircular envelope disturbed by the noise generated by the graininess of the film is depicted. In the lower half, a theoretically best weighting curve for finding the center (dashed line) is compared with a practical weighting scheme (bar graph) which could be realized using density wedges and balanced photometry.

(OVERLEAF BLANK)

tracing along the long axis of a flash pattern might reveal, a roughly semi-circular envelope disturbed by film noise.

Under certain circumstances, the optimal weighting procedure is known. If, for example, the noise is gaussian and uniformly additive, the best weighting curve is the derivative of the envelope. Thus under these circumstances, a parabolic envelope would dictate a linear, or true center-of-gravity, weight, giving the most emphasis to the most steeply sloping parts of the undisturbed envelope. Optimal methods offer the advantage that approximately optimal methods are nearly indistinguishable from optimal. Under realistic circumstances, the noise will not be gaussian nor uniformly additive, and the exact envelope shape will be subject to film nonlinearities. For these reasons, it is thought prudent to use the theory only as a qualitative guide, and to perform experiments with approximate weighting schemes as indicated schematically in the lower half of Fig. 6.5.

The dashed curve in Fig. 6.5 is intended to suggest what might be an optimal weight for the pattern in the upper part of that figure. Since one way to perform the weighting in practice would be to superpose density wedges upon the image, and since negative transmissions are not possible, it is proposed that two weighting functions be used, shown by the bar graphs in the lower half of Fig. 6.5. The two are to be exact mirror images of one another. Their relative positioning so that transmission through each is a standard amount and achieves exact equality provides the estimation of the location of the image center. Such a procedure is readily implemented in a photometric optical measuring machine that may be devised, for example, as a modification of standard apparatus. The procedure is also readily simulated in a computer.

D. H. Cooper

6.6 Computer Simulation[†]

For a computer simulation of the procedures described in connection with Fig. 6.5, a realistic simulation of film noise is required. Microdensitometer tracings of density step wedges,[5] made on red-extended Royal-X Pan, are being prepared for this purpose and recorded on punched paper tape. Preliminary tracings, recorded graphically, were obtained using an Ansco microdensitometer through the courtesy of D. C. O'Connor[6] and transcribed to paper tape. These data were processed on a digital computer, first to prepare replicas of the original tracing using the Calcomp plotter, so that transcribing errors could be checked and removed. Then, statistical processing resulted in a probability density histogram shown in Fig. 6.6, and an autocorrelation plot shown in Fig. 6.7.

The autocorrelation plot clearly indicates that the correlation is governed by the aperture used in the microdensitometer, 10 microns, so that the film noise has a finer structure than that. Since this is less than the 20 microns corresponding roughly to the Baker-Nunn resolution, such a resolution may be assumed for the sampling interval in the computer program with the assurance that the noise is white relative to that. Thus, samples taken at such intervals will, in the simulation be made to be statistically independent.

Further microdensitometer tracings will be made through the courtesy of Professor K. Yoss of the Astronomy department, using their Jarrel-Ash Projection

---

[†]This work was supported in part by the National Aeronautics and Space Administration under Grant NsG 443.

[5]Courtesy of L. H. Solomon, Smithsonian Astrophysical Observatory.

[6]Geodesy, Intelligence, and Mapping Research and Development Agency, Fort Belvoir, Virginia.

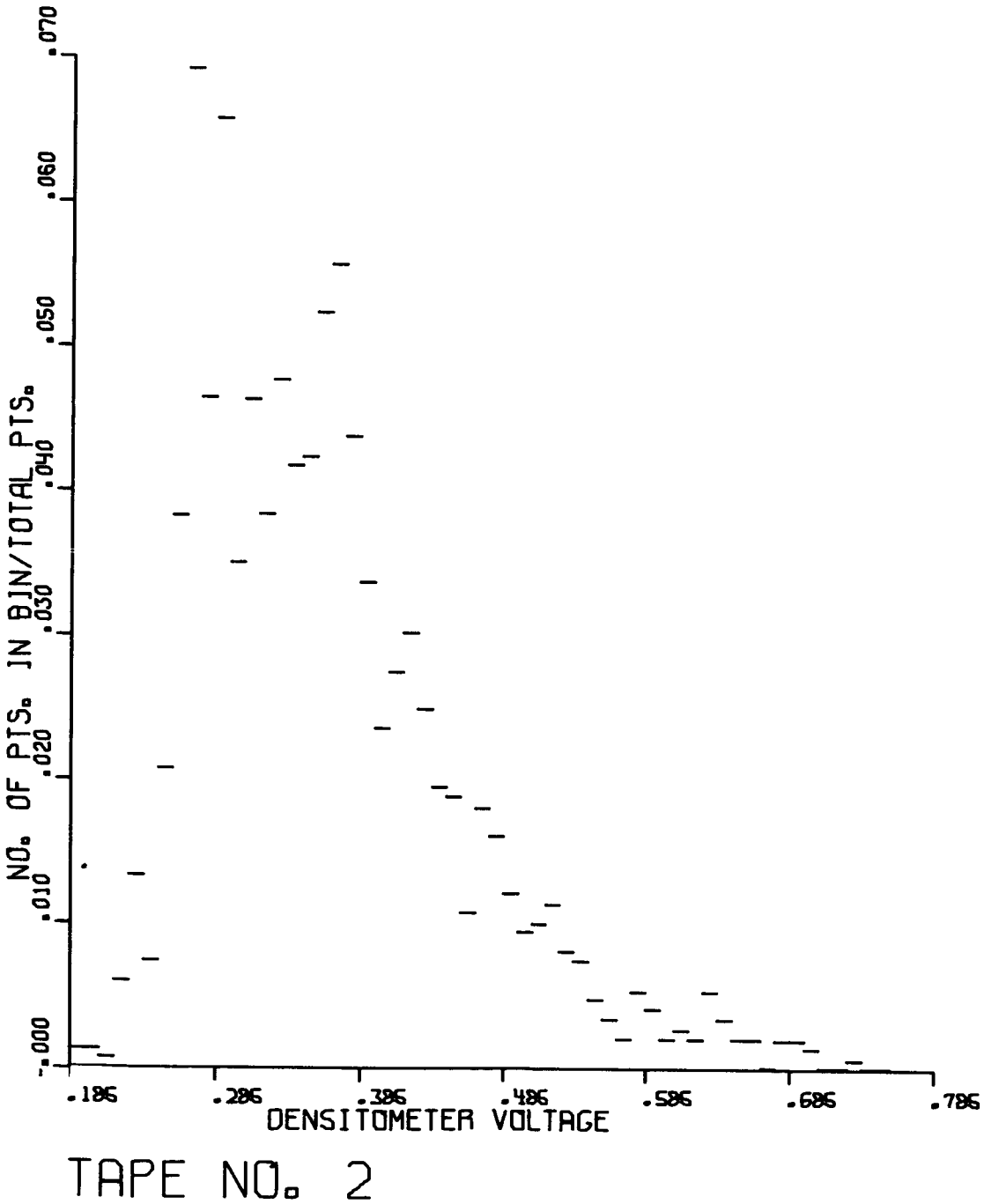

Fig. 6.6. Plot of probability distribution measured from a specimen of red-extended Royal-X Pan film. The "densitometer voltage" is in units of the usual logarithmic measure of density.

(OVERLEAF BLANK)

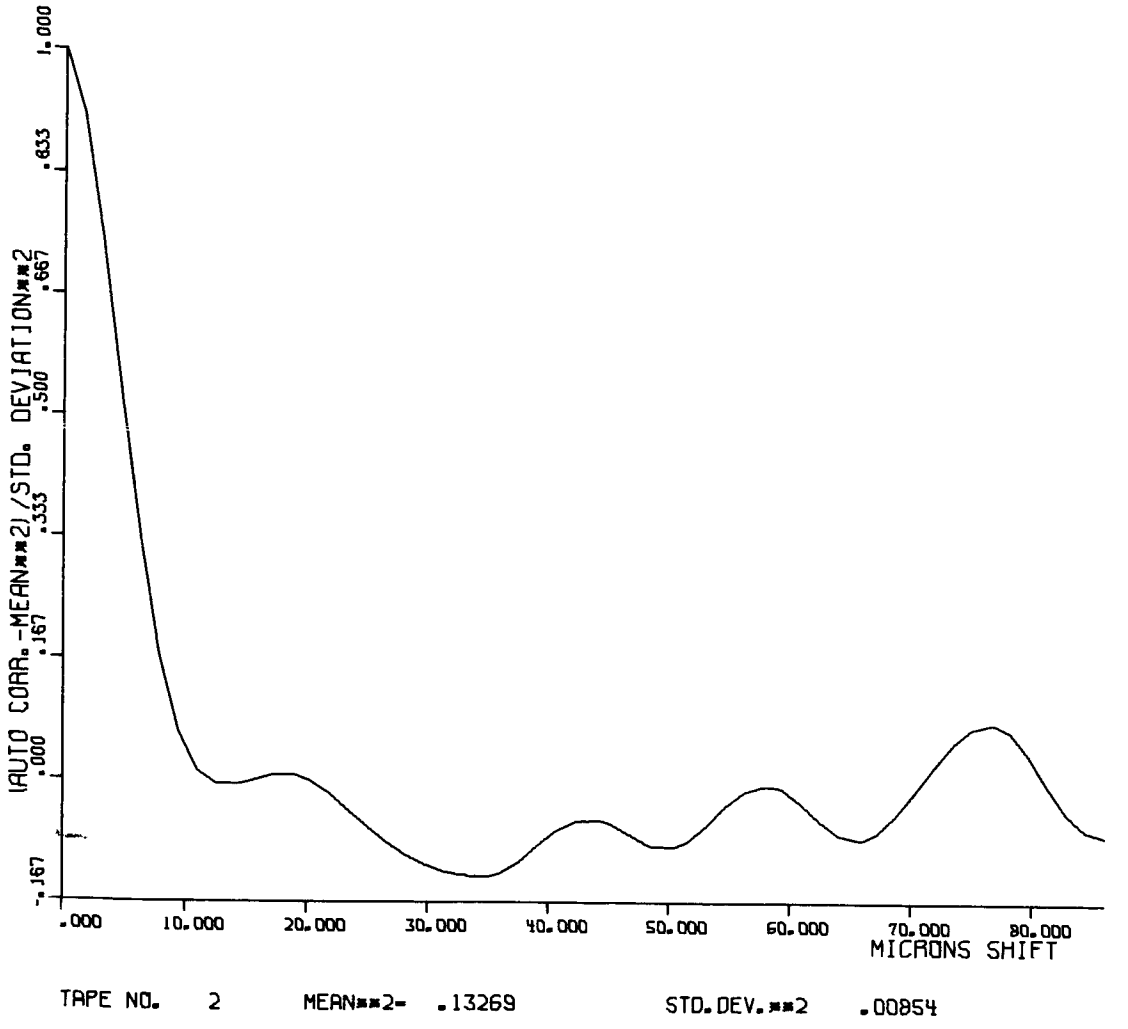

Fig. 6.7. Plot of the autocorrelation function for the film specimen of Fig. 6.6. The film-graininess noise is seen to be essentially uncorrelated at distances greater than the densitometer aperture, 10 microns.

(OVERLEAF BLANK)

Photometer, at 20 micron resolution. Probability histograms like that shown in Fig. 6.6 will be calculated for a variety of average densities. The computer-simulated noise will be adjusted to fit such data.

Programming of the computer simulation has begun, and some trial runs have been made. When the film noise statistics have all been obtained, so that the computer-simulated noise may be fitted to it, it will be possible to make many runs at a variety of peak-density levels and finally make a plot of measuring error versus peak density (or exposure).

D. H. Cooper
W. J. Bouknight
B. D. Krikwood
H. C. Morrison

6.7 Photographic Simulation[†]

A cylindrical optical system has been designed by which distorted images of the sun's disc may be photographed on 35mm red-extended Royal-X Pan film. The sun's disc will be distorted into an elliptical image with major and minor axes of about 1800 and 10 seconds of arc respectively. For the long axis, the effective focal length of the system matches that of the Baker-Nunn camera so that the overall simulation would be to scale. The overall resolution, though not yet determined exactly, is expected to be broader than 10 seconds of arc, so that the illumination of the long, narrow image is expected to show a tapering in the long direction which would be a realistic simulation of the brightness distribution for the glitter pattern of the satellite flashes.

The optical parts are at hand, and work has begun in fitting these parts to a Leica camera body equipped with a reflex housing. The primary optical

[†]This work was supported in part by the National Aeronautics and Space Administration under Grant NsG 443.

element is a pair of convex, short focal-length cylindrical mirrors arranged so that a double image will be formed. The single objective lens is an astigmatic refractor whose cylindrical and spherical (20-inch focal length) components complemer the astigmatic properties of the cylindrical mirrors. The image is expected to be bright enough so that chromatic aberration may be controlled through the use of color filters, while the overall resolution may be controlled by adjusting the numerical aperture which will be about f:50 at widest.

It is proposed that the Jarrel-Ash projection photometer, with a specially-built dual-photomultiplier measuring station replacing the standard one, be used to try the measuring technique outlined in an earlier section. With matching density wedges across the divided slit, and the two halves previously balanced on a uniform or blank image, the Mann measuring stage will be adjusted with the simulated image in place until balance is restored. The procedure will be repeated for the second image of the same frame. Statistics will be accumulated for the difference in measured position of the two images, for many pairs of images, and also with exposure as a parameter.

D. H. Cooper
B. D. Kirkwood

6.8 Ionosphere Program†

All of the objectives of this program have been successfully completed and CSL's participation in this project has been brought to an end. Summarizing briefly, the first phase of the project involved the design, construction and execution of a radio propagation experiment employing rocket probes to determine electron density and collision frequency from measurements of differential

†This work was supported in part by the National Aeronautics and Space Administration under Grant NsG 504.

absorption and Faraday rotation in the "D" region of the ionosphere.[7] The system was used in a series of 17 rocket launches made from Wallops Island, Va., and a NASA sea-going, mobile-launch platform. CSL personnel executed 14 rocket experiments, 13 of which were operationally successful.

The system has been transferred to the Aeronomy Group of the Electrical Engineering Department at this university, which will continue to conduct similar experiments. Up to this time they have executed three rocket experiments, two of which were operationally successful and a third partially so.

The second phase of this project was to develop an automatic data processing system for extracting the differential absorption and Faraday rotation data from the series of 15 successful and one partially successful experiments. The work reported below completes this phase, and a final report containing all of the extracted differential absorption and Faraday-rotation data is being prepared.

D. Skaperdas

6.9 Differential Absorption Data Reduction[†]

Two earlier reports[8,9] give a description of the method of storing the differential absorption data on a 145-hertz carrier. The following is a description

---

[†]This work was supported in part by the National Aeronautics and Space Administration under Grant NsG 504.

[7]"High Resolution Radio Frequency Measurements of Faraday Rotation and Differential Absorption with Rocket Probes," Knoebel *et al*, CSL Report R-273, Dec. 1965.

[8]CSL Progress Report for Mar., Apr., and May 1964.

[9]*High Resolution Radio Frequency Measurements of Faraday Rotation and Differential Absorption with Rocket Probes*. CSL Report R-273, Knoebel *et al*.

of a method for transferring the data from its 145-hertz carrier to punched paper tape that can serve as an input to a digital computer. The digital computer can then be programmed to give a printout and plot of differential absorption vs. time.

During the rocket flight, the extraordinary power level is recorded, on its 145-hertz carrier, on a magnetic tape recorder at 30 inches per second tape velocity. In the processing of the data these tapes are reproduced at 1/16 this velocity (1-7/8 inches per second) to provide compatibility between the desired number of samples per second and the paper-tape-punch capabilities.

Figure 6.8 is a block diagram of the data reduction system. The slowed-down data from the magnetic tape recorder is dc-coupled to a full-wave rectifier where the signal is rectified and filtered through a low-pass filter so that the carrier frequency is eliminated and the modulation representing the extraordinary power level is retained.

Figure 6.9 is a schematic diagram of the rectifier-filter. This circuit places the rectifying diodes in the feedback loop of a Burr-Brown type-1503 operational amplifier, which has the effect of decreasing the diode nonlinearity to a very small value. The balanced output of the rectifier is fed to the low-pass R C filter. The R C time constant of the filter is adjusted to be compatible with the sampling frequency, while rejecting the rectified carrier frequency and preserving the modulation.

From the filter the data is fed to an analog-to-digital converter and paper-tape-punch system, and to a graphical pen recorder that provides a low-resolution analog plot of the data as it is processed.

K. V. Krone

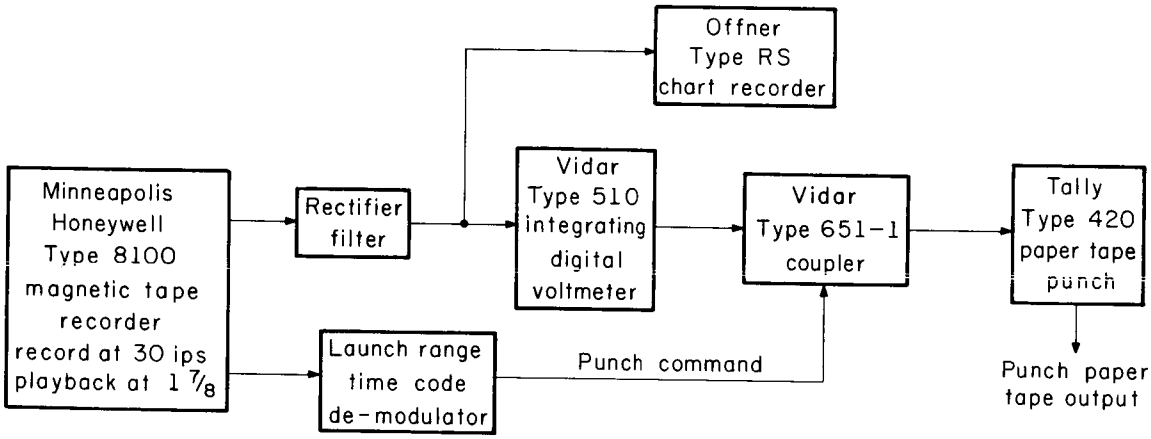

Fig. 6.8. Block diagram of differential-absorption data reduction.

(OVERLEAF BLANK)

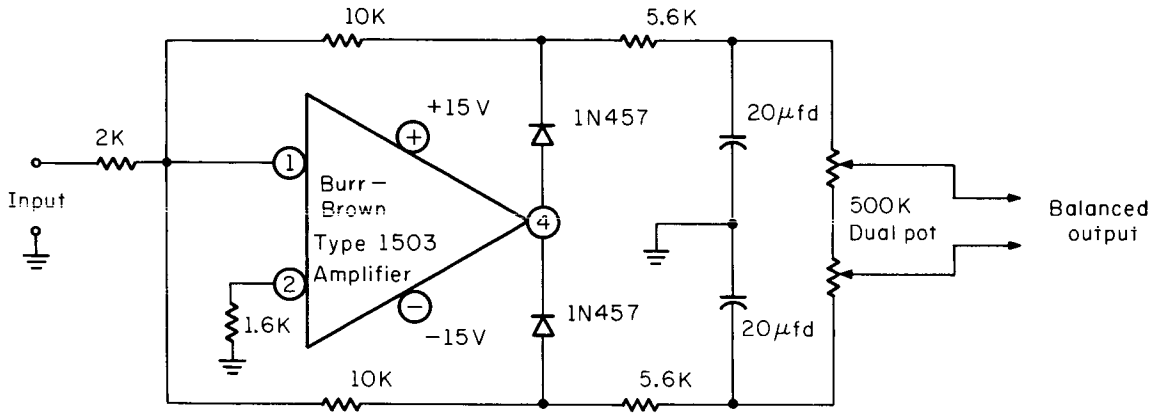

Fig. 6.9. Schematic diagram of the rectifier-filter circuit for the differential-absorption data-reduction system.

(OVERLEAF BLANK)

7. PLATO

D. L. Bitzer
B. M. Arora
M. Axeen
C. Bridges
J. A. Easley, Jr.
L. Fillman
J. Gilpin
W. Golden
H. Guetzkow
T. Hastings
B. Hicks
J. Holshouser
R. Johnson
H. Kiess
P. Koo
J. M. Kraatz
S. Krueger
E. R. Lyman
W. E. Montague
M. K. Myers
J. Norton
C. E. Osgood
J. Rubovits
S. H. Schwartz
M. Secrest
S. Singer
T. L. Smith
B. Stake
K. Tatsuoka
P. Taylor
M. Uretsky
B. Voth
J. Walker
M. Walker
A. Wearing
C. E. Webber
D. Weeks
M. Wilkins

7.1 Introduction[†]

The purpose of the PLATO project has been to develop an automatic computer-controlled teaching system of sufficient flexibility to permit experimental evaluation of a large variety of ideas in automatic instruction including simultaneous tutoring of a large number of students in a variety of subjects. The PLATO system differs from most teaching systems in that the power of a large digital computer is available to teach each student, since one such computer controls all student stations. The project work has fallen into three categories, no two of which are wholly separate from each other: (1) development of the tools for research; (2) provision of a prototype for multi-student teaching machines; (3) learning and teaching research. Under the first category has come the development of three successive versions of the PLATO equipment with PLATO IV, which includes an audio facility, now under construction. The twenty-student-station classroom provides the prototype for multi-student teaching

[†]This work was supported in part by the Advanced Research Projects Agency through the Office of Naval Research under Contract Nonr-3985(08) and by the Office of Education under Contract No. OE-6-10-184.

machines mentioned in the second category. Research is also underway on designs for remote installation PLATO station equipment. The installation in May of the CDC 1604 computer, a gift of the Control Data Corporation solely for the use of the PLATO project, has enormously helped to satisfy the increasing demand for initiating new projects using the PLATO system.

The learning and teaching research, the third area of PLATO work, has covered curriculum studies, college teaching, and behavioral science research. Cooperative projects are carried on with the University of Illinois Committee on School Mathematics and with several departments and colleges of the university: psychology, political science (University of Illinois and Northwestern University), library science, commerce, education, etc.

7.2 PLATO III System Equipment

During the past six months, work leading to the realization of a 20-station, computer-based teaching system has been completed to the extent that all 20 stations are checked out and are consistently available to the presentation of lesson material. That is, all 20 stations can be used concurrently with essentially no difficulties arising from cross-talk, drift, or equipment failure for periods of at least 24 hours, and typically much beyond 24 hours.

However, even though the system is in a very usable state of development for use with most lesson material, further technical development would improve its effectiveness, especially in endeavors requiring great consistency in the visual aspects of the presented material. As an example, not all stations present electronic book pages with consistent intensity, shading, and size with respect to other book pages; and not all stations present blackboard information which is blemish-free, and which is not delayed slightly in reaching full intensity. Furthermore, there are electronic scanning inaccuracies related

to both the electronic book and blackboard which often cause small misregistrations on the written material of the blackboard and book.

The shading and intensity variations of the electronic book are largely the result of variations in electro-optical sensitivity characteristics of the book hardware as well as film density variations related to exposure and photo processing. Remedies are straightforward, but nevertheless would require extensive revision of present electronic book hardware.

The blemish of blackboard-presented information is related to the storage tube. According to the manufacturer, blemish formation can be eliminated through a different mode of operation of the storage tubes and would require only a small increase of circuitry. Intensity delay has not been investigated, but is thought to be largely circuit-related and if so, would yield to simple circuit changes. Also related to image quality, but of minor consequence, is a rather slow drift of storage-tube beam current which produces a fading of presented material over long intervals. The consequent need for adjustment from time to time can be eliminated, it is thought, by some means of regulation of the beam current.

The matter of scanning accuracy can be improved, in the case of the electronic book, by scanning-correction devices and better-quality optical hardware. In the case of the blackboard, probably a redesign of the storage tube is required to eliminate fully the wall-charge-induced scanning inaccuracies.

Development work concentrating on the above matters continues at very low priority. To date only problems regarding storage-tube blemish and book-scanning accuracy have been looked into. Some experimental circuitry has been devised and is undergoing evaluation.

New system equipments currently under study and development are those which will provide the PLATO system with audio capabilities, in addition to its

visual-display capabilities. The study of the audio storage continues. Various schemes employing magnetic-oxide film and photographic film have been considered. Some basic apparatus for the evaluation of schemes using magnetic-oxide film has been devised.

To date, development of the motion-picture equipment has progressed to the point where generation of 16 mm frames will soon begin. Early results indicate that the commercial oscilloscope which is to be used will produce only mediocre-quality frames due to a short-term raster drift peculiar to the scope cathode-ray tube itself. A new scope, free of drift, is planned, and is expected to be complete within the next six months. In the meantime at least one short film sequence using the present scope is planned.

B. Voth

7.3 PLATO Learning and Teaching Research

7.3.1 University Courses

7.3.1.1 Electrical Engineering 322--Circuit Analysis

During March 1966 two types of programmed instruction (inquiry and tutorial) were used on the PLATO System to teach a basic introduction to Laplace-Transform theory and its application to network analysis. During a specified learning period, one test group of students received all instruction from the tutorial teaching logic while a second group received all instruction from an inquiry teaching logic. Both instruction sequences were developed using the same set of lesson objectives, i.e. ideally, the students in both groups would attain the same behavior or knowledge by completing the instruction sequence. Both groups of students were given the same pretest and post-test to evaluate how well the lesson objectives were attained by the students and to provide a measure of the effectiveness of the two teaching methods. A detailed discussion of the study and

the data obtained from the student records, comments, and test scores are presented in CSL Report R-297 which was prepared in the following months.

The present study has shown that the lesson material taught in EE 322 Network Analysis can be adapted and used effectively on a computer-based instruction system such as PLATO. Although the inquiry method of teaching seemed to have some advantages over the tutorial method, it would be difficult to make a definite conclusion as to which method should be used. It is felt that a teaching logic which would incorporate the characteristics of both teaching logics would be more desirable. No definite conclusions were drawn from the analysis of student performance although some indications were obtained from the data. The students commented most frequently on the manner in which the system allowed them to participate actively in the learning process; they felt that this was a definite improvement over conventional types of instruction. Future work in the areas of lesson material and the designing of teaching programs should involve improved and more extensive help sequences and references.

Roger L. Johnson

7.3.1.2 FORTRAN Programming Course for Business Students.

During this period responses from the latest student sessions were analyzed. As a result, plans were undertaken to modify the teaching logic to provide for automatic branching, wash-forwards and wash-backs. These will be used in connection with a modification in the learning program. A judging subroutine is currently being written to enable on-line interpretive compilation of FORTRAN programs. This facility will permit us to examine the results of having the problem-solving behavior integrated directly into the teaching program.

M. Uretsky

7.3.1.3 Library Science 195--Introduction to Library Use.

The PLATO version of the university course Introduction to the Use of the Library (Lib Sci 195) was given during the second semester to a group of thirteen students. This was the second group to take the course from PLATO instruction rather than conventional classroom instruction. Conclusions on the comparative study of PLATO vs. classroom instruction for this course will not be made until response data is available from a third group who will take the course in the fall semester of 1966.

M. Axeen

Data derived from the students' responses from the first two groups (fall semester 1965, spring semester 1966) were processed by a "doping routine" during the spring and summer. The doping routine sorted the student responses and printed them sequentially so that the pattern of an individual's procedure through each lesson could be followed. At the end of each session a table was presented showing for each student the number of wrong answers, number of answers correctly given on the first trial of a question, the number of times the student asked for help, the number of times the student asked the computer for the answers to questions, the number of times the reverse key was pushed, the number of spelling errors, the number of screen erasures, and the individual's lapsed time for the session. A collection of the comments made during the year's sessions was also made from the dope by using a special COMMENT routine.

E. R. Lyman

7.3.2 Mathematical Instructional Projects

7.3.2.1 ARITHDRILL. About twenty low-achieving seventh-grade students from Champaign junior high schools used ARITHDRILL during April and May. Working in groups of six or seven, the students worked an average of six 50-minute

sessions. Previous findings, that these short-attention-span students would work dependably thru 50-minute sessions, were in the main substantiated, although more isolation between booths would be helpful during sessions, and a clear effect of changes in the weather on student performance from one session to another was noted.

Student output for these sessions was analyzed largely by hand. Clear evidence of improvement in performance was found, but there was some evidence of "concurrent interference" among the items being learned. Further sessions to be held in the fall will seek to confirm formally the first of these findings and to explore systematically the second.

A dope-analysis program for ARITHDRILL has been completed and debugged, and the ARITHDRILL program has been annotated in handscript.

John Gilpin
J. Kraatz
B. Wilson

7.3.2.2 PROOF. Program PROOF, which permits the construction of valid complete proofs has been used to prove a number of theorems in algebra from axioms inserted as parameters in the program. More work is required before its general capabilities can be fully realized.

J. A. Easley, Jr.
T. Smith
J. Kraatz
W. Golden

7.3.3 Project SIRA (System for Instructional Response Analysis).

Student response data collected by the use of three short instructional programs (a 1-hour test, a 4-hour lesson on arrays for 4th grade children, and a 9-hour unit on recursive definitions for high school students) are now being analyzed by means of three separate programs. The first, SPECTRE, which replays events on the screen of each station, has long been available but not extensively

used for feedback to authors. The second, TEXTDOPE, a program capable of graphing time and error and listing sequences of keyboard events, and the third, DOPESELECT, are new developments of project SIRA. The latter selects subsets of dope records of keyboard (and other) data in terms of subsets of values on each variable (station, key, time, and mode) typed in by the operator. An abbreviation mode for assigning short names to commonly used subsets of values and a general recursive property of the program give it the power to select from the complete dope record (and from future dope records containing many more variables) precisely the facts desired. The main difficulty in using it is that the information desired must be requested in a language that is often quite far removed from the language an author uses to talk about his lesson material. A preliminary design for an information-request language for tutorial-teaching instruction has been explored, but a more general language is desired to handle inquiry logics and unusual uses of tutorial logics.

Authors' behavior in analyzing and modifying their lessons is being recorded anecdotally for guidance in the design of a more general fact-retrieval system.

Work has continued on editing capabilities in tutorial logics with the object of gaining enough experience in editing instructional programs to author specifications to be able to design a general-purpose teaching logic with editing capabilities that are engineered to quite-general author characteristics.

K. Tatsuoka has developed a generalized classification procedure using a function which maps multiple, convex categories in n space onto a single dimension. It is hoped that her procedure will facilitate the process

of retrieving instances of general types of instructional-event sequences.

Charles Bridges
J. A. Easley, Jr.
William Golden
J. Thomas Hastings
Jim Kraatz
Scott Krueger
John Norton
Jim Rubovits
Robert E. Stake
Kikumi Tatsuoka
Peter Taylor

7.3.4 Behavioral Science Projects

7.3.4.1 Group Interaction Program. Dr. Hicks visited a number of groups in England in the period June 20 to July 8 and discussed various applications of PLATO in teaching and in the behavioral sciences. Especially relevant to the Group Interaction Program were visits to the Peace Research Centre at Lancaster University, to the Mankind 2000 project in London, and to Professors Halsey and Clark and their colleagues at Oxford University. There apparently is no man-computer system like PLATO in England now.

Two inter-nation simulations will make use of the GIN-1 PLATO program in whole or in part: Guetzkow's INS and Osgood's Security Game. Application of GIN-1 to specific simulations has been delayed by an unrecognized contradiction in the program and by the postponed arrival of Professor Seki, who is to design the specific INS simulation to be used on the PLATO System. On July 21, however, Professor Seki, Professor Smoker, and other visitors from Professor Guetzkow's group visited the PLATO group for discussions of INS and GIN-1. These discussions will lead, in the near future we hope, to choice of the specific situation to be simulated and to necessary training of new research people in the use of PLATO. Professor Smoker is visiting Northwestern University from the Peace

Research Centre and Professor Seki is visiting Northwestern University from Tokyo.

The basic contradiction in the GIN-1 program has been removed. A Fortran program written at Northwestern for up-dating the data banks has been transferred to the PLATO computer. Slides and descriptive material have been prepared as a first stage in the training of INS participants.

B. L. Hicks
H. Guetzkow
J. Holshouser
S. Singer
J. Walker
M. Walker
D. Weeks

7.3.4.2 Learning and Retention of Verbal Materials Research.

This project involves the utilization of PLATO for studies in the learning and retention of paired associates. In one experiment, paired associates were learned under several conditions and retention tested after 24 hours. Collection of data from this experiment was completed during the spring and summer and is currently being analyzed.

A second experiment, begun this year, involves learning of paired associates which have previously been scaled for ease of learning. Data is being collected to relate speed of learning and ease of retention with the previous scaling of the pairs.

W. E. Montague
H. Kiess
A. Wearing
C. E. Webber

7.3.4.3 A Study of Propositional Control of Behavior.

A psychological experiment involving 240 subjects was carried out using the PLATO System. The study attempted to test a theory of propositional control of behavior in a concept-attainment situation. The PLATO system's ability

to display, judge, and act upon student-generated data within a short period of time enabled consideration of variables normally not obtainable in such studies.

The subjects were given the task of determining the concept or classification rule by which certain instances (sentences) were always classified as examples, while other sentences were always classified as nonexamples. On each trial the subject either created, selected, or received, depending on the treatment condition, a sentence, guessed as to whether it was an example or a nonexample of the concept, and indicated their hypotheses concerning the possible relevance of various words in the sentence to the correct concept. The PLATO System displayed each sentence, the subjects' responses, and the actual correct classification for that sentence. By consideration of these sentences and the accompanying feedback from the system as to the correct classification of each sentence, a subject could in time determine the classification rule the system was using.

The results are currently being analyzed and readied for publication.

Steven H. Schwartz

7.3.4.4 Experimental Satiation of Semantic Features.

This research was designed to measure Osgood's semantic features through examining subjects' responses to experimental satiation treatments. The study was completed in late May, and, after organizing the subject data via a PLATO output routine, analysis was completed on the IBM 7094.

Results failed to confirm the presence (or hypothesized operation) of semantic satiation. This situation could have arisen from a multitude of sources, e.g., inadequate design of criterion items or excessive machine time required to generate the experimental items. However, the study was productive in a way not altogether anticipated. Results provide an interesting view of cognitive

interaction: the amount of subject indecision and error as a function of cognitive congruence. Aside from the well-known acquiesence response (the tendency for subjects to say 'yes', whatever the item), subjects showed an overwhelming tendency to endorse the socially 'good' words, e.g., words representing strength, activity, morality, etc. This tendency was stronger for the adverb member of the item pair than for the verb member. Important information would be gained if this latter finding were to be substantiated, and the effects of recency disentangled from the effects of linguistic word class.

C. E. Osgood
M. Wilkins

7.3.4.5 Animation of Abstract Visual Forms. This project involves filming computer-generated figures in order to provide animated scenes of interpersonal behavior. Unfortunately, it has not yet reached the production stage; effort has been devoted entirely toward the development of the required display system. Mrs. Koo, working in collaboration with B. Voth and M. Johnson of the PLATO group, has currently been providing test programs for the measurement of this new system.

A major difficulty lies in the control of shading: between the extremes of black and white, the effect of changing brightness is not known (but known to be nonlinear). The appearance of changing brightness is also suspected to be a function of the particular camera or particular film used. For this reason, a program was written to test distinguishable differences in shading for any given film or camera. As a further safeguard, the "circle" program (described in the previous progress report) has been modified to adopt variable "break points" of distinguished shades--thus allowing cameras or films to be interchanged without further changes in the program.

The oscilloscope involved in the display system has also presented a problem. Since there is no oscilloscope assigned exclusively to this project, it has been necessary to tune and adjust different ones each time. (A program written specifically for calibrating the oscilloscope should spare much of this effort.) Furthermore, the shape of the scanning line (across a single frame) has been irregularly variable. This may be due to the oscilloscope itself or to other components in the system, e.g., camera or picture tube, but must be eliminated before actual production work can begin.

C. E. Osgood
M. Wilkins

7.3.4.6 PROGMAT. A program which uses PLATO to collect data on Raven's Progressive Matrices Test has been written and debugged. The PMT is a non-verbal test of pattern-handling capabilities. The PLATO program will be used to collect data from low-achieving seventh- and eighth-graders using new UICSM curriculum materials, in an attempt to determine whether the test can distinguish those "low achievers" who have more realizable potential for learning from those who have less. Latency data will be considered as well as error data.

PROGMAT calculates and stores performance information while the students are working. Analysis routines built into the program are activated at the end of the session and a complete summary of the data is outputted to the printer.

J. Gilpin

7.3.5 French Instruction. Preliminary work necessary for instructional programming in French has been completed. Author- and student-mode keyboards have been laid out, and the characters (93 altogether) necessary for plotting French text, phonetic help text, and translation help texts, have been designed, checked, and revised. The initial program is concerned with the facilitation of skill in reading printed French. A teaching logic has been laid out and

construction of the program scheduled for August-December 1966. Provision for training in oral-aural skills is included in the planning, and relevant programming will be undertaken when the PLATO audio becomes available.

M. K. Myers

7.4 Some Operational Details in the PLATO Group

7.4.1 The 1604 Computer. A new CDC-1604 computer system was installed in the Coordinated Science Laboratory in May. It is the generous gift of the Control Data Corporation on a rent-free basis for eighteen months and it is designated as solely for the use of the PLATO group. The new equipment includes the 1604 computer, a 1607 magnetic-tape system, and a 1612 line printer. Use of the other Coordinated-Science-Laboratory 1604 had been limited to five hours a day, but it was not long before at least 12-16 hours a day were being utilized on the new computer for PLATO research and "student runs." Use of the new computer is carried on with an "open-shop" policy after careful check out of each user by a computer engineer. A few modifications on the new computer and tape units have been made such as "fast read," "fast write," and some inverse instructions.

D. L. Bitzer

7.4.2 Systems Programming. CATORES (resident program for CATO programs) has undergone major revision in connection with the change in the method of automatic recording on magnetic tape of student responses, a procedure known as "doping." Two subroutines, called SETDOPE and DOPE, respectively, have been added which provide the PLATO authors and teachers with a choice of items to be recorded in suitable bytes. The "dope" is now recorded in binary mode, instead of BCD as before, in a format similar to the FORTRAN library format.

The new method is more efficient in time and in its use of magnetic tape, in addition to giving the users the information in more suitable form.

Many other minor corrections and improvements have been and are now being made to the CATO Systems program. The next revised edition of the PLATO manual will include these changes.

M. Secrest

7.4.3 The PLATO Manual. The PLATO System Manual for users of the PLATO system has been completed and distributed on a limited basis to current users for reference, suggested additions and comments.

L. Fillman

7.4.4 Production Facilities for PLATO Lessons and Programs. Production facilities have been organized to accommodate the anticipated increase of PLATO users. These facilities include: reference files of CAI activity, reference files of PLATO publications, and photographic files of PLATO hardware, software, and lessons. Forms and programming information are also provided to aid programmers in constructing PLATO lessons and programs and in writing reports of PLATO research.

L. Fillman

7.4.5 PLATO Seminars. The final series of PLATO seminars for the academic year 1965-66 (open to any interested persons) consisted of a capsule series of summary talks which were held in late May and early June. The subjects and speakers were as follows:

SIRA (System for Instructional Response Analysis), Professor J. A. Easley, Jr., Associate Professor of Education, Research Director, University of Illinois Committee on School Mathematics.

PROOF (Mathematical Problem Solving), T. L. Smith, Research Assistant, University of Illinois Committee on School Mathematics.

PLATO University Courses (LIB SCI 195), Miss Marina Axeen, Assistant in Library Science, University of Illinois.

PLATO University Courses (EE 322), Mr. Roger Johnson, Assistant in Electrical Engineering, Coordinated Science Laboratory.

GIN-INS Program (Group Interaction, Inter-Nation Simulation), Professor Bruce L. Hicks, Research Professor, Coordinated Science Laboratory.

The Display Tube, Professor D. L. Bitzer, Research Associate Professor, Coordinated Science Laboratory and Professor G. Slottow, Senior Research Engineer, Coordinated Science Laboratory.

Paired Associate Learning: Interface Studies, Professor William Montague, Assistant Professor of Psychology, University of Illinois.

Comparative Psycholinguistic Studies, Professor C. E. Osgood, Professor of Psychology, Institute of Communications Research.

E. R. Lyman

7.4.6 Demonstrations and Workshops. Seventy-eight demonstrations of the PLATO system were given in the past six months. Some were in the form of talks with remote station demonstrations, others actual "audience-participation" demonstrations held in the PLATO classroom.

Two three-to-four-week workshops to teach the details of preparing and programming lesson material for the PLATO system were presented during June, one to six members of the United States Naval Academy and one to four faculty members from the Homewood-Flossmoor (Illinois) school district. Dr. Bitzer and Dr. Easley presented the lectures for the workshop. Participants were given ample opportunity to prepare, program, and test lesson materials directly on the PLATO system.

E. R. Lyman

8. COMPUTER SYSTEMS AND APPLICATIONS

H. G. Slottow
G. Crawford
L. Hedges
J. Knoke
D. Lee
V. Metze
E. Neff
J. Stifle
R. Trogdon
P. Trombi

8.1 Introduction

The computing facility at CSL now includes two Control Data 1604 computers, the CSX-1 computer, and a variety of peripheral equipment. One of the 1604 computers has, since 1962, been the principal computer for the Laboratory. The second 1604 has been loaned to CSL by the Control Data Corporation and is used exclusively by the PLATO group in its computer-based education system. The CSX-1 is a short-word-length computer designed and constructed at CSL.[1] This computer has an order code and an interrupt capability that make it particularly appropriate for on-line, real-time operation.

The computer group maintains all three computers and operates the Laboratory-owned 1604 and the CSX-1.

An important responsibility of the group is the continued development of both the equipment and the programming systems for this facility.

8.2 CSX-1 Computer

Period: 1 March 1966 to 1 September 1966

Total Running Time:	4139.6 hours
Average Per Day (7 day week):	22.47 hours
Operational Time: 99.25%	4118.6 hours

[1] R. M. Brown, R. D. Jenks, J. E. Stifle, R. L. Trogdon "Manual for the CSX-1 Computer" Report R-136, Coordinated Science Laboratory, Univ. of Illinois, April 1962.

Scheduled Maintenance Time:	.38%	16.0 hours
Emergency Maintenance Time:	.12%	5.0 hours

L. E. Hedges

8.3 CDC 1604 Computer

8.3.1 Operations

Period: March 1 to August 31, 1966

Total Running Time:		2397.40 hours
Average Per Day (7 day week):		13.03 hours
Operational Time:	96.87%	2322.40 hours
Preventive Maintenance Time:	2.61%	62.50 hours
Engineering Time:	0.00%	0.00 hours
Emergency Maintenance Time:	0.52%	12.50 hours

E. Neff

8.3.2 CRT Display. Construction of the CRT display unit continued during the preceding six months. At the present rate of construction, the display should be ready for initial check out by November.

The display is a digitally operated device designed for on-line operation with a CDC 1604 computer. Two CRTs are provided; a 16" tube for direct viewing and a 5" tube for photographic recording of displayed data. The display contains 12-bit digital-to-analog converters which provide more than 16×10^6 points on the CRT. Also contained in the display are a line generator and a character generator. The display operator may converse with the computer via a console typewriter or with a light pen.

Briefly the display operates as follows: The computer transmits a MODE CONTROL WORD (MCW) to the display. The MCW directs the processing of all

succeeding data. The display remains in a given mode until receipt of a new MCW. Seven modes, including character and line-generation modes will be available initially. Detailed descriptions of the modes can be found in the previous progress report.

A modification has been made in the 1604 computer which permits any portion of the computer memory to be operated as a circulating memory to refresh the display. This modification greatly simplifies display programming and at the same time eliminates the need for a separate display memory.

A report is being written describing the display system in detail and will be issued on completion of this project.

J. Stifle
L. Hedges

8.3.3 Programming System for 1604 Computer. A versatile programming system has been prepared for the CDC 1604 computer and is now in use on an experimental basis. With minor exceptions the system is compatible with both the existing FORTRAN and machine-language systems.

In its present form it includes a monitor, an edit routine, an assembler (ILLAR), and a modern version of FORTRAN. Other languages can be added as they are needed. The FORTRAN compiles directly in ILLAR, and a programmer can use both FORTRAN and ILLAR in one program, changing from one to another when he desires. A detailed description of this programming system is being prepared.

D. Lee

8.4 Special Equipment

8.4.1 Plasma Data Processor. If a signal of known frequency is imbedded in noise, the signal to-noise ratio can be determined by polarity coincidence

techniques.[2] Equipment has been constructed to gather data from an improved polarity-coincidence detector (PCD) used in plasma-physics experiments.[3] The PCD scheme involves sampling four times for each cycle of signal frequency, so that, including a counter for clock pulses, five conventional counters would be required. Only three counters are required if two of the counters can count forwards and backwards, and this fact has been exploited in the design of this equipment.

The device constructed contains three data registers of eight decimal digits each, and has the logical structure of a serial-decimal arithmetic unit. The three registers may be incremented, decremented, or their contents combined, as determined by "wired-in" programs. Subtraction is implemented by ten's-complement addition.

The device has two instructions available to the user that may be initiate electrically. Each instruction allows as many as five register modifications, the actual number executed being determined by incoming data. In addition, one may initiate certain subtraction operations manually. This feature offers a convenient method of converting data in complement representation to positive representation.

The equipment employs a method of control sequencing called a pre-sequenced control (PSC), which involves storing the desired sequence of operations in flip-flops prior to the execution of each instruction. The PSC consists of interconnected logical circuits called sequencing blocks. Sequencing blocks may be readily adapted to speed-independent operation and may be exploited by the circuit designer for high-speed operation. The PSC offers a systematic and

---

[2] M. Raether and D. Bitzer, Rev. Sci. Instr., 35, 837 (1964).

[3] Coordinated Science Lab., Progress Report for March, April, May, 1965, pp. 56.

straightforward design procedure, is amenable to modification, and lends itself particularly well to diagnosis of malfunction and to electrical checking of the sequencing operation.

R. Trogdon

8.4.2 S. M. P. Film Drive Servo System. Figure 8.1 is a block diagram of a servo system and associated control circuitry that was designed to provide the capstan driving power for a 70-mm film-projection system. The projection system provides for the scanning and viewing of three 1000-foot reels of film simultaneously, individually, or in combinations of two.

The drive system is capable of driving the film very slowly for frame positioning or at velocities up to 1000 feet per minute. Acceleration between velocities is accurately controlled to avoid tearing the sprocket holes in the film, and to provide compatibility with the take-up and supply-reel servo systems. The system is reversible and drives in either direction with the same characteristics. A shaft-encoder and display system provide an indication of the frame number that is being viewed.

The system has two methods of control. In one the operator uses a manual speed control and can operate the servo at slow speeds for frame positioning, or can drive the film at maximum velocity by moving the control to its extreme. The other method of control is an "automatic frame-finding" mode. This mode provides a method for going quickly from any particular position on the film to another specific position some distance away. The automatic mode utilizes an on-line computer (data is normally fed from the projection system to the computer) in conjunction with other digital circuitry to generate the necessary drive signals to bring the desired frame into position. Also incorporated with this mode is a "single-frame advance" control that advances the film one frame each time the control button is depressed.

A direct-drive dc torque motor with wound armature and permanent-magnet field was chosen as the servo actuator. The dc torque motor is designed for high torque, low-speed operation for positioning and speed-control systems. Since it has high-torque capabilities at low speeds, it can be directly coupled to the load shaft, thereby eliminating the complexity and problems of a geared system Additionally, it is capable of operating over a large speed range. A dc tachometer generator of the same type as the motor is attached to the motor shaft and provides rate feedback for the system. A servo system of this type is considerably less complex than the conventional ac servo system.

The servo electronics (refer to Fig. 8.1) consists of two summing networks, acceleration-limiting circuitry, pre-amplifier, and power amplifier. The acceleration-limiting circuitry is in essence an integrating circuit made up of three operational amplifiers in a feed-back arrangement with the integrating time constants chosen to limit acceleration to the desired level. It operates linearly for slowly-varying input voltages, but transfers to the maximum-acceleration curve when the input command attempts to change the velocity too rapidly.

The pre-amplifier is a Burr-Brown type-1506 silicon-transistor operational amplifier. Its inputs are from the acceleration-limiting circuitry and the tachometer generator. Potentiometers in external circuitry around the pre-amplifier provide [illegible] and "zero-speed" adjustments. Power for the pre-amplifier is [illegible] precision power supplies incorporated on the amplifier ch[illegible]

A pair [illegible] take the output of the pre-amplifier and provide sufficien[illegible] the power transistors. One of the drivers provides the inversion [illegible] provide a push-pull signal for the power

The pre-amplifier is a Burr-Brown type-1506 silicon-transistor operational amplifier. Its inputs are from the acceleration-limiting circuitry and the tachometer generator. Potentiometers in external circuitry around the pre-amplifier provide "loop-gain" and "zero-speed" adjustments. Power for the pre-amplifier is provided by ±15-volt precision power supplies incorporated on the amplifier chassis.

A pair of driver amplifiers take the output of the pre-amplifier and provide sufficient drive current for the power transistors. One of the drivers provides the inversion necessary to provide a push-pull signal for the power

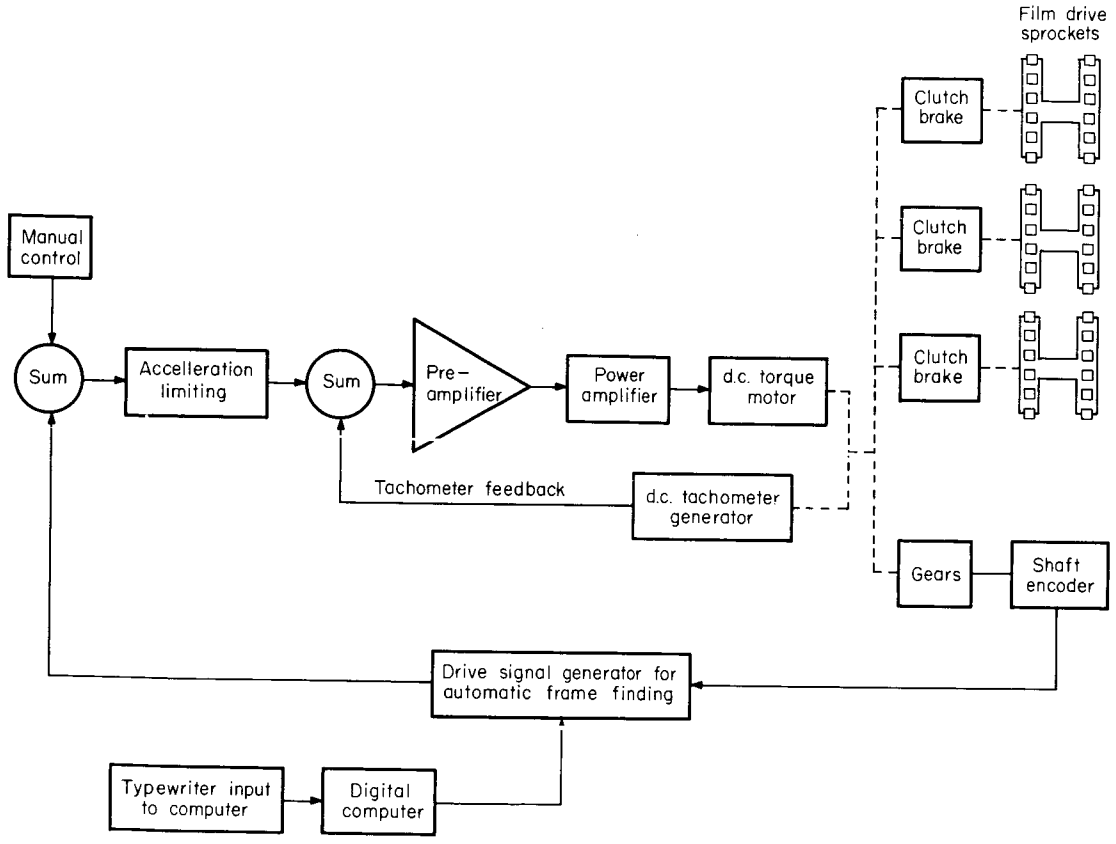

Fig. 8.1. Block diagram of film-drive servo system and control circuitry.

(OVERLEAF BLANK)

amplifiers. The power amplifier consists of two single-ended, push-pull amplifiers, operating independently, but in push-pull with each other. These provide a ±32-volt push-pull voltage to the motor. The output power transistors are mounted on heat sinks cooled by forced air, and operate considerably below their maximum-power-output capability. A regulated power supply provides +35 volts for the power amplifier. Current-limiting circuitry within the power supply provides protection for both motor and transistors in the event of accidental overload or motor stall.

V. Krone

(OVERLEAF BLANK)

9. PLASMA DISPLAY[†]

D. L. Bitzer
H. G. Slottow
B. M. Arora
M. L. Bunting
R. L. Johnson
E. Stredde

9.1 Introduction

The invention at CSL of the Plasma Display Panel was the culmination of research that was stimulated by the needs of the PLATO computer-based education system. This display responds directly to digital signals from a computer; it retains its images without need for regeneration from an auxiliary memory; and it provides a bright display that can be viewed satisfactorily in high ambient light. The device can also be interrogated by the computer, and it seems likely that the observer can enter graphical information directly into the display by one of several kinds of pens. Moreover the possibilities of developing multi-color displays are encouraging.

The members of the Plasma Display Group are engaged in research on the properties of this new device, in limited development of the display, and, where appropriate, in the guidance of industrial development.

Briefly, the Plasma Display Panel is a rectangular array of bistable gas-discharge cells. The cells are separated from the exciting electrodes by glass panels and the memory in each cell is provided by charge storage on the insulating end walls of the cells. In the "one" state, these charges, which flow to the walls during short, intense glow discharges, combine with induced charges to fire the cell once every half cycle of a high-frequency sustaining signal. The duration of each discharge is typically 50×10^{-9} sec. In the "zero" state, the wall charges are such that the cell cannot fire. The cells are addressed by coincident-voltage techniques. More-detailed information is

[†]Supported in part by the Syracuse University Research Corporation under Contract SURC 66124.

provided in the previous two progress reports,[1,2] and in two laboratory reports.[3,4]

Until this reporting period, experimental research on the display was concerned principally with the properties of a single discharge cell. Although this work is still by no means complete, our understanding of the cell properties was sufficient to make it appropriate to plan experiments with small arrays. In the following section we discuss some results of these experiments which include the successful writing and erasing of characters on a 4X4 matrix. Subsequently, we report some measurements of the spectral characteristics of the light from the display, and we describe a mode of operation in which the memory cell can be in either of two distinct "on" states.

9.2 Display of Characters

The experimental display is an 8X8 array to which connections are made only to the center four rows and columns. Each conductor is connected to an amplifier, and all eight amplifiers are driven by a single 500-KHz generator. The amplitude of the output signal at each line is set to one of three levels by transistor switches that are in turn controlled by manual switches, or through interface circuitry by the CDC 1604 computer.

---

[1] Coordinated Science Laboratory Progress Report Dec. 1965, Jan., Feb. 1966.

[2] Coordinated Science Laboratory Progress Report Mar., April, May, 1966.

[3] Bitzer, D. L., Slottow, H. G., and Willson, R. H., Preliminary Description of the Plasma Display Tube, Nov. 1965.

[4] Willson, R. H., A Capacitively Coupled Bistable Gas Discharge Cell for Computer Controlled Displays, CSL Report R-303, June, 1966.

In the sustaining mode the signals on all lines are at the intermediate voltage level; the combined signals across the cells are all within the sustaining range; and the pattern on the display remains unchanged. When the signals on each of two intersecting conductors are raised to the highest level, the combined voltage across the cell at the intersection exceeds the firing voltage, and the cell is turned on. The voltage across the other cells adjacent to the selected lines also rises, but not enough to fire the cells. Similarly, when the signal on two intersecting lines is reduced to the lowest level, the voltage at the intersection falls below the minimum sustaining voltage and the cell is turned off. The voltage across the remaining cells along these lines is also reduced, but it also stays within the sustaining range.

Figure 9.1 shows the appearance of several characters after the appropriate cells have been selected and after the selection signals have been removed. The external-voltage conditions are therefore the same for each character. The distance between the centers of adjacent cells is 0.025 in, and the actual height of each character is just under 0.1 in.

This method of driving the display, since it requires a line driver for each line, is neither the most economical nor the most elegant. It was used here because it is straightforward and was the easiest to implement quickly at this stage of development.

9.3 Effects of Parameter Variations

If every cell in the display had identical electrical characteristics, and the various exciting voltages were the same for all lines, the conditions on the write voltage, the erase voltage, and the sustaining voltage would be

$$V_w > V_F,$$

$$V_e < V_E,$$

$$V_E < V_s < V_F, \tag{1}$$

in which V_F is the firing voltage; V_E is the minimum sustaining voltage; V_s is the sustaining voltage; V_w is the write voltage; and V_e is the erase voltage. Under these rather unrealistic conditions, the necessary separation between the firing voltage V_F and the minimum sustaining voltage V_E can be arbitrarily small. On the other hand, it seems intuitively clear that for reliable operation of the display the relative separation between these voltages should be large. This idea can be made precise by relating this memory margin to the variations in the signals and in the cell voltages.

We redefine the above symbols as mean values, and we express the voltage spreads in the usual way by means of increments. For example, the firing voltages of all cells falls in the range $V_F \pm \Delta V_F$. It is then easy to show that the restrictions on the mean write, erase, and sustain voltages are

$$V_w > V_F + \Delta V_F + \Delta V_w,$$

$$V_e < V_E - \Delta V_E - \Delta V_e, \tag{2}$$

$$V_E + 3\Delta V_E + 2\Delta V_e + \Delta V_s < V_s < V_F - 3\Delta V_w - 2\Delta V_w - \Delta V_s.$$

We now define the memory margin as

$$\alpha = (V_F - V_E)/\tfrac{1}{2}V_F \tag{3}$$

and substituting in Eq. (2) we find that

$$2 - \alpha + (3\Delta V_E + 2\Delta V_e + \Delta V_s)/\tfrac{1}{2}V_F < V_s/\tfrac{1}{2}V_F < 2 - (3\Delta V_F - 2\Delta V_w - \Delta V_s)/\tfrac{1}{2}V_F \tag{4}$$

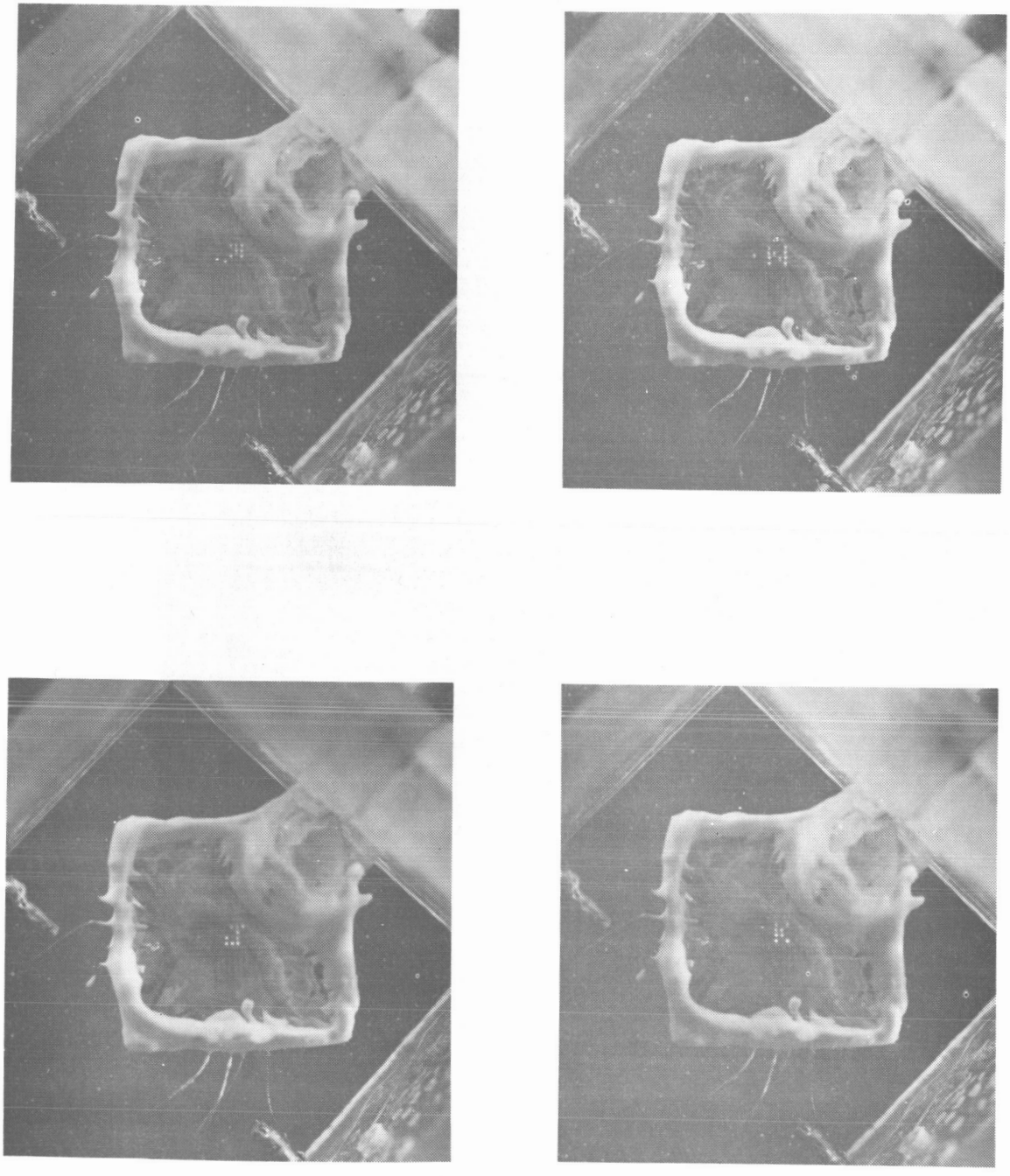

Fig. 9.1. Characters on a 4x4 Plasma Display.

(OVERLEAF BLANK)

The minimum acceptable value of α is obtained in the limit when these inequalities become equalities. Then the minimum memory margin is

$$\alpha_{min} = (3\Delta V_E+3\Delta V_F+2\Delta V_e+2\Delta V_w+2\Delta V_s)/\tfrac{1}{2}V_F \quad (5)$$

If for simplicity we assume that the variations for all voltages are the same we obtain

$$\alpha_{min} = 12\Delta V_F/\tfrac{1}{2}V_F \quad (6)$$

Table I shows the influence of the variations on α when $\Delta V_F/\frac{1}{2}V_F$ varies from zero to 0.05. Table II shows the actual values of α, $\Delta V_F/\frac{1}{2}V_F$, V_E, and V_F that correspond to the photographs of Fig. 9.1.

For reliable operation of the display, the voltage variations should be as small as possible, and the memory margin should be large. The regulation of the signal voltages V_w, V_s, and V_e is governed by the external circuits, and can be made small by good design. In contrast the firing voltage V_F, the extinction voltage V_E, and the memory margin α, which depends on these voltages, are characteristics of the gas-discharge cells. Fortunately, there exists a range of gas conditions for which α is large and the variations in V_F and V_E from cell to cell are small. Figure 9.2 shows the influence of nitrogen on these properties when the total pressure of a neon-nitrogen gas combination is held constant at 700 Torr. The lower curve shows the average of ΔV_E and ΔV_F. The upper curve shows the voltage difference between $\frac{1}{2}V_E$ and $\frac{1}{2}V_F$. When nitrogen accounts for about 9% of the total pressure, the memory margin, α, is about 0.7, and the average of $\Delta V_E/\frac{1}{2}V_F$ and $\Delta V_F/\frac{1}{2}V_F$ is less than 0.05. The minimum-acceptable value of α under these conditions is about 0.60.

Table I. Dependence of α_{min} upon values of $\Delta V_F/\frac{1}{2}V_F$.

α_{min}	$\Delta V_F/\frac{1}{2}V_F$
0.12	0.01
0.24	0.02
0.36	0.03
0.48	0.04
0.60	0.05

Table II. Values corresponding to Fig. 9.1.

α	$\Delta V_F/\frac{1}{2}V_F$	V_E	V_F
0.71	0.048	520	820

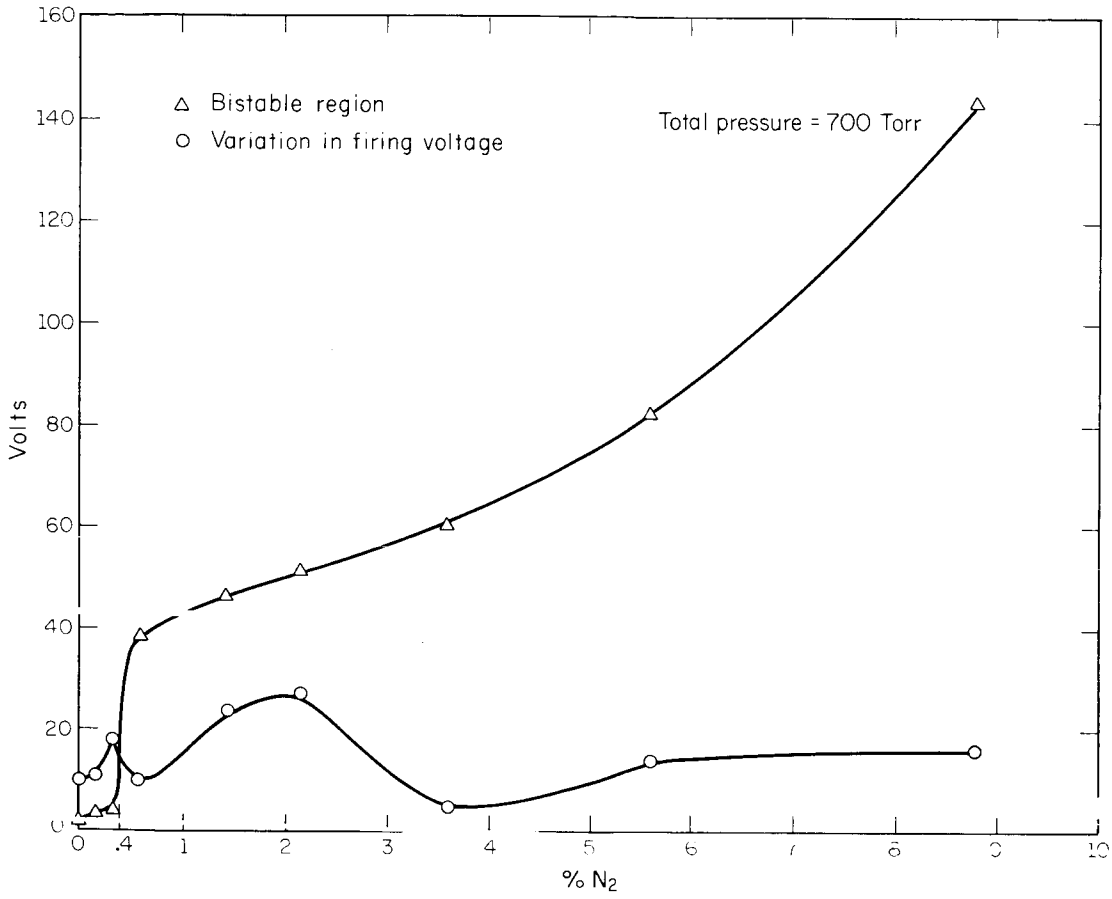

Fig. 9.2. Influence of nitrogen content on bistable voltage range and on parameter variations.

(OVERLEAF BLANK)

We attribute the small variation in V_F and V_E to the fact that the portion of the Paschen curve that corresponds to these pressures is relatively flat. The critical voltages are thus insensitive to variations in pressure and in thickness. Even the widths of the deposited electrodes, which vary by as much as 2:1, have little effect. This insensitivity is shown in another way by the two photographs of Fig. 9.3. Fig. 9.3a shows the light output from a single cell on a time scale of 50×10^{-9} sec/cm. Figure 9.3b shows the light from 12 cells on the same time scale. The oscilloscope gain for this photograph has been reduced by a factor of 10. Within our ability to measure these records, the twelve cells are turned on and off together without any evidence of time stagger.

9.4 Light Output

As a first step in measuring the brightness of the display, the spectral content of the light was measured using an EMI-9552B photomultiplier and a Bosch-and-Lomb monochromator. These measurements, corrected for the response of the photomultiplier are shown in Fig. 9.4. The most surprising feature of this curve is the evidence of radiation in the near ultraviolet, particularly in view of the fact that it is heavily attenuated by the soda-glass panels. In the visible region of the spectrum the dominant line is at 5800 Å. This line is contributed by the neon, but the color of the neon-nitrogen discharge differs slightly from the pure-neon discharge in that the orange is tinged with blue.

No absolute brightness measurements have yet been made. However, it is sufficiently bright in a normally-lighted room, and without attentuation, it provides too much light in a darkened room. A rough indication of brightness was obtained by illuminating the display by a 1000 watt lamp held about 4½ feet from the display. The character on the display was still visible to an observer, and its image could also be seen on a photograph taken under these conditions.

9.5 Existence of Several Stable States

When a cell is in the "one" state, the wall voltage, proportional to the wall charge, alternates at each discharge between levels that are equal in magnitude, and opposite in polarity. Since the leakage of charge on the surfaces is negligible on this time scale, the amounts of charge transferred at each discharge are equal. A cell in the "zero" state, on the other hand, has a wall voltage that is, ideally, zero. The transition between these states is marked by a series of discharges in which the amounts of charge transferred at each discharg are not equal. Because the amount of charge increases rapidly with the slope of the existing voltage, the transition process is very rapid and reaches equilibrium within several cycles. With a sinusoidal signal, there is a single equilibrium state in which the discharges occur at times when the slopes are equal.

Figure 9.5a shows the approach to equilibrium when the exciting signal (lower trace) is switched on. The upper two traces show the same light output, the offset being provided to simplify comparison with the exciting voltage wave.

An appropriately chosen nonsinusoidal signal can provide two distinct equilibrium states, in both of which the cell is "on" in the sense described above. This situation is shown in Fig. 9.5b which is a tracing of an oscillogram. The upper trace shows the wave shape of the existing signal. The second trace shows the light output in one of the two states. The wall voltage after the second discharge in the pair is such that the reverse pulse (at the left of the photograph) cannot provide the conditions for discharge. The third trace shows a similar response in the second state.

The demonstration of this process suggests a number of applications, particularly in the use of the Plasma Display as a memory. Perhaps its greatest

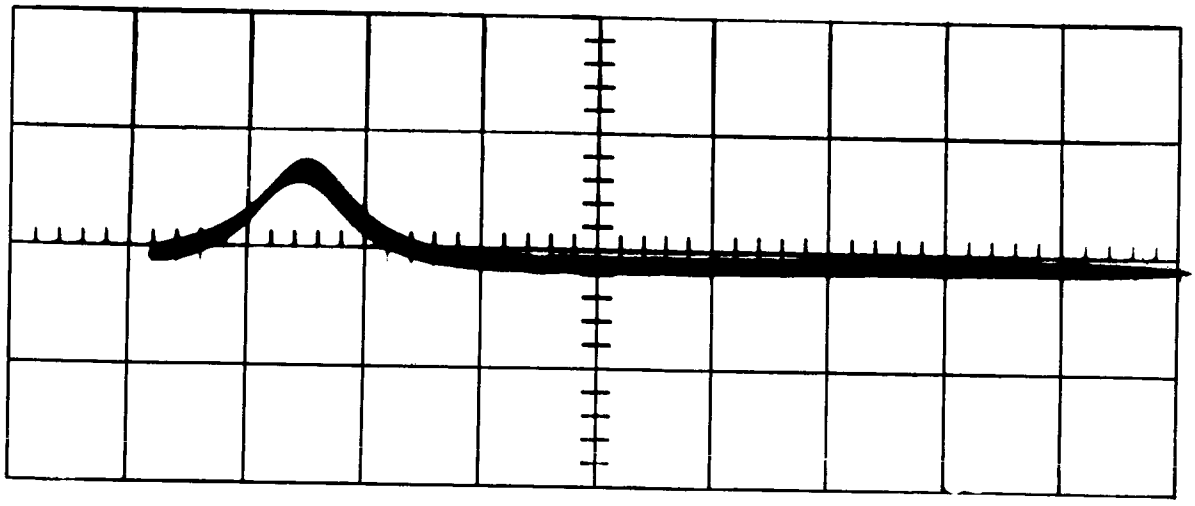

Fig. 9.3(a). Light signal from single cell. Time scale: 50×10^{-9} seconds/division.

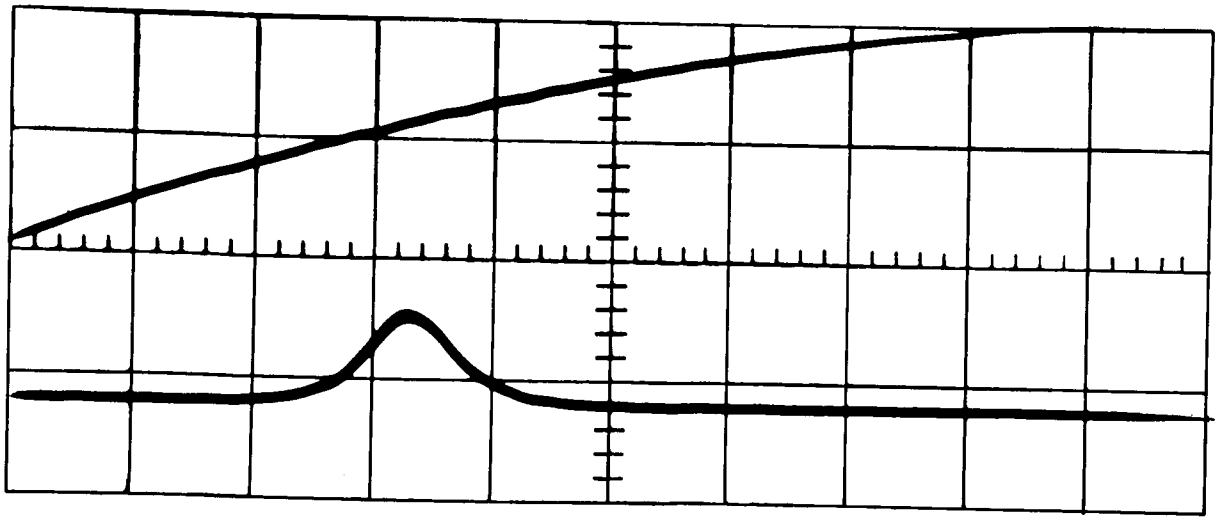

Fig. 9.3(b). Light signal from 12 cells. Time scale: 50×10^{-9} seconds/division, and vertical-amplifier gain reduced by factor of 10.

(OVERLEAF BLANK)

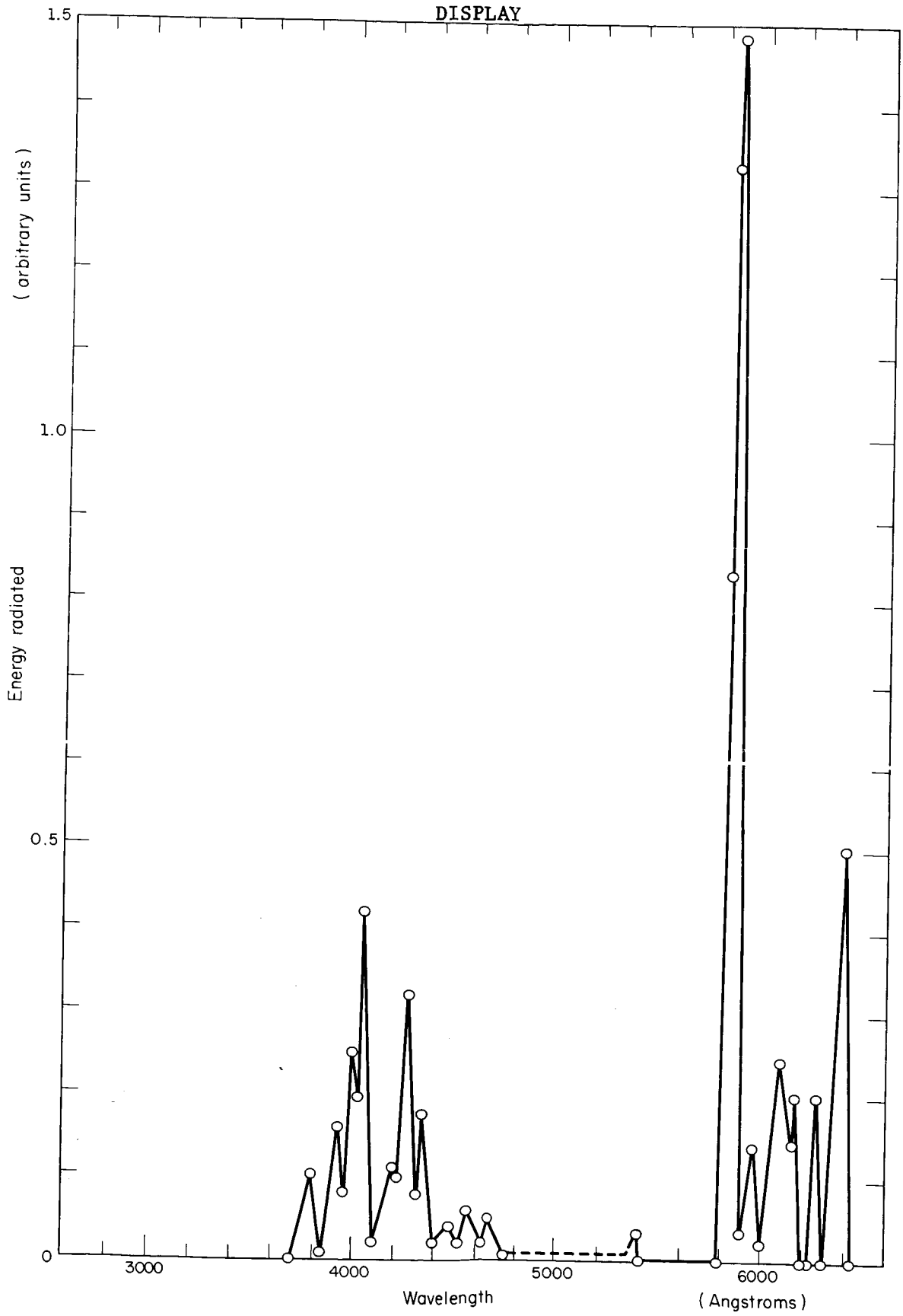

Fig. 9.4. Spectral response of Plasma Display cells.

(OVERLEAF BLANK)

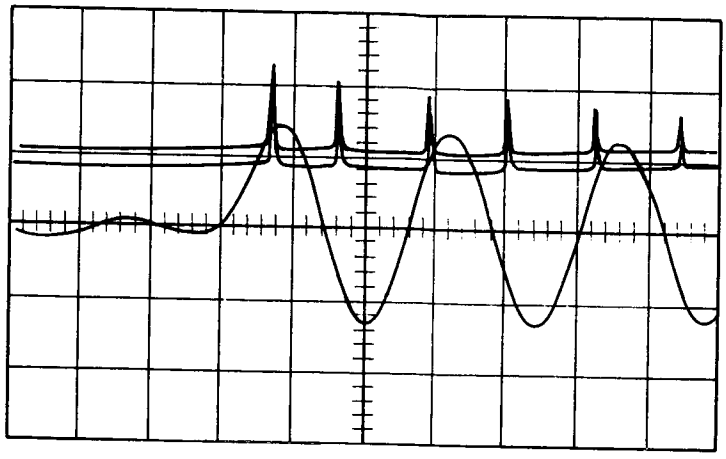

Fig. 9.5(a). Approach to equilibrium after turn on.

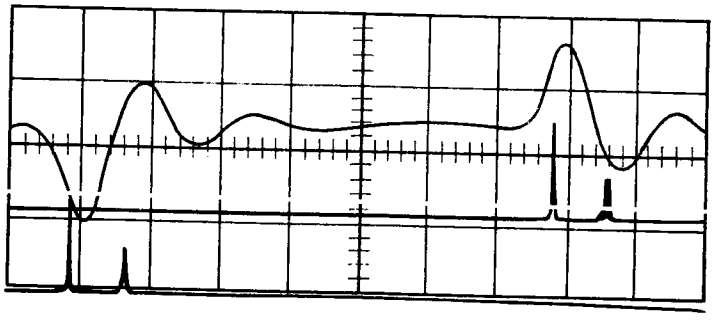

Fig. 9.5(b). Two stable "on" states in Plasma Display cell.

(OVERLEAF BLANK)

importance, however, is that, since its existence was predicted on the basis of our model of the basic cell processes, its demonstration reinforces our confidence in the model itself.

B. Arora
D. L. Bitzer
H. G. Slottow

(OVERLEAF BLANK)

10. INFRARED CONVERTER

W. D. Compton
W. P. Bleha
S. Depp
J. T. Jacobs
R. N. Peacock
A. Tulumello

10.1 Introduction

In December, 1965, Professor W. D. Compton suggested that the tunneling of minority carriers between two semiconductors be used to directly convert infrared photons to visible photons. The operation of such a device can be understood by reference to Figs. 10.1 and 10.2. A semiconductor-insulator-semiconductor (SIS) sandwich is constructed of two semiconducting materials of different forbidden band gaps (Fig. 10.1). Consider the case for two n-type semiconductors. In the absence of a bias, and neglecting band bending at the surface, the Fermi levels will coincide as shown in Fig. 10.2. The band gap energy of Ge and CdS are used for illustration.

Consider the system biased as shown in Fig. 10.3. Absorption of photons in the narrow-band-gap material generates free electrons and holes. With the system biased such that the valence bands are at nearly the same energy, the holes can tunnel into the wide-band-gap semiconductor, recombine with the majority carriers, giving photons having an energy of the wide-band-gap material. At $77^{\circ}K$, the edge luminescence of CdS has a spectral distribution between 5100 and 5400 angstroms (2.43 to 2.30 eV).[1] Thus, photons of energy about 0.8 eV can be converted to photons of energy about 2.4 eV. Energy conservation is provided by the electric field.

A number of fundamental problems must be solved before the feasibility of such a device can be evaluated. For example, the injection of minority carriers

---

[1] J. J. Lambe and C. C. Klick. Phys. Rev. 103, 1715 (1956).

into the II-VI semiconductors is quite difficult, although tunneling of minority carriers between metals and II-VI compounds is known to occur.[2] The successful solution of this problem, however, would allow these materials to be used in a wide variety of electroluminescent display devices. The efficiency of tunneling minority carriers between two semiconductors depends upon such factors as the lifetimes of the minority carriers and the magnitude of the band bending that occurs at the semiconductor-insulator interface. Utilization of thin-film techniques presents special problems since the luminescence of thin films of the II-VI phosphors are normally low and since the resistivity of films of Si and Ge is difficult to control.

The applied-physics group has initiated a number of projects that are designed to provide information about the fundamental nature of some of these processes. It is ultimately intended that application of these ideas will be made to a wide variety of solid-state display problems.

10.2 Experimental Results and Procedures

This initial work was aimed at a feasibility study of making the SIS device just described. The experimental work began with the formation of single-crystal CdS-evaporated SiO-evaporated Au sandwich devices as previously reported.[2] Green electroluminescence (EL) at 77°K was observed for voltages as low as 1.8 volts applied across the device. A gold film evaporated directly on the CdS crystal gave no EL even at much higher voltages and currents. To make the SIS device just described, a semiconductor with a small band gap was used instead of a metal as the third element in the device. Attempts at making Ge and Te films by vacuum evaporation resulted in films that did not adhere

---

[2] R. C. Jaklevic, D. L. Donald, J. Lambe, and W. C. Vassel, Appl. Phys. Letters, 2, 7 (1963).

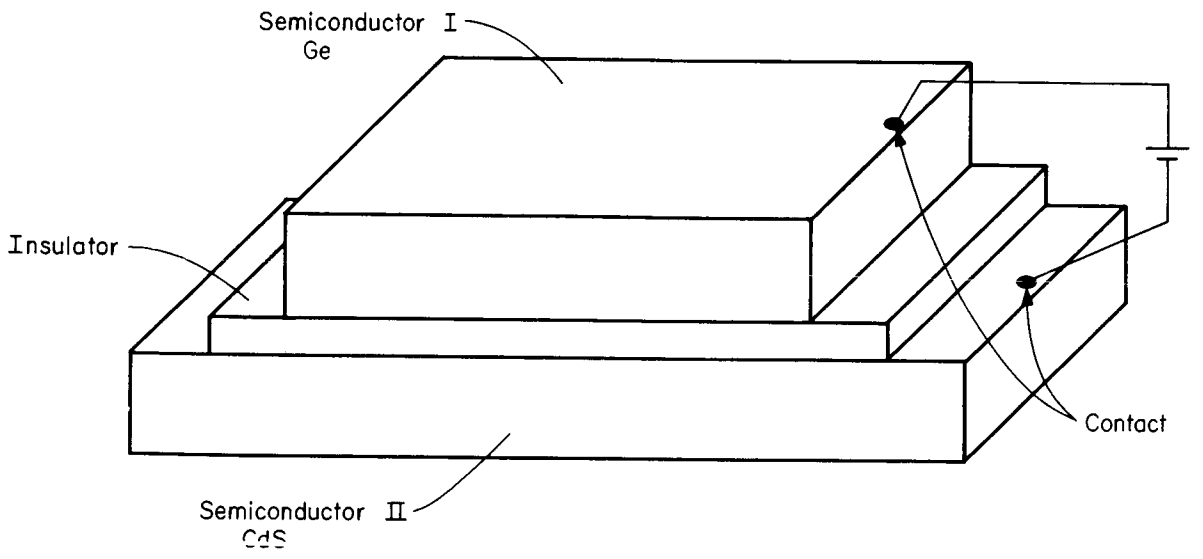

Fig. 10.1. Diagram of a SIS structure.

(OVERLEAF BLANK)

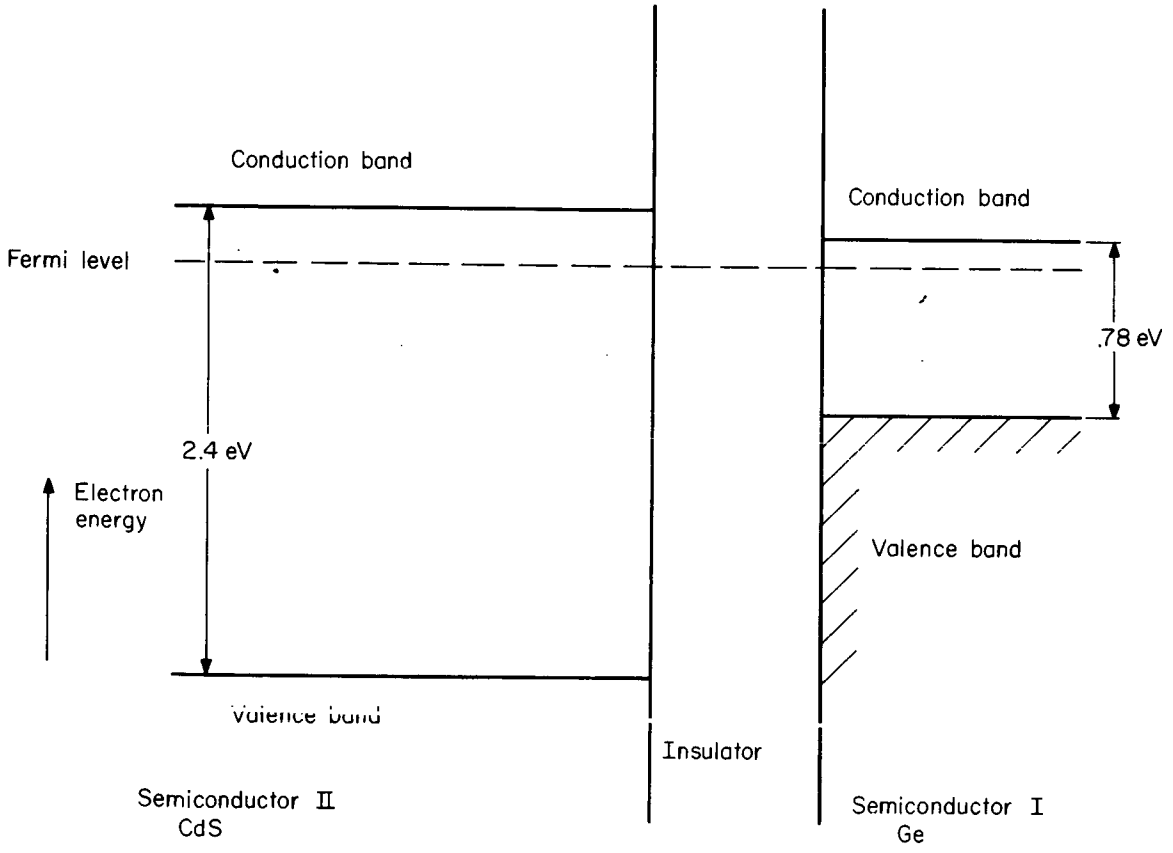

Fig. 10.2. Energy band diagram of a zero biased SIS structure.

(OVERLEAF BLANK)

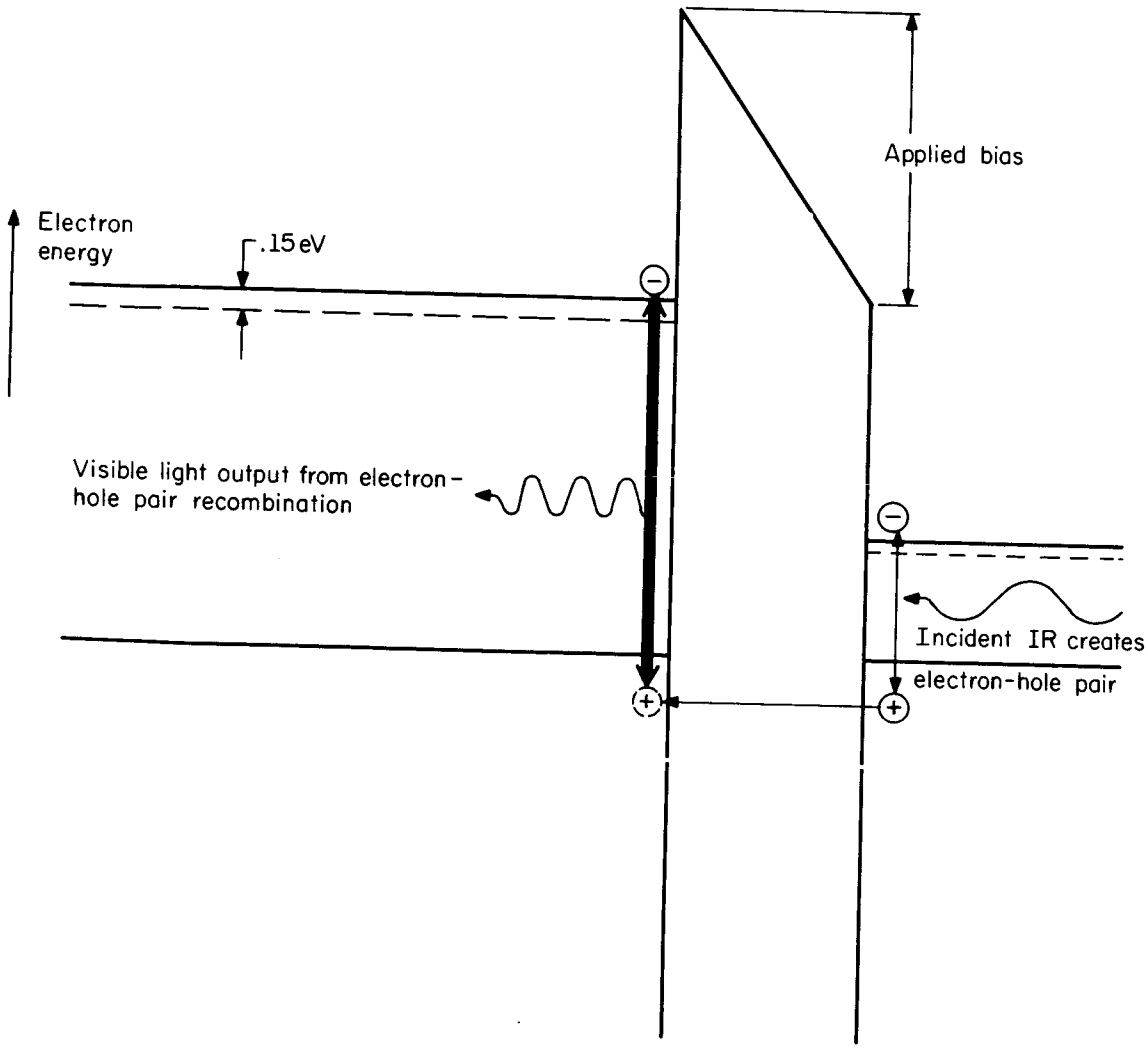

Fig. 10.3. Energy band diagram of a biased SIS structure.

(OVERLEAF BLANK)

to the SiO-coated CdS and thus electrical measurements were not possible.

While developing the techniques required for depositing Ge and CdS thin films, it was decided to make junctions by pressing together pieces of sawed-and-polished Ge and CdS, with and without an intervening SiO evaporated layer.

Preparation of this type of device consisted of polishing the Ge and CdS crystals to a flat, smooth finish and then chemically etching away surface damage in standard chemical etches. In some samples 50-100 Å of SiO was vacuum evaporated on the Ge or CdS or both. The pieces were then pressed together in the atmosphere and held by spring clips. Electrical contacts were made by indium solder to the CdS (which makes an ohmic contact). Contacts were made to the Ge by tin contacts, Cerro-seal solder, or sandblasting the surface of the Ge and using Cu pressure contacts. The Si was contacted by baked Al films or stainless-steel pressure contacts. For measurements a sample was suspended in liquid nitrogen, and light from a flashlight or high intensity tungsten light source filtered by a Corning-Glass 7-56 IR filter was used to illuminate the sample. The sample could be illuminated through the CdS or, alternatively, on the Ge. Qualitatively similar results were obtained for IR illumination from the CdS side or the Ge side.

Visual observation of the green luminescence indicated that it originated as small spots at the CdS-SiO interface. These spots probably result from thinner regions in the insulating barrier where tunneling is enhanced or from the presence of a contact point with the Ge.

This method was used for a variety of dopings of both n- and p-type Ge. The CdS used was UHP 10-30 ohm-cm, purchased from the Eagle-Picher Co.

Electroluminescence was seen from samples made with all dopings of Ge used. EL was seen in samples using intrinsic Ge, 70 ohm-cm n-type Si and 100 ohm-cm

p-type Si. This effect was seen only in cases where there was at least a 20% change in current through the device.

The magnitude of the current at the EL point was largely controlled by the number of actual contacts made in pressing the two pieces together. Different samples of similar materials showed wide variation in EL-point currents, though in general the higher the doping the higher the EL-point current. With intrinsic Ge, currents at the EL point varied from 0.1 ma to 2 ma for different samples. This uncontrollable variation in current severely limits the usefulness of this method of fabrication of devices.

The voltage applied across the device was also higher in most cases than that predicted by theory. The voltage across the device includes resistive drops in the Ge (Si) and CdS, contact resistances, and the actual resistance of the junction region. Measurement of the EL voltage across the CdS-SiO layers indicated that voltages of the proper order of magnitude were across the junction in a few samples, while most of the samples had EL-point voltages higher than that predicted by theory.

Since the resistance of the Ge or Si can be changed by a factor of 100 with the intensity of IR used in illuminating these samples, it is possible that this effect controls the luminescent process. If the junction region is of comparable resistance to the unilluminated Ge (Si), the illumination with IR will lower the resistance of the Ge (Si), thereby increasing the potential across the junction region. This voltage change will effectively alter the bias across the junction and significantly increase the electron tunneling probability into the conduction band of the Ge (Si) (Fig. 10.4).

Measurements of the voltage across the CdS-SiO section of the device showed a voltage increase when IR illuminated the samples indicating a change of

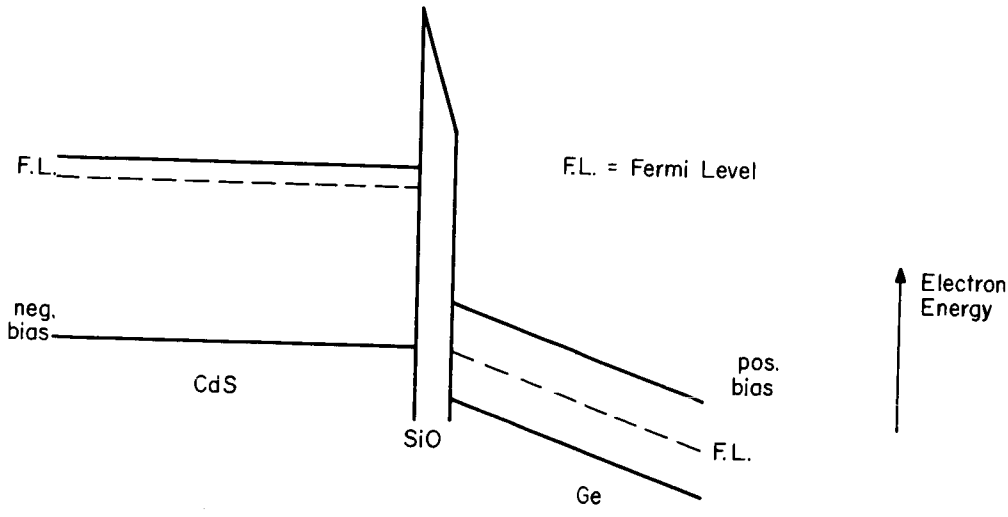

Fig. 10.4. Energy band diagrams of photoconductivity controlled electroluminescence.

(OVERLEAF BLANK)

resistance across the junction since the resistance of the CdS remained constant. This IR-induced EL was also seen in p-type Si where the number of holes available in the valence band of the Si for tunneling is not significantly increased by the IR. The effect has not been seen in strongly-doped n-type semiconductors where the change in the number of holes in the valence band of the Ge would be at a maximum.

A measurement of the variation of the current and the intensity of the luminescence with the variation of intensity of incident IR is under way. A linear relation would suggest valence-band tunneling as the dominant mechanism, whereas a nonlinear relation would indicate conduction-band tunneling since the density of available states in the conduction band would change as more voltage was applied across the insulating barrier and the tunneling probability would change nonlinearly as more voltage was applied across the junction region.

From experiments performed, one cannot determine the necessity of an insulating barrier between the CdS and Ge. The necessity of such a barrier was previously shown[2] for tunneling between metals and CdS, but in the present study some sandwiches exhibited EL even though they had no oxide interface. A barrier in these cases could be caused by absorbed surface contamination, surface damage, or be the result of band bending due to the difference of electron affinities in the two semiconductors. Water vapor and other absorbed gases were not carefully controlled on the surfaces in the preparation of samples.

The evidence for band bending at the surface comes from the injection efficiency of holes. The efficiency of injection of holes into CdS increases with increasing n doping of the Ge (Si) indicating that the insulating barrier may be effectively increased by band bending at the surface of the Ge (Si).

In a metal-semiconductor junction the band bending increases, and hence the barrier width becomes narrower as the doping is increased. Thus the lower currents and lower EL intensity for devices made with high-resistance Ge and Si may be due to an increase in the effective barrier width. Also supporting this is the fact that the EL voltage for a degenerate n-type Ge sandwich approaches that of a metal sandwich. This is expected since the degenerate semiconductor acts like a metal and significant band bending will not occur.

In summary, the following observations have been made during this feasibility study on pressed contacts:

1) high-resistance semiconductors are necessary to see IR-induced electroluminescence;
2) it may be possible to utilize the surface barrier as the tunneling barrier;
3) it has not been shown conclusively whether the observed processes result from tunneling from the valence band or from the conduction band of the Ge (Si).

The problem of making thin-film devices is being investigated from two directions. One is the preparation of electroluminescent cadmium-sulfide films on glass, germanium, and silicon substrates. This work is performed by Dr. A. Tulumello. The results of his study are discussed in the following section. The other approach is to prepare photoconductive germanium and silicon films on cadmium sulfide. The status of this program is reported below by S. Depp.

W. D. Compton
R. N. Peacock
J. T. Jacobs
W. P. Bleha

10.3 Preparation of Ge Films

Work has been carried out for the design and construction of a system capable of producing high-quality germanium films. A literature survey suggested that at least two processes had been developed to produce epitaxial growth of germanium films that are compatible with the requirements imposed by the present device: disproportionation of GeI_2 and hydrogen reduction of $GeCl_4$. Both methods involve the use of an available open-tube furnace and can, in general, use the same gas-feed equipment. Therefore, a single convertible unit is being constructed which will allow investigation of both methods.

From preliminary trials using the GeI_2 mechanism, it was found that careful control of gas-flow rate through the furnace, gas composition, temperature, substrate orientation, physical relationship between the reactants, etc., is necessary for reproducible depositions. With these parameters in mind, flowmeters and temperature-control equipment will be used along with traps and purifiers to reduce the impurity content of the gases.

It is hoped that the system will allow sufficient control to accurately predict conductivities and mobilities of the depositions. Eventually, controlled doping of the films by adding a known amount of impurity to the reactants will be attempted. Since this system can readily be converted for the deposition of silicon, it may be possible to control the cobalt doping of silicon with sufficient accuracy to adjust the Fermi level, a necessity for a device currently under consideration.

S. Depp

10.4 Preparation of CdS Films

Equipment was assembled to deposit CdS by sublimation at 1100°C and condensation at 800°C in an atmosphere of H_2S and H_2.

CdS was prepared in three different ways each of which might be applied to making CdS films:

1) Pure CdS was sublimed at 1100°C and condensed at 800°C in an atmosphere of H_2 and H_2S.
2) Cd was volatilized in an atmosphere of H_2 and H_2S at 900°C and the resulting CdS condensed at 800°C.
3) CdS was prepared by the thermal decomposition (at 400°C) of a spray of $CdCl_2$ and thiourea by the reaction,

$$2H_2O+CdCl_2+(NH_2)_2CS \rightarrow CdS+2NH_4Cl+CO_2.$$

Of the three methods used, only the first two showed the green edge luminescence of interest. Method 3 showed a red luminescence in experiments performed to the present. Further experimental work may well be expected to yield green edge luminescence.

It has been shown that high-purity CdS (99.99%) which was red luminescent under uv excitation as obtained from the supplier, was converted to the green luminescent material when heated in an atmosphere of H_2 and H_2S at 1100°C.

For Further Work:

1) Temperature controllers are being devised for the maintenance of the elevated temperatures necessary for the sublimation of CdS.
2) Red-luminescent CdS films prepared in various ways will be baked in an H_2-and-H_2S atmosphere at 400°C in an effort to obtain green edge luminescent CdS from red-luminescent material at lower temperatures.

3) In view of the experience of Chamberlin and Skarman[3] in obtaining green-luminescent CdS, a further study will be made of the effect of solution variables on the films produced by spray deposition.

4) A more careful study will be made to establish criterion for correlating the luminescence with previous conductivity and Hall-effect measurements reported by Kröger.[4]

(OVERLEAF BLANK)

[3] R. R. Chamberlin and J. S. Skarman, J. Electrochem. Soc. 113, 86 (1966).

[4] F. A. Kröger, H. V. Vink, and V. van den Boomgaard, Z. Physik. Chem. 203, 1 (1954).

11. INFORMATION SCIENCE

R. T. Chien
R. B. Ash
L. Bahl
J. T. Barrows
D. Chow
C. Hartman
H. T. Hsu
T. Kasami
V. Lum
F. P. Preparata
R. J. Tracey
K. K. Tzeng

11.1 Introduction

The purpose of this research is to develop methods for the design and optimalization of digital systems for the transmission, retrieval and processing of information.

Further progress is reported in all areas under investigation. New studies in information retrieval systems have been initiated and progress made to-date is reported. Also reported are results in the connection assignment problem of diagnosable systems.

11.2 Algebraic Theory of Cyclic Codes[†]

Two related aspects of the BCH codes have been investigated. The problems are (1) to have a better knowledge concerning their minimum distances, and (2) to find decoding methods not limited by the BCH bounds. Progress made during the last six months is summarized in a technical report R-306.

A theory is presented which enables one to determine if a particular BCH code has minimum distance larger than its BCH bound. The derivation of this new theory is based on the Mattson-Solomon approach. The new results are easy to apply as illustrated by several examples. They are applicable to many codes including the well-known Golay (11,6) code over GF(3).

A general algebraic full-power decoding method is outlined. In addition, two different methods are presented for the two special cases:

[†]Supported in part by the National Science Foundation under Grant NSF GK-690.

(1) the decoding of the two Golay perfect codes to its full error-correcting capability, and (2) the decoding of concatenated codes. All decoding methods are found to be quite practical.

V. Lum
R. T. Chien

Weight distribution formulas are of considerable importance in evaluating the performance of codes and in address design of random access communication systems. Two classes of weight distribution formulas have been obtained. The first class of formulas, relating to a class of cyclic codes, is reported in Report R-285. The result may be summarized as follows.

"Let $h_1(X)$ and $h_2(X)$ be different irreducible polynomials such that $h_1(\alpha^{-2^n-1}) = 0$ for some $n(0<n<m)$ and $h_2(\alpha^{-1}) = 0$, α being a primitive element of $GF(2^m)$. This report presents the weight distribution formula of the code of length 2^m-1 generated by $(X^{2^m-1}-1)/[h_1(X)h_2(X)]$ for any m and n. Some applications to the cross-correlation problem between two different maximum length sequences are presented."

Another class of weight distribution formulas obtained relates to BCH codes. They appear in Report R-317. The following is an abstract of the report.

Several techniques useful for finding weight distributions of the binary Bose-Chaudhuri-Hocquenghem codes (the BCH codes) of length 2^m-1 and some other cyclic codes are presented. By using (1) a relation between the BCH codes and the Reed-Muller codes, (2) the invariant property of the BCH codes (extended by the addition of an overall parity check) under a doubly transitive group of permutations on digit positions and (3) the power moment identities, explicit weight distribution formulas are derived for $(2^{m-1}-2^{m/2-j}-1)$-BCH codes

with j = 0 and 1, $(2^{m-1}-2^{(m-1)/2+j}-1)$-BCH codes with $0 \leq j < 2$, the dual codes of double-error-correcting BCH codes, the dual codes of triple-error-correcting BCH codes, and some other class of cyclic codes. Here, for odd d, a d-BCH code is a BCH code of length 2^m-1 which has $\beta, \beta^2, \ldots, \beta^{d-1}$ but not β^d as roots of its generator polynomial where β is a primitive element of $GF(2^m)$.

T. Kasami

11.3 Coding Methods for Information Retrieval[†]

An invesitgation has been made on the application of threshold decoding to information retrieval. Threshold decoding is easily instrumented. If a code can be decoded by threshold decoding, the error vector is obtainable from the syndrome. Hence threshold decoding is applicable to information retrieval. Massey has shown that the maximal length code, the first order Reed-Muller codes and the Hamming codes can all be L-step orthogonalized.[1] We will now show that all Reed-Muller codes and all modified Reed-Muller Codes can be L-step orthogonalized, hence threshold decodable. The results obtained are useful in error correction as well as information retrieval.

Theorem 1: Reed-Muller Codes can be L-step orthogonalized.

The decoding method[2] proposed for Reed-Muller Codes uses majority voting to determine the value of some information digits and then the sum of certain base vectors is subtracted from the received vector according to these decoded

---

[†]Supported in part by the National Science Foundation under Grant NSF GK-690.

[1]Massey, James: Threshold Decoding, The MIT Press, 1963.

[2]Peterson: Error-Correcting Codes, p. 75. The MIT Press, 1961.

information digits. We can then obtain another information digit from this resulting vector and repeat the process. The general idea of proving this theorem is that we can derive a set of modified parity checks to vote for a certain sum of noise bits from the set of equations which is used to vote for an information digit. Then, these known sums of noise bits can be used to form another set of modified parity checks to vote for a different sum of noise bits in a way similar to the original decoding approach.

Definition: Let α be a primitive element of $GF(2^m)$ $(m>1)$ and

$$\alpha^f = \sum_{i=0}^{m-1} v_{if} \qquad 0 \leq f < 2^m-1,\ v_{if} \in GF(2).$$

Let all $n = 2^m-1$ digits of v_0 be "ones," thus

$$v_0 = (11\ldots1),$$

and let

$$v_i = (v_{(i-1)0}, v_{(i-1)\ 1}, \ldots, v_{(i-1)2^m-2}) \quad (1 \leq i \leq m).$$

The ν-th order modified Reed-Muller Code is defined to be the code generated by the vectors $v_0, v_1, \ldots, v_m$ and all vector products of these vectors ν or fewer at a time.

Theorem 2: ν-th order Modified Reed-Muller Codes can be ν-step orthogonalized.

The general idea of the proof is that the minimum distance of the modified Reed-Muller Codes is one less than the minimum distance of the ν-th order Reed-Muller Codes. Since ν-th order modified Reed-Muller Code is derived from the ν-th order Reed-Muller Code by deleting the first digit and permuting the remaining digits, we lose only one equation by deleting the first digit.

There are still enough equations to vote for error digits in modified Reed-Muller Codes. The v-step orthogonalization can also be proved easily.

A modified Reed-Muller Code differs from a Reed-Muller Code by only one bit in code length, minimum distance, the number of parity check bits, and, also, a modified Reed-Muller Code is a cyclic code. Hence the advantages of the cyclic property can be utilized.

Other results related to the threshold decoding are stated below.

Theorem 3: If a (n,k) code generated by g(x) with $g(1) \neq 0$ can be L-step orthogonalized, then the (n,k-1) code generated by (x-1)g(x) can be L-step orthogonalized.

Proof: Let d be minimum distance of the (n,k) code, we can form d-1 modified parity checks to determine certain selected sum of noise bits. Since d-1 is even, we can form additional modified parity check by adding over all parity check to these d-1 parity checks. Hence we can obtain d modified parity checks to determine the same selected sum of noise bits in the (n,k-1) code. Hence the (n,k-1) code can also be L-step orthogonalized.

Massey suggested an important area of research to be the investigation of L-step orthogonalization for block linear codes. The following theorem states an interesting result in this direction. The proof is omitted.

Theorem 4: All double error correcting codes for $n = 2^m-1$, $m \geq 5$ cannot be L-step orthogonalized.

Another result relating to modified Reed-Muller Codes which is useful for the permutation decoding will also be stated without proof.

Theorem 5: There exist a group G of permutations of order $(2^m-1)(2^m-2)\ldots(2^m-2^{m-1})$ which leaves the modified Reed-Muller code invariant.

A detailed account of the results summarized here will be presented in a forthcoming technical report.

D. Chow

11.4 Coding for Compound Channels[†]

Compound channel codes obtained can be classified in two classes, namely, class K and class P codes. Class K codes are developed by combining generating polynomials of Fire codes (for burst correction) and those of BCH codes (for correction of independent errors). Class P codes are developed by modifying the usage of BCH codes and Gorog codes.

During the past six months a number of significant improvements have been made in our theory of class K codes. We shall state the final version of our principal theorems without proof.

Theorem 1: Assume that a shortened cyclic code generated by $(x^c-1)g_o(x)$ has minimum distance 2t+2 and also can correct every single burst error of length b_o or less. Then, this code can correct both every random error of weight t or less and every single burst error of length $\min\{c, b_o\}$ or less.

Theorem 2: Let $g_o(x)$ be the generator polynomial of a cyclic code of length n and minimum distance not less than 2t+1. Let m_o be the sum of the degrees of those irreducible factors of $g_o(x)$ whose periods are equal to n. If C is a shortened cyclic code of length n generated by $(x^c-1)g_o(x)$ then C can correct every single burst of length less than $\text{Min}\{m_o+1, \frac{1}{2}c+(3t-1)/4\}$.

A lower bound on r of a compound channel code given n, t, and b can be shown as

$$2^r \geq n2^{b-1} + \sum_{i=0}^{t} \binom{n}{i} - n \sum_{i=1}^{t} \binom{b-1}{i-1}$$

[†]Supported in part by the National Science Foundation under Grant NSF GK-690.

where the last term enumerates those error combinations that are burst errors of length not greater than b and of weight not greater than t.

A computer program has been completed to search for Class K and Class P codes. Several runs have been made and an extensive list of both classes of codes have been compiled. The computational results as well as the theoretical results are presented in a forthcoming technical report.

H. T. Hsu
T. Kasami
R. T. Chien

11.5 Coding for the Time-Discrete Gaussian Channel

A time-discrete communication channel which accepts for transmission a vector $\underset{\sim}{x}$ of real numbers, and whose output is $\underset{\sim}{y} = \underset{\sim}{x}+\underset{\sim}{n}$, where $\underset{\sim}{n}$ is a vector of independent Gaussian random variables, is called a Gaussian channel. Certain explicit codes that satisfy an average power limitation $|\underset{\sim}{x}|^2 \leq nM$ are being studied for use on such a channel. These codes are subsets of the n-dimensional point lattice corresponding to a given positive definite quadratic form $f(x_1,\ldots,x_n)$, and are used in conjunction with a bounded discrepancy decoder. The minimum distance in the lattice, as well as the density of its points in n-space, can be determined from the coefficients of the form; these quantities can then be used to estimate the transmission rate and probability of error for the code. The densest point lattices are those corresponding to the so-called absolutely extreme forms, which are known explicitly in eight or fewer dimensions. For example, an eight-dimensional code with 240 words generated from such a form has been evaluated; it compares favorably with several other known codes, even though the bounded discrepancy decoder is only suboptimal. Several directions of research are open. The best result would be to determine absolutely extreme forms in more than eight dimensions; at the present, this appears to be a formidable problem. Also, specific

forms may be investigated in order to determine codes with desirable properties, such as ease of decoding. Finally, the degradation in performance of the codes caused by the suboptimal decoder can be investigated.

R. B. Ash
R. J. Tracey

11.6 Digital Addressing[†]

Progress for the last six months in the area of digital addressing has been summarized in a forthcoming technical report.

Methods of obtaining matrix switches from block designs have been formulated by Singleton and Neumann. The first part of the report extends Singleton method for designing unipolar switches to the design of bipolar switches. A new class of low-noise switches is obtained by permutation of the winding matrix of noiseless switches and it is shown how these new switches are related to block designs.

The latter part of this report is concerned with methods of constructing error-correcting codes from block designs. Some of these codes obtained are found to be optimal.

L. Bahl

11.7 Information Retrieval Systems

The research project on information retrieval systems was initiated this summer with the cooperative effort of an interdisciplinary team consisting of Dewey Carroll, Graduate School of Library Science; Charles D. Hendricks, Department of Electrical Engineering; Sylvian Ray, Department of Computer Science; Paul Weston, Electrical Engineering Research Laboratory; and the authors.

[†]Supported in part by the National Science Foundation under Grant NSF GK-690.

The research program in information retrieval emphasizes two related studies of computer-based systems, namely: (1) Non-Subject Content-Centered Indexing and Analysis, and (2) Implementation and Comparative Analysis of Retrieval Systems. The following sections give a brief account of the significance of these problem areas and progress made to-date.

11.7.1 Non-Subject Content-Centered Indexing and Analysis. In a typical situation in which a user interrogates a document store, most conventional subject-content-centered retrieval systems will result in a reasonably satisfactory yield of relevant materials, provided the area of interest as specified by the requestor is relatively broad and homogenous. These conditions are frequently absent, however, from requests for scientific information originated by research workers. Instead of specifying a single relatively standardized area of interest, their requests are frequently aimed at a combination of several interrelated, complex, and narrowly-defined subjects. Such combinations are most often exceedingly difficult to describe in conventional indexing systems; the specific information desired is usually only very roughly approximated in translation into the retrieval language and contaminates the retrieval output with a large proportion of irrelevant material. What is needed in refining the requestor's target and in improving the retrieval yield is to provide for the utilization of all those readily identifiable relationships in the published literature which are thematically consistent with the requestor's specific problems, immediate situation, and ultimate goals, though these relationships may neither be explicitly nor implicitly specified or indicated by the simple naming of subject interests. Such thematically-consistent relationships do exist in relatively large numbers in subject literatures, though they have heretofore not been exploited in a systematic manner by conventional retrieval systems. Moreover, most such relationships readily lend themselves

to coding and machine processing. Thus, such inherent factors in the published literature as co-authorship linkages, organizational affiliations, institutional bylines, acknowledgments, shared methodologies and instrumentation, and especially the reference citations from one document to another may be computer manipulated in order to bring the total informational context of the retrieval output into a much closer conformity to the original need and request. Obviously, retrieval and analysis of this kind are not presumed to displace conventional subject-content-centered methods; rather, they anticipate a coordinated use in conjunction with some well-tried and preferably relatively simply-designed conventional-subject-indexing system. Our research objectives call for the following necessary steps in implementing the program:

(i) Establishment of a general and flexible experimental retrieval system;

(ii) By a combination of both theoretical and experimental investigations, determine the specific groups of citation linkages that are most useful for retrieval purposes and determine whenever possible the optimum combination(s);

(iii) Select and determine the proper-matching and subject-indexing scheme to complete the design of the retrieval system.

It is quite obvious that (iii) cannot be done without first accomplishing (i) and (ii). Furthermore, our knowledge of subject-oriented retrieval systems surpasses our knowledge in non-subject content-centered retrieval systems by great margins. Hence, we have so far concentrated our efforts mainly in areas (i) and (ii).

In regard to the experimental system, we have initiated compiling a data base of 500 journal articles from a group of leading research journals in the area of computer science. The citation linkages will be coded in a form

convenient for direct processing. The list structures will be imbedded in a programming language to be chosen as the base language for the manipulations of these structures. The programs will be processed on our CDC 1604 computer.

Work has also begun in the investigation of the usefulness of citations in context. A particularly interesting problem seems to be determining the marginal effectiveness of the linkage information as we condense it at various levels of classification. It was discovered that at least two additional levels of classifications are possible besides the level of full context and the level of no context (cited or not cited type of classification). Each level of classification dictates a certain level of storage requirement which may in turn strongly influence systems implementation or retrieval strategy.

11.7.2 Implementation and Comparative Analysis of Retrieval Systems. The objective of an optimum implementation is to achieve a best match between, on the one hand, the capabilities and limitations of a hardware-constrained computer and, on the other hand, the features and specifications (sometimes not well-defined computationally) of an information-oriented indexing-retrieval scheme. While it is clear that relevancy in the retrieval output may be a function of the indexing-retrieval scheme alone, depending on the specific implementation employed, the processing time required for the retrieval operation may vary over wide ranges. The analysis of indexing-retrieval schemes in the light of computational complexity and actual implementation thus adds a new dimension toward the goal of comparing retrieval systems from the point of view of cost-effectiveness. It is also expected that valuable insights will be gained during the course of investigation of the organization and logic of ideal information retrieval machines.

Presently under investigation are implementation problems relating to mass storage files that are random access at the unit level and sequential access

at the bit level. These new mass-storage files cast a different equipment constraint on the system and may lead to radically new file organization and search strategies. Also under investigation are combinational techniques for cluster generation and automatic indexing.

F. P. Preparata
R. T. Chien

11.8 Information Retrieval -- Key-to-Addressing Transformation[†]

An important problem in the design of a system for information storage and retrieval is key-to-address transformation. The key-to-address transformation provides an internal indexing structure so that the average search time of information items can be greatly reduced.

In this study two known methods of transformation are analyzed, extended in scope, with performance evaluated in relation to the statistical characteristi of the key set. A new method based on the Chinese Remainder Theorem is developed.

A. Division: With this scheme, the address R is the remainder of the division process which divides the key K by a constant A. All items are assumed to be expressed in decimal for simplicity of discussion. Let us consider a key set consisting of clusters C_i of length t_i. A set of simple conditions on A have been found to ensure unique assignments of addresses; contrary to ordinary belief A does not have to be a prime number.

B. Folding: This is actually a sub-case of division. Three cases of folding are considered, namely (a) folding without carry, (b) folding with carry and end-around carry and (c) folding with carry but not end-around carry. The merits of each approach is discussed and compared. Simplicity in implementatior is the main advantage of this approach.

[†]Supported in part by the National Science Foundation under Grant NSF GK-690.

C. Method Based on the Chinese Remainder Theorem: The Chinese Remainder theorem asserts that given m_i $(i = 1,2,\ldots,t)$ such that they are pairwise relatively prime, the numbers of the range $D \leq \sum_{i=1}^{t} m_i - 1$ can be uniquely represented by the residues modulo m_i, $(i = 1,2,\ldots,t)$. By grouping the digits of a key and assigning the appropriate m_i to the groups, one could achieve a significant amount of compression.

A detailed account of the results summarized here will appear in a forthcoming technical report.

J. T. Barrows
R. T. Chien

11.9 Connection Assignments of Diagnosable Systems[†]

The problem of automatic diagnosis of digital systems with multiple faults has been investigated. The systems are assumed to be decomposed into n units $u_1, u_2, \ldots, u_n$ and each unit is potentially assumed to be used as test equipment for the correct operation of any other unit. This leads to a graph-theoretic model of a diagnosable system: The nodes of the graph are the undecomposable portions of the system, and a directed link from node u_i to node u_j signifies that there is a test in which u_i is given an opportunity to evaluate u_j. The outcome of each test is binary.

This theoretical model and the corresponding diagnosis philosophy draw some motivation from current trends in the computer technology as regards the advent of integrated circuitry and the packaging of digital systems. It does not seem unreasonable to expect that digital systems of the next generation will consist of single-chip units containing several hundreds of active components;

[†]Supported in part by the National Science Foundation under Grant NSF GK-36 and NSF GK-690.

these units would therefore exhibit the properties of being undecomposable for diagnosis purposes and of possessing the computational complexity implied by the outlined philosophy.

A diagnosable system S is therefore identified by its units and by their connection, or more concisely by its connection matrix.

The first problem which has been solved is the relation between the number t of defective units and the minimum number n of units in the system for which diagnosis is theoretically possible.

Once this lower bound on n ($n \geq 2t+1$) is obtained, we are confronted with the problem of designing efficient connections. In this context, we have adopted two diagnosis strategies: 1) one-step diagnosis, in which the entire set of defective units is determined, without replacement, by inspection of the set of outcomes (diagnosis pattern), 2) sequential diagnosis, in which at least one defective unit can be determined without replacement.

The problem of one-step diagnosis has been investigated and a lower bound on the number of links has been obtained; furthermore, connections have been designed which meet the aforementioned lower bound and are therefore optimal.

The problem of sequential diagnosis is somehow more delicate. Lower bounds on the number of units have been obtained when the units of the system are cyclically connected (single-loop), and connections have been designed for a number of units comprised between the absolute minimum (2t+1) and the single-loop minimum, but no evidence is given of their optimality.

The approach has disclosed several areas for future research, especially as regards exploring the capabilities of different topological arrangements of units, which may be best suited for the actual layout of digital systems.

The results of the described investigation are being published as a CSL report.

F. P. Preparata
G. Metze
R. T. Chien

(OVERLEAF BLANK)

12. NETWORKS[†]

M. E. Van Valkenburg
J. J. Bourquin
T. Kamae
W. Mayeda*
T. Murata
J. A. Resh
G. H. Stumpff
S. Toida
T. N. Trick
N. Wax*

12.1 Linear Graphs

Since knowing all trees is enough to analyze electrical networks, it is desirable to find a simple method of generating all trees of a linear graph by a digital computer.

A new method which is comparable to one[1] given previously, but may be simpler for computer programming, is obtained. For convenience a fundamental form of a matrix is defined to be of the form $[M_{11}U]$ where U is a unit matrix. The new method is as follows: Let $A = [A_{11}U]$ be a fundamental cut-set matrix of a linear graph G. Let the columns of U representing a tree t_o be $\{a_1 a_2 \ldots a_{v-1}\}$. Also let the symbol $T[a_{j_1} \ldots a_{j_k}; t_o]$ be the collection of all trees obtained from t_o by replacing edges $a_{j_1}, a_{j_2}, \ldots$, and a_{j_k} which are in $\{a_1, a_2, \ldots, a_{v-1}\}$ with the chords of the graph as shown in previous work.[1] Now $T[a_{j_1} \ldots a_{j_k}; t_o]$ can be obtained by knowing the non-singular majors of $A[a_{j_1} \ldots a_{j_k}]$ which are obtained from A by deleting all rows which do not have 1 at one of the columns $a_{j_1}, a_{j_2}, \ldots$ and a_{j_k}, and deleting all columns of U. Notice that the finding of the trees of G is the same as obtaining all non-singular majors of A. Thus obtaining $T[a_{j_1} \ldots a_{j_k}; t_o]$ is the same as obtaining all trees of G, but the size of

---

[†]This work was supported in part by the Air Force Office of Scientific Research under Grant No. AFOSR 931.66.

*On leave.

[1]W. Mayeda and S. Seshu, "Generation of Trees without Duplications," IEEE Trans. on Circuit Theory, CT-12, 181-185, June, 1965.

the corresponding matrix is smaller. For example, consider a linear graph whose fundamental cut-set matrix is

$$A = \begin{array}{c} \begin{matrix} e_1 & e_2 & e_3 & a_1 & a_2 & a_3 \end{matrix} \\ \begin{bmatrix} 1 & 0 & 1 & 1 & 0 & 0 \\ 1 & 1 & 0 & 0 & 1 & 0 \\ 0 & 1 & 1 & 0 & 0 & 1 \end{bmatrix} \end{array}.$$

From this it is known that $t_o=\{a_1a_2a_3\}$. Thus the trees in t_o and $T[a_1;t_o]$, $T[a_2;t_o]$, $T[a_3;t_o]$, $T[a_1a_2;t_o]$, $T[a_1a_3;t_o]$, $T[a_2a_3;t_o]$ and $T[a_1a_2a_3;t_o]$ are all the trees of the given graph. To obtain $T[a_1;t_o]$ for example, consider $A[a_1]$ which is

$$\begin{matrix} e_1 & e_2 & e_3 \end{matrix}$$
$$[1 \quad 0 \quad 1].$$

There are two non-singular majors in this matrix which consists of columns e_1 and e_3 respectively. Thus, there is obtained

$$T[a_1;t_o] = \{e_1a_2a_3, e_3a_2a_3\}.$$

To obtain $T[a_1a_2;t_o]$, consider $A[a_1a_2]$ which is

$$\begin{matrix} e_1 & e_2 & e_3 \end{matrix}$$
$$\begin{bmatrix} 1 & 0 & 1 \\ 1 & 1 & 0 \end{bmatrix}.$$

Obtaining all non-singular majors of this matrix can be done by considering a fundamental form of this matrix to be a given cut-set matrix. Thus, this new process consists of two steps one of which is to obtain a tree of distance unity

from a reference tree and the other is to make a fundamental form of a matrix. Complete trees can be obtained by a simple modification of this method.

This process has been programmed for a digital computer. However, we found that there is much more to be done before analysis of networks by a digital computer becomes useful. One future problem is to make some modification of a given network before finding its trees. Often, there are many thousands of trees in a given network, but only a few trees in a simply modified network.

W. Mayeda

12.2 System Reliability Study

An investigation of certain algebraic properties and formulations of the system reliability function, R_s, for a system which operates whenever one or more subsets of its elements operate simultaneously is complete. Using the set of distinct variables which represent the known element reliabilities, and the real number 1, as a set of generators, a polynomial ring, H, is formed with respect to a multiplicative "star" operation, under which each variable and R_s itself is idempotent. Although primary consideration is given to systems with independently operating elements, certain dependencies among elements are also investigated. Analysis of systems containing dependencies, as well as the general formulation of R_s itself, is significantly simplified by the definition of the star operation.

For that subclass of systems, whose reliability models can be represented by weighted linear graphs or nets, where the weights are the reliabilities (variables) of elements, and for which the systems perform successfully whenever there exists a connected sequence of edges and nodes (a path) between two points of the net, a number of interesting properties are obtained. For example, for a planar net, R_s of the dual net is $1-R_s$ of the original (planar)

net. Also, the system unreliability $(1-R_s)$ for either directed or undirected reliability nets can be determined by forming the summation of alternating sums of unreliability products of increasing unions of collections of cutsets separating a pair of nodes i to j -- in an analogous way to that developed for R_s using the set of all paths from i to j. For reliability nets which are series-parallel, it is found that R_s has unity coefficients, with sign determined by $(-1)^{e-n+1}$, where e is the number of edges represented by a given term of R_s, and n is the number of nodes upon which these e edges terminate. This basic idea is used to introduce the new concept of a directed reliability net, where it is found that terms of R_s for such nets are acyclic and always have such unity coefficients. Certain transformations between directed nets and undirected nets are defined. One of the advantages of such transformations is that when R_s is for a large, complex, undirected net, it may be more economically determined by first formulating R_s for its directed equivalent.

Using H, and based on established laws of probability theory, a recursive, generating function Φ for R_s is developed, which is amenable to computer programming, and which, because of its recursive nature, allows the removal of cyclic terms from R_s as they occur, thereby reducing computer time and storage requirements. Also, Φ under star is found to have some interesting algebraic properties.

Finally, consideration is given to the relative sensitivity (for a given change in R_s) between pairs of elements (edges and nodes) of the net in relation to the topology of the net. It is found that series elements and parallel elements have well-defined relationships, but that for more complex structures, the topology alone is not sufficient to evaluate the relative sensitivity between elements. In fact, for very complex nets the topological

influence is almost completely obscured by the importance of the relative reliability values of other elements in the net. The details of this study will be contained in the forthcoming CSL Report No. 300, dated August, 1966.

G. H. Stumpff

12.3 Switching Functions and Minimum Feedback Cut Set

12.3.1 Switching Functions. Given switching functions F_{ab} and F_{bc} between any two of three vertices a, b, and c in the contact network, the third switching function, that is F_{ac}, satisfies the following equation:

$$F_{ac}+F_{ab}\cdot F_{bc} = F_{ac}$$

where "·" is Boolean multiplication and "+" is Boolean addition.

From this we can deduce the following by induction. Let F_{ab} be a switching function between a and b. Also let $F_{bc},F_{cd},\ldots,F_{ma}$ be switching functions between any two vertices in a path between a and b. Then

$$F_{ab}+F_{bc}\cdot F_{cd}\cdots F_{ma} = F_{ab}.$$

If given switching functions are single contact functions, then for any three vertices a, b, and c in the contact network the following equation holds:

$$F_{ab}*B_{bc} = F_{ac},$$

where

$$x_i*x_j = x_i\cdot x_j \quad \text{if } x_i \neq x_j$$

$$x_i*x_j = 1 \quad \text{if } x_i = x_j.$$

If the above relation holds for any three vertices in the contact network, then the network is single contact.

12.3.2 Minimum Feedback Cut Set. If the number of edges in a minimum feedback cut set is less than 4, the minimum feedback cut set is obtained as follows:

(1) Find an edge which is contained in the largest number of circuits in a given graph (original graph).

(2) Remove the edge obtained in (1) and the circuits destroyed by it from the given graph.

(3) Go to (1) if there are any circuits left.

Otherwise end.

It is conjectured that the above procedure may be extendible to a graph with a minimum feedback cut set of more than 3 edges.

S. Toida

12.4 Hamilton Circuits in a Tree Graph

Trees t_1 and t_2 of a given network N are said to be adjacent if t_1 and t_2 share exactly v-2 edges, where v is the number of vertices in N. The tree graph associated with a given network N is defined to be a linear graph in which the vertices are in one-to-one correspondence with the trees of N and the edges with the adjacencies of the corresponding trees. R. L. Cummins first proved the existence of a Hamilton circuit in a tree graph in his Ph.D. thesis at the University of Illinois. His proof consists of the following:

(1) Any nonseparable graph can be derived from a simple circuit of two edges by the operations called the edge insertion and the vertex insertion, both of which were defined in his paper.

(2) These two operations do not affect the property of a tree graph having a Hamilton circuit.

A new proof has been given for the existence of a Hamilton circuit in a tree graph. This new proof is more concise and straightforward than the existing one. It can be efficiently applied to the generation of all the trees of a given network. Details will be reported soon.

T. Kamae

12.5 Frequency Entrainment

The locking or synchronization of an oscillator to an external signal has been the subject of a great deal of study. The method of the variation of parameters, either in the van der Pol form, or in the Krylov-Bogoluibev form, has been used successfully in obtaining a first approximation to the solution of the locking problem. However, both of these methods suffer, at times, from the "problem of small divisors." The problem of small divisors arises whenever terms, supposed small, appear in the solution with denominators which are the differences of equal, or nearly equal numbers.

In work just completed a variant of Struble's method,[2] which combines, effectively, the two classic techniques of variation of parameters and perturbation series to avoid the problem of small divisors, is used to study frequency entrainment. Asymptotic quasi-sinusoidal solutions of the vector equation

$$\ddot{x}+\Omega x = u\, f(x,\dot{x},t)$$

(x and f are vectors, Ω is a diagonal matrix of positive elements, t is the time, and u is a scalar constant, $0 < u \ll 1$) are treated. The results will be published shortly.

N. Wax

---

[2] R. A. Struble, Nonlinear Differential Equations, McGraw-Hill Book Co., New York, 1962.

12.6 Stability of Nonlinear Networks

As mentioned in the previous Progress Report, a "small-perturbation" stability criterion has been developed for linear time-invariant networks which contain periodic sources of period T and a nonlinear element whose first and second derivatives exist over a certain allowable operating range of the nonlinear device. It is assumed that for small enough inputs the steady-state response is unique and periodic of period T. The network is said to be stable to small perturbations if the input voltage is changed by some small increment Δe and the resulting transients decay to a unique periodic solution with period T. The stability criterion determines the maximum allowable input voltage such that the transients decay to the desired response for "very small" changes in the input voltage. This stability criterion has now been compared with other criteria and with experimental results obtained from a subharmonic oscillator circuit.

This comparison shows that the perturbation approach to the stability of sinusoidally-forced nonlinear networks is superior. A larger allowable dynamic operating range is tolerated with this new approach over previous stability criteria. Also, when the stability criterion is applied to the subharmonic oscillator circuit, an unstable system by our definition, the results are good. A report is now in preparation covering these results.

T. N. Trick

12.7 Subharmonic Oscillations in Parametric Amplifiers

Quite often parametric amplifiers and frequency converters will go into undesirable subharmonic oscillations. Since parametric-amplifier designers do their designs on the basis of a time-varying model, the problem of subharmonic oscillations is sometimes very baffling to them. Actually the parametric device

is nonlinear, and subharmonic oscillations are the result of nonlinear phenomena. To date, analytic and topological techniques have mainly been applied to second-order nonlinear differential equations. Recent results in the study of nonlinear oscillations due to Hale[3] and others have led us to the following conjecture: It is believed that subharmonic oscillations in a nonlinear system will occur only at or near the eigenvalues of a linearized model for the nonlinear system.

In order to test this conjecture a fourth-order circuit containing an abrupt-junction varactor diode was constructed. The eigenvalues of a linearized model of the above circuit were found. The circuit was then pumped at a frequency of twice each of the eigenvalues. The experimental results showed that this circuit went into one-half subharmonic oscillations whenever the pump frequency was around twice one of the eigenvalues, and only then. These results will soon be compared with a theoretical analysis which is being completed.

T. N. Trick

12.8 Stability of Distributed Systems

Irrational functions of the complex frequency variable s, such as functions of ϵ^{Ts}, $\sqrt{s}$, and $\epsilon^{\sqrt{Ts}}$ are appearing more frequently as transfer or driving-point functions in present-day literature. Often one of the methods of analysis applied to such functions is similar to that applied to rational functions of s: In F(s) = A(s)/B(s) the poles of F(s) are taken as the values of s for which B(s) = 0. If any such points lie in the right-half s-plane, it is decided that the corresponding system is unstable; if there are none, then it is assumed stable. In some cases there are an infinite number of zeros of B(s).

[3] J. K. Hale, Oscillations in Nonlinear Systems, McGraw-Hill, 1963.

In these cases only a finite number of such points are usually observed; only those closest to the origin of the s plane are considered dominant, the number of which depends on the desired accuracy of the resulting approximation to the true time response.

That the above procedure may not always yield accurate results can be illustrated by two examples. Consider first $f(t) = t^n \sin t^\alpha$ ($\alpha > 1$; $n = 1,2,\ldots$). This function obviously describes an unstable occurrence. Yet $F(s) = \mathcal{L}[f(t)]$ is an entire function and therefore possesses no singularities in the finite plane.

Next consider a system for which the transfer function $F(s) = 1/(1+\sqrt{s})$. Solving $B(s) = 0$, one obtains $\sqrt{s} = -1$, and $s = 1$. A pole exists in the right-half s plane, and it seems that the system should be unstable. Yet, the unit-step response is $\mathcal{L}^{-1}[1/(1+\sqrt{s})s] = 1-\epsilon^t \operatorname{erfc}\sqrt{t}$ which approaches 1 as $t \to \infty$. It is obvious that care is necessary in the analysis of such systems as illustrated here.

The stability criterion of systems for which F(s) is a rational function of ϵ^{Ts} has long been established in terms of a region of the z plane, for $z = \epsilon^{Ts}$. In 1961[4] the stability criterion of systems for which F(s) is a rational function of $\sqrt{s}$ was established in terms of a region of the $\sqrt{s}$ plane. Proceeding now is an attempt to establish the stability criterion of systems for which F(s) is a rational function of $\epsilon^{\sqrt{Ts}}$ in terms of a region of the ξ plane, where $\xi = \epsilon^{\sqrt{Ts}}$.

J. J. Bourquin

---

[4] I. A. Brin, "On the Stability of Certain Systems with Distributed and Lumped Parameters," Automation and Remote Control, 23, 798, July 1962.

13. CONTROL SYSTEMS

J. B. Cruz, Jr.
S. D. Agashe
O. Balasaygun
M. S. Davies
R. L. Gonzales
J. P. Herner
R. A. Hoyt
W. R. Perkins
D. C. Reddy
D. M. Salmon
M. Schoenberger
M. Sobral, Jr.
R. Werner

13.1 Introduction

This group is concerned with the analytical, computational, and simulation aspects of control system analysis and design. Three major projects are underway currently. The first involves a detailed investigation of parameter variation effects (sensitivity). Emphasis is placed on the formulation of sensitivity measures, and on the use of these measures not only for system analysis, but also for design of low-sensitivity systems. The relation between sensitivity and optimality also is receiving attention.

The second project is a study of stability problems. Important generalizations of several Popov's results concerning sufficient frequency-domain stability conditions have been obtained.

The third problem is a study of optimal control theory. New insight into the Maximum Principle has been obtained, especially involving the perturbation process used in obtaining the Principle.

13.2 Sensitivity of Dynamical Systems

13.2.1 Comparison Sensitivity.[†] Work has continued on the study of parameter-variation effects in open-loop and closed-loop linear systems. A direct comparison of output deviations due to parameter variations in open-loop

[†]This work was supported in part by the Air Force Office of Scientific Research under Grant No. AFOSR 931.66.

and closed-loop systems has led to comparison-of-sensitivity performance indices. Several time-domain and frequency-domain criteria for analysis and design of comparitively insensitive systems have been developed.

Investigation of the sensitivity of nonlinear systems has begun. Necessary and sufficient conditions for the insensitiveness of one system relative to another have been obtained for a class of nonlinear systems with small parameter perturbations. Furthermore, a suboptimization scheme for choosing a feedback realization is suggested.

This work is reported in "Criteria for System Sensitivity to Parameter Variations" presented at the Third Congress of the International Federation of Automatic Control, London, England, June, 1966. Related simulation studies are reported below.

W. R. Perkins
J. B. Cruz, Jr.

13.2.2 Sensitivity Comparison of Open and Closed Loop Nonlinear Control Systems.[†] Cruz and Perkins have developed a general method of comparing the sensitivities with respect to plant parameters of open-loop and closed-loop nonlinear control systems having equal nominal outputs. A specific example to which this general method has been applied is a servomotor with variable derivative and unity-output feedback control. The gain and time constants of the motor were chosen as two parameters that may be subjected to variations. The system has been simulated on the analog computer and the open-loop and closed-loop first-order sensitivity functions were obtained for various values of the tachometer feedback constant.

Oray Balasaygun

[†]This work was supported in part by the Air Force Office of Scientific Research under Grant No. AFOSR 931.66.

13.2.3 Synthesizing Comparatively Insensitive Systems.[†] Work is continuing on the problem of designing linear feedback systems that are simultaneously optimal with respect to a quadratic index and insensitive in comparison with open-loop systems. This problem has been described in detail in the Progress Report for Sept., Oct., Nov., 1965.

In the solution of this basic problem, it has been necessary to find a convenient method of extending the result that for all ω the optimal control law F obey

$$|1-F\Phi_p(j\omega)\underline{b}|^2 \geq 1$$

for multiple-input systems.

To the matrix Ricatti equation

$$PBL^{-1}B^TP-A^TP-PA = W$$

with $LF = -B^TP$ for the linear regulator problem add sP-sP, premultiply by $B^T\bar{\Phi}_p{}^T(-s)$, and postmultiply by $\bar{\Phi}_p(s)B$. After adding L-L, the result is

$$[I-F\bar{\Phi}_p(-s)B]^TL[I-F\bar{\Phi}_p(s)B] = L+B^T\bar{\Phi}_p{}^T(-s)W\bar{\Phi}_p(s)B.$$

Following directly from the above equation, if the weighting matrix of Perkins and Cruz is F^TLF, we have

$$S^{-1}{}^T(-j\omega)F^TLFS^{-1}(j\omega) = F^T[I-F\bar{\Phi}_p(-j\omega)B]^TL[I-F\bar{\Phi}_p(j\omega)B]$$

$$= F^TLF+F^TB^T\bar{\Phi}_p{}^T(-j\omega)W\bar{\Phi}_p(j\omega)BF.$$

[†]This work was supported in part by the Air Force Office of Scientific Research under Grant No. AFOSR 931.66.

Since the second term is positive semidefinite, there obtains

$$S^{-1}(-j\omega)F^{T}LFS^{-1}(j\omega) \geq F^{T}LF$$

Note that this choice of weighting matrix $F^{T}LF$ weights only those errors that are affected by the feedback configuration, because, if one has

$$\underset{\sim}{e}^{T}(-j\omega)F^{T}LF\underline{e}(j\omega) = 0$$

then it follows that

$$F\underset{\sim}{e}(j\omega) = 0. \tag{1}$$

However, $\underline{e}_o$ and $\underline{e}_c$ are related by

$$\underset{\sim}{e}_c(j\omega) = \underset{\sim}{e}_o(j\omega)+\Phi_{f'}(j\omega)BF\underset{\sim}{e}_o(j\omega) \ , \tag{2}$$

so that (1) and (2) imply

$$\underset{\sim}{e}_c(s) = \underset{\sim}{e}_o(s).$$

Another interpretation of using the weighting matrix $F^{T}LF$ is that, since (A,F) is completely observable, reduction in errors in $F\underset{\sim}{x}$ necessarily implies that errors in $\underset{\sim}{x}$ are reduced. Proof of the above conjecture is being investigated at the present time.

J. P. Herner

13.2.4 Optimal Controls of Plants with Varying Parameters.[†] Work is continuing on worst-case design of optimal control linear regulators with quadratic performance indices. We are given a single-input plant in a state-space

[†]This work was supported in part by the Air Force Office of Scientific Research under Grant No. AFOSR 931.66.

representation

$$\dot{\underset{\sim}{x}} = A\underset{\sim}{x}+\underset{\sim}{b}u$$

with parameters in A only partially defined, that is, A is only defined as some range of parameters called $\bar{A}$. For this plant, we wish to find the control u(t) which satisfies

$$\min_{u(t)\in U}\{\max_{A\in\bar{A}}\{\int_0^T [\underset{\sim}{x}^T Q\underset{\sim}{x}+u^2(t)]dt\}\}.$$

The above is a formal representation of the solution, but computational algorithms for this min-max design are needed.

At present, work is being done on the sub-optimal problem where the constraint that

$$u(t) = \underset{\sim}{c}^T\underset{\sim}{x}$$

is employed. From preliminary studies, it appears that for certain ranges, $\bar{A}$, the min-max computation can be reduced to a finite number of standard minimization problems, i.e.,

$$\min_{u\in U}\{\int_0^T (\underset{\sim}{x}^T Q\underset{\sim}{x}+u^2)dt\}$$

for

$$\dot{\underset{\sim}{x}} = A_i\underset{\sim}{x}+\underset{\sim}{b}u$$

$$u = \underset{\sim}{c}^T\underset{\sim}{x}$$

where A_i's are certain special A's in the range $\bar{A}$ (usually boundary points). The above results have been established for lower-order examples. General proofs for higher-order cases are being sought.

R. Hoyt

13.2.5 Sensitivity Analysis of Dynamic Systems. Investigation has continued into the problem of change in the performance indices for a particular class of time-weighted functionals of the form

$$\int_0^\infty t^r \underset{\sim}{x}^T \underset{\sim\sim}{Q} \underset{\sim}{x}\, dt, \quad Q > 0,$$

for free, stationary, linear, multivariable systems. No general results were apparent which would conveniently relate eigenvalue and eigenvector sensitivities to the change in the performance indices mentioned above. However, when the $\underset{\sim}{A}$ matrix of the system in the special case

$$\dot{\underset{\sim}{x}} = \underset{\sim\sim}{A}\underset{\sim}{x}$$

is symmetric with $r = 0$, it is possible to relate any change in the performance indices to both the eigenvector and eigenvalue sensitivity.

Also, in the previous Progress Report, perturbations affecting only a single element a_{ij} of the $\underset{\sim}{A}_1$ matrix, as defined below were considered:

$$\dot{\underset{\sim}{x}} = \underset{\sim}{A}_1\underset{\sim}{x} + \underset{\sim\sim}{B}\underset{\sim}{u},$$

$$\underset{\sim}{u} = \underset{\sim\sim}{F}\underset{\sim}{Y},$$

$$\underset{\sim}{Y} = c\underset{\sim}{x},$$

In general, the above-mentioned perturbations could affect not only more than a single element of the $\underset{\sim}{A}_1$ matrix but also elements of the $\underset{\sim}{B}$, $\underset{\sim}{F}$, $\underset{\sim}{C}$ matrices. So the general parameter-variation problem was considered, and a simple formula for the evaluation of eigenvalue sensitivity was derived. Specifically, assuming distinct eigenvalues of the matrix $\underset{\sim}{A}$, where $A = A_1 + \underset{\sim\sim}{BFC}$, the eigenvalue sensitivity of λ_j with respect to α_i is given by

$$\frac{\partial \lambda_j}{\partial \alpha_i} = \frac{\text{Trace of Adjoint}\{[\underset{\sim}{A}-\lambda;I][\partial \underset{\sim}{A}/\partial \alpha_i]\}}{\text{Trace of Adjoint}[A-\lambda_j I]}$$

where

λ_j is the $j^{\underline{th}}$ eigenvalue of the matrix $\underset{\sim}{A}$

and

$\alpha_i \in \{\alpha_1, \alpha_2, \ldots, \alpha_n\}$.

The problem of the relation of invariance to eigenvalue-of-eigenvector sensitivity was investigated. The necessary and sufficient conditions for an invariant response were obtained.

A study of a class of matrices -- circulants -- was undertaken. It was found that the eigenvectors of these matrices were invariant with respect to any parameter variations, i.e. the eigenvectors were not functions of the elements of the $\underset{\sim}{A}$ matrix.

Using the concept of eigenfunction sensitivity, the effect of parameter variations on the system response of a problem of practical interest was undertaken. A possible design procedure was evolved which reduced the sensitivity of the response for the above mentioned problem.

The results of this whole investigation will appear in a forthcoming CSL research report.

D. C. Reddy

13.2.6 Minimization of Multiparameter Sensitivity.[†] A new multiparameter sensitivity index for control system analysis and design has been

[†]This work was supported in part by the Air Force Office of Scientific Research under Grant No. AFOSR 931.66.

developed. This index involves either the integral-square deviation error or the mean-square deviation error due to parameter variations. A first-order approximation to the change in system transmission is used to simplify these expressions. In addition, sensitivity-analysis techniques for worst-case conditions have been developed to deal with parameter specifications in the form of tolerances.

Synthesis procedures permitting the minimization of these indices, and incorporating stability and physical-realizability conditions, have been developed. Specific numerical examples have been studies with the aid of the CDC 1604 computer to verify the accuracy and usefulness of the approach. The results are reported in detail in Report R-312, "Control System Sensitivity to Minimize Multiparameter Sensitivity."

R. L. Gonzales

13.3 Stability of Nonlinear Control Systems

Work has continued on the stability of systems involving a number of nonlinearities. The general problem is described in detail in the Progress Report for Dec., 1965, Jan. and Feb., 1966. Several useful results have already been obtained[1], but the stability criteria have been found unwieldy when applied to particular systems. It is hoped that it will be possible to find criteria which are more easily exploited. At present it is possible to simplify the criteria only when considering systems of a particular form, and even then the sufficient conditions for stability are weaker than those mentioned above.

M. S. Davies

---

[1] The Absolute Stability of Systems with Multiple Nonlinearities, CSL Report R-288, May, 1966.

13.4 Some Topics in Optimal Control Theory

A critical examination of the perturbation process involved in the proof of the Pontryagin Maximum Principle has been carried out. This has resulted in a simpler description of the perturbation process and in a new proof of the constancy of the Hamiltonian function for time-invariant systems.

A new definition of the "impulse" response has been proposed. This definition is rigorous, physically meaningful and allows the convolution-integral form of response to an input to be derived naturally and rigorously. This new interpretation of impulse response was suggested by the consideration of the perturbation process mentioned above.

Finally, a connection between optimality and controllability has been discovered. Using this, sufficient conditions for controllability are obtained from necessary conditions for optimality.

S. D. Agashe

(OVERLEAF BLANK)

14. STRUCTURAL-SYSTEM DESIGN[†]

S. J. Fenves

R. duPreez

A doctoral thesis on the application of symbolic network transfer functions to structural-engineering problems is in the process of being completed. The symbolic-network topological approach is directly applicable only to lumped-parameter structural systems in which the branch admittances and variables are expressed by scalars or scalar functions. For such problems, efficient parameter-optimization design procedures can be developed. Further research is needed to apply the approach to general structures, where the branch variables are vectors and the branch admittances are square submatrices.

Two demonstration programs for simple structural design problems, using on-line typewriter input and cathode-ray-tube output, have been written. One of these is being adapted to PLATO, and will be used by Civil Engineering classes in the Fall. The programs are characterized by the fact that no "teaching logic" is built into them; it is entirely up to the student user to determine the sequence of operations in specifying, modifying, and comparing trial designs.

(OVERLEAF BLANK)

[†]Supported in part by the University of Illinois.

15. SWITCHING SYSTEMS

G. Metze
L. Abecassis
W. J. Bouknight
S. C. Chang
E. D. Crockett
R. duPreez
S. Fenves
T. Gaddess
F. Hohn
D. Howarter
R. Marlett
G. Martens
Miss L. Minning
T. Powell
F. Preparata
R. Schneider

15.1 Diagnosis of Combinational Networks[†]

Several new techniques for the diagnosis of faults in combinational networks are under investigation. As usual, at most one fault is assumed to exist in the network at any time, and logical faults only, i.e., lines, inputs, or outputs stuck at 0 or 1 are considered. In all of these procedures, selected inputs are applied to the network, and the corresponding outputs are used to determine which fault (or class of indistinguishable faults) is present in the network.

Report R-292 describes a method for selecting a subset of the input vectors suitable for a test procedure. Since, for each input vector, each of the possible output vectors determines a class of indistinguishable faults, and since the fault partitioning resulting from the application of several input vectors in some sequence can be obtained by forming the set intersections of the fault partitions which correspond to the individual input vectors, a set of test inputs which yields a complete diagnosis can be selected either for a combinational test procedure, in which a fixed set of inputs is applied in any sequence, or for a serial test procedure, in which the outcome of the current test determines which of a predetermined subset of inputs is to be applied next.

[†]This work was supported in part by the National Science Foundation under Grant NSF GK-36.

Armstrong[1] recently described a procedure for the selection of suitable inputs for failure detection tests which is based on the technique of path sensitizing. A report on an extension of this method to failure location tests is in preparation.[2]

Chang's procedure[3] for the selection of tests which locate a fault to within a module but do not necessarily identify the faulty circuit in more detail records only whether a test passed or failed. A modification of this method which utilizes the available information about how the test failed is under development.

W. J. Bouknight
D. Howarter
T. Powell

15.2 Self Diagnosis of Digital Computers[†]

A new approach for deriving self-diagnosing programs for digital computers is reported in report R-293. The derivation procedure is based on only a micro-orde description of the computer to be tested. The detailed logic information is not needed. This approach is made possible by "standardizing" computer realization techniques by means of a set of design principles. This report describes such a set of design principles which guarantees the existence of a relationship between the behavior of a computer under a large number of failures and alterations of the

---

[1] D. B. Armstrong, "On Finding a Nearly Minimal Set of Fault Detection Tests for Combinational Logic Nets," IEEE Trans. on Electronic Computers, EC-15, 66, (1966).

[2] D. Howarter, "The Selection of Failure Location Tests by Path Sensitizing Techniques," CSL Report R-316.

[3] H. Y. Chang, "An Algorithm for Selecting an Optimum Set of Diagnostic Tests," IEEE Trans. on Electronic Computers, EC-14, 706, (1965).

[†] This work was supported in part by the National Science Foundation under Grant NSF GK-36.

micro-order specification for that computer. The micro-order "alterations" are then used to characterize a computer under failure for every machine instruction so that test programs can be written which check for over 93% of all failures. Such programs check for "symptoms of failure" rather than the actual component which caused the failure, since the logic is not necessarily assumed to be known. This procedure can be programmed so that diagnostic programs can be generated by a computer. An experiment is also described which substantiates the theoretical findings.

Further work is indicated particularly with respect to the design of diagnosable instruction decoders. The design principles developed so far should be subjected to a full-scale test by using them in the design of an entire digital system.

R. Marlett

15.3 Ternary Switching Circuits[†]

If the assignment of the values of a physical variable, such as voltage, to the logic values 0, 1, and 2 of ternary Post algebra satisfies certain simple conditions, then the only types of circuits which are necessary for the realization of any ternary switching function are diode-resistor OR and AND circuits identical to those used in binary switching networks, and some simple triode or transistor circuits which employ a single switching threshold.[4]

[†]This work was supported in part by the National Science Foundation under Grant NSF GK-36.

[4]M. Yoeli and G. Rosenfeld, "Logical Design of Ternary Switching Circuits," IEEE Trans. of Electronic Computers, EC-14, (1965).

A study of some of the properties of ternary switching has led to the development of procedures for the detection and elimination of static and dynamic hazards and is reported in report R-310.

L. Abecassis
F. Preparata

15.4 Quasi-Linear Sequential Machines

The study of procedures for the realization of a sequential machine as a quasi-linear sequential machine continues.

If a maximum-length-cycle set is found under one input (or a sequence of inputs), then a valid state assignment can be obtained by a rather simple method. The state assignment can then be used to check whether this machine has a quasi-linear realization. If no maximum length cycle set can be found for any input, the method works partially except for the case where at least two cycles are associated with any cycle length in the set.

If a tree exists under one input (or a sequence of inputs), one can match a valid tree-type state sequence to the tree, with the state assignment arbitrary up to the same tree level, to get a transition matrix T. Let $S_n PTP' S_n = L$, where S_n is Preparata's standard matrix,[5] P is a permutation matrix on the 2^n states, and n is the dimension of the state vector space. Using the conditions for quasi-linearity on the matrix L, one can solve for the unknowns in P. A 32-state machine has been analyzed by this method.

S. C. Chang

---

[5] F. P. Preparata, "State-Logic Relations for Autonomous Sequential Networks," IEEE Trans. on Electronic Computers, EC-13, 542 (1964).

15.5 Synthesis of Sequential Networks†

The study of modular decompositions of sequential machines using graph-theoretical methods continues. The suggested approach makes it possible to select a desired type of decomposition without having to try various possibilities. Furthermore, the method employs matrix techniques which could be programmed on a digital computer.

E. D. Crockett

15.6 Design of an Error-Detecting Arithmetic Unit†

The study of the implementation of an error-detecting arithmetic unit has led to a suitable design for an adder, and an algebraic proof that any single fixed fault in the adder results in at most a distance-1 error in the sum, for this particular design. The design of a practical checking circuit for the chosen codes, distance-1 codes of the type An+B, is being pursued.

T. Gaddess
F. Preparata

15.7 Algebraic Network Synthesis†

State equations in the form

$$px = Ax+Bu$$

$$y = Cx+Du$$

may be used to characterize the dynamic behavior of time-varying and time-invariant systems. A, B, C, and D are matrices of real constants or functions of time, x, u, and y are column matrices of state-variables, driving functions and responses, respectively, and p denotes d/dt. For linear time-invariant systems the driving functions may be related directly to their responses by an

†This work was supported in part by the National Science Foundation under Grant NSF GK-36.

input-output matrix. The state equations determine the input-output matrix uniquely. However, the converse is not true.

The problem considered here is the synthesis of active and passive RLC networks which realize a given set of time-varying or time-invariant state equations.

A characterization is given for the state equations of an RLC network with sources. It is shown that the coefficient matrix of the state equations must be representable as a product of two factors satisfying necessary symmetry conditions. Each factor may be interpreted as the input-output matrix of a resistive network. It is also shown that, except for degenerate cases, an input-output matrix must satisfy a divisibility property.

An algebraic procedure, utilizing the divisibility property, is developed for inserting variables to generate a near-primitive hybrid matrix from a given input-output matrix. This procedure is analogous to the node-insertion procedure developed by Hohn and Schissler[6] for the design of switching circuits. The near-primitive hybrid matrix determines a positive-definite diagonal matrix and a hybrid matrix which satisfy the necessary symmetry conditions and, after the permutation of submatrices, yield the required product representation for the coefficient matrix of the state equations. The characteristic polynomial of the A matrix is identical with the minimal polynomial of A and the monic common denominator of the input-output matrix.

Active RC and active RLC network realizations for time-varying as well as time-invariant linear state equations are obtained. The only active elements are dependent voltage and current sources. In the time-varying case

---

[6] F. E. Hohn and L. R. Schissler, "Boolean Matrices and the Design of Combinational Relay Switching Circuits," B.S.T.J., 34, 177 (1955).

the only time-varying elements are dependent sources such as mixers and modulators. Thus it is shown that any linear system, time-varying or time-invariant, can be simulated by an active network.

This work has been reported in report R-294.

G. O. Martens